UNIVERSIDAD NACIONAL DE COLOMBIA

Control strategy to share reactive power and regulate voltage in microgrids with autonomous mode operation

EDER ALEXANDER MOLINA VILORIA

Doctorado en Ingeniería – Automática

Facultad de Ingeniería y Arquitectura

Universidad Nacional de Colombia

Manizales, Colombia

2019

Control strategy to share reactive power and regulate voltage in microgrids with autonomous mode operation

Eder Alexander Molina Viloria

Thesis presented as a partial requirement to obtain the title of:

Doctor en Ingeniería

Línea de Investigación en Automática

Advisor:

John Edwin Candelo Becerra, PhD

Advisor:

Fredy Edimer Hoyos Velasco, PhD

Doctorado en Ingeniería – Automática

Facultad de Ingeniería y Arquitectura

Universidad Nacional de Colombia

Manizales, Colombia

2019

Estrategia de control para compartir potencia reactiva y regular tensión en micro redes operando en modo autónomo

Resumen

El objetivo de esta tesis es desarrollar una estrategia de control para los sistemas de generación distribuida (DG), que permitan lograr compartir la potencia reactiva y regular el voltaje en las microrredes operadas de manera autónoma. Las estrategias de control propuestas presentan diferentes alternativas para mejorar la compartición de potencia reactiva entre las diferente DG que conforman la microrred y para regular el voltaje en los nodos. Por lo tanto, es posible contribuir a la superación de los problemas causados por la conexión y desconexión continua de las cargas, evitando el disparo de DG en esta situación. El alcance de las estrategias propuestas cubre una amplia gama de posibilidades, desde la regulación del voltaje en los nodos de la microrred basada en la conexión y desconexión del vehículo eléctrico, hasta las cargas residenciales urbanas y rurales. La utilidad de estas estrategias de control se centra en los sistemas de DG que funcionan en modo autónomo con una gran integración de energías renovables, principalmente ubicadas en áreas remotas. Por lo tanto, en esta investigación trabajamos en la comparación del consumo de las comunidades rurales y urbanas para obtener diferentes variaciones de cargas para probar la estrategia de control en la microrred. Las estrategias de control incluidas en esta investigación son: voltaje RMS virtual, impedancia virtual variable, corriente virtual y voltaje virtual.

Palabras claves: Compartición de potencia reactiva; microrredes; voltaje virtual; corriente virtual; regulación de voltaje.

Abstract

The objective of this thesis is to develop control strategies for distributed generation (DG) systems, that allows to achieve reactive power sharing and regulate voltage in microgrids operated autonomously. The proposed control strategies present different alternatives to improve reactive power sharing among DGs that conform the microgrid and to regulate the voltage in the nodes. Thus, it is possible to contribute to the overcoming problems caused by the continuous connection and disconnection of power loads, avoiding DG tripping under this situation. The scope of the proposed strategies covers a wide range of possibilities, from regulating voltage in the nodes of the microgrid based on electric vehicle connection and disconnection, to urban and rural residential loads. The usefulness of these control strategies is focused on DG systems that operate in isolated mode with great integration of renewables, mainly located in remote areas. Therefore, in this research we worked on the comparison of both the consumption of rural and urban communities to obtain different load variations to test the control strategy in the microgrid. The control strategies included in this research are: virtual RMS voltage, variable virtual impedance, virtual current, and virtual voltage.

Keywords: reactive power sharing; microgrid; virtual voltage; virtual current; voltage control.

Acknowledgment

Poor person who thinks that something like this is achieved alone. First, I want to thank God, for giving me health, knowledge and the necessary perseverance to complete successfully this goal. Also, to my advisor John Candelo for the trust and collaboration during these four years. Besides, to my advisor Fredy Hoyos who was always willing to support me in all technical decisions. I also want to thank the entire community of the Universidad Nacional de Colombia, Sede Medellín and Sede Manizales.

Finally, I thank my parents with my heart for all the help, patience, affection and dedication they have had during every second of my life; because without a doubt getting here would not have been possible without their love, their encouragement and understanding. Also, I thank my friends who in one way or another have been present in my life.

Table of contents

1

Introduction

The research work developed in this Doctoral Thesis was conducted at the National University of Colombia, within the Applied Technologies research group (GITA), in the research topic related to modeling and simulation of electrical systems. This thesis is presented as a compendium of scientific papers, either published or submitted to recognized scientific journals [2–7]. These papers comprise Chapters 2–7 and bring together the most significant aspects of the studies conducted between February 2016 and September 2019.

The main objective of this study is to develop control strategies for power inverters in Distributed Generation (DG) systems when disturbances occur as a result of the variation of electric loads while managing to share the reactive power and regulate the voltage in the nodes of the microgrid operating in island mode.

Basically, these control strategies allow defining the behavior of the inverter or group of inverters connected to the microgrid (MG) in autonomous (island) mode. Throughout this thesis, the power inverters will be the main tool that modifies the behavior of the DGs. For this, the proposed control strategies can vary the references of active and reactive power so that it is possible to respond adequately to changes in loads that can lead to network instability or collapse.

The operating mode of an MG introduces new challenges because the dynamics are no longer dominated by the main power grid. The island mode requires the implementation of an accurate control and management mechanism to maintain the balance between power demand and supply. The power inverters that are shunt-connected can be organized following a hierarchical architecture that is divided into

three control levels: primary, secondary, and tertiary.

A better use of DG resources is to consider DGs and loads as a subsystem or MG. Therefore, the MG can be managed as if it were a complete, predictable generation and consumption unit. This approach allows certain benefits for users of the MG, such as improving continuity of the power supply, optimizing the location and quantity of internal generation, or controlling power injection to maintain generation availability in the form of reserve. However, this may present a medium-term demand management problem as it is not always possible to manage generation and consumption mismatches, and an additional investment in installing more power units may be necessary.

The first generation of MGs was installed for large industrial or institutional facilities, where demand is well known and the required generation can be easily predicted. It is these types of installations that have served as a reference to develop an adequate framework, which allows the extension of the concept of MGs and makes it compatible with an efficient and reliable management of the distribution network.

An isolated MG works like those isolated power systems and experiences major problems associated to system size such as system stability. The isolated MG has the invaluable contribution of electronics in the form of power converters, which are responsible for integrating the DG as a voltage source where the magnitude and frequency can be controlled and, consequently, the stability of the system.

The performance of the MG has been studied from different perspectives such as the compensation needed to improve power quality [1], programming [2], power management and control [3], [4], protection [5], and communication [6]. A control strategy for network connection and island mode has been presented in the literature [7]–[9].

When the MG is connected to the power grid, the MG is typically controlled as an entity that follows the network. Some control strategies adopted for the network monitoring operation are discussed in [7] and [8]. In the island mode, there are two master–slave and multi-master strategies that have been considered in MGs with an electronically coupled power source [9], [10].

1.1 Problem statement

When the MG works in autonomous (island) mode, it is important to maintain the stability of the system and manage power sharing to the loads among shunt-connected DGs [11]. However, the problem of sharing reactive power is influenced by the impedance mismatch of the feeders and the different DG units. Additionally, nonlinear loads and unbalanced loads further affect the reactive power sharing [11].

Sharing reactive power between generators in high voltage networks is not usually a major concern due to capacitive compensation and power transfer of transmission lines. However, in low voltage MGs, there is a reduced capacity to supply reactive power from generation sources and compensators to the loads and the reactive power sharing is not sufficiently accurate to avoid overloads [11].

In a low voltage MG, the impedance of the distribution feeder is mainly resistive [12]; in this case, the droop control method is subject to poor transient stability [12] due to the poor reactive power coupling between DG units when no additional inductance is present [12]. Line impedances and DG output impedances significantly affect the accuracy of reactive power control during the operating mode connected to the network and the reactive power sharing during the operation in island mode due to voltage drops [12]. The accuracy of reactive power sharing is further deteriorated if there are local loads at the DG output [12].

Consequently, the concepts of droop control have been widely adopted to provide decentralized power without relying on communications [8]. However, communications, in addition to droop control, can be used as a noncritical element in an upper control layer, known as “secondary control,” to improve the performance of the island MG without reducing system reliability [13]. Although the frequency droop control technique can be used to achieve accurate real power distribution, the voltage droop control technique commonly results in a poor distribution of the reactive power [14]. This is due to the lack of coincidence in the voltage drops across the DG (unit feeders), which is induced by the mismatch in the impedance feeder and/or the differences in the powers of the generation units [15].

At present, the voltage controllers in the MGs are unable to share the demand for reactive power among even identical inverters in shunt operation [9]. Some researchers have previously worked on this issue, as in [16], which proposes an alternative controller for sharing reactive power between shunt inverters with nominal

voltages. The method requires that each unit have a common load voltage measurement, which limits its applicability in more complex MG scenarios with multiple loads.

Similarly, the centralized secondary control architecture proposed in [17] for the distribution of reactive power from generation units requires communication with a central controller. In addition, the distribution of the voltage regulator proposed in [18] and [19] requires all DGs to be able to communicate directly with each other.

One of the main issues in MGs operating in autonomous mode or connected to the power grid is the ability to share reactive power to loads as the voltage regulation and reactive power distribution are contradictory objectives due to line impedance. Then, as defined above, the following question arises: What is the most appropriate way to share the reactive power and regulate the voltage in the nodes in an autonomous MG?

The answer to this question can be derived through several initial questions: How can reactive power be distributed efficiently in the different loads of the MG while regulating the voltage in the different nodes of the load? How does the MG regulate the voltage when different types of loads change? What MG topology allows better voltage regulation in autonomous MGs? How should the stability of an implemented control strategy be tested without causing failure?

1.2 Proposal

The limitations in droop control reveal that shunt inverters must have the same

impedance per unit in order to share the reactive power to the load accurately and in proportion to their reactive power values when a conventional droop control is adopted. The droop controllers must also generate the same voltage for the inverters and both conditions are difficult to meet in practice, which leads to errors in reactive power sharing between DGs that interact in the MG.

The voltage regulation and the distribution of reactive power are contradictory objectives in the DGs that interact in an MG due to the line impedance of local loads connected to each DG and the output impedance of each DG. Accurate voltage regulation in the DG leads to large errors in the distribution of reactive power.

In this work, it is proposed to perform an improved slope control strategy in order to achieve a more accurate proportional distribution of reactive power within the upper and lower limits of each DG. There is also a dependence on the homogeneity of the linear reactance, which can possibly be solved with a control that considers a constant virtual impedance when the load changes.

In this thesis, it will be possible to develop a control strategy based on primary and secondary controls to solve the problem that currently exists in MGs in order to meet the demands requested by different loads. In addition, a stable voltage must be maintained at each DG bus, something that so far has not been achieved in MGs operating in island mode. After developing this control strategy, a stability test must be applied that will confirm that the control strategy works in an optimal way.

The primary control will be responsible for regulating the proportional reactive power

in the different DGs, maintaining the desired voltage, and improving these values as obtained in the primary control. The secondary control will be in charge of optimizing the reactive power and the voltage to the desired values; the errors are canceled very quickly thanks to this new stage.

1.3 General objective

The main objective of the research work of the thesis is to design a control strategy to share the reactive power and maintain the voltage regulation of the nodes when different load changes occur in an MG operating in island mode.

1.4 References

[1] Rashad M. Kamel*, Aymen Chaouachi, Ken Nagasaka: Wind power smoothing using fuzzy logic pitch controller and energy capacitor system for improvement Micro-Grid performance in islanding mode," *Energy*, vol. 35, no. 5, pp. 2119–2129, May 2010.

[2] M. Tasdighi, H. Ghasemi, and A. Rahimi-Kian, "Residential Microgrid Scheduling Based on Smart Meters Data and Temperature Dependent Thermal Load Modeling," *IEEE Trans. Smart Grid*, vol. 5, no. 1, pp. 349–357, Jan. 2014.

[3] A. Bidram and A. Davoudi, "Hierarchical Structure of Microgrids Control System," *IEEE Trans. Smart Grid*, vol. 3, no. 4, pp. 1963–1976, Dec. 2012.

[4] S. V. Iyer, M. N. Belur, and M. C. Chandorkar, "A Generalized Computational Method to Determine Stability of a Multi-inverter Microgrid," *IEEE Trans. Power*

Electron., vol. 25, no. 9, pp. 2420–2432, Sep. 2010.

[5] T. S. Ustun, C. Ozansoy, and A. Ustun, “Fault current coefficient and time delay assignment for microgrid protection system with central protection unit,” *IEEE Trans. Power Syst.*, vol. 28, no. 2, pp. 598–606, May 2013.

[6] T. Dragicevic, J. M. Guerrero, and J. C. Vasquez, “A Distributed Control Strategy for Coordination of an Autonomous LVDC Microgrid Based on Power-Line Signaling,” *IEEE Trans. Ind. Electron.*, vol. 61, no. 7, pp. 3313–3326, Jul. 2014.

[7] J. Rocabert, A. Luna, F. Blaabjerg, and P. Rodríguez, “Control of Power Converters in AC Microgrids,” *IEEE Trans. Power Electron.*, vol. 27, no. 11, pp. 4734–4749, Nov. 2012.

[8] F. Blaabjerg, R. Teodorescu, M. Liserre, and A. V. Timbus, “Overview of Control and Grid Synchronization for Distributed Power Generation Systems,” *IEEE Trans. Ind. Electron.*, vol. 53, no. 5, pp. 1398–1409, Oct. 2006.

[9] J. A. P. Lopes, C. L. Moreira, and A. G. Madureira, “Defining Control Strategies for MicroGrids Islanded Operation,” *IEEE Trans. Power Syst.*, vol. 21, no. 2, pp. 916–924, May 2006.

[10] “Review of primary control strategies for islanded microgrids with power-electronic interfaces,” *Renew. Sustain. Energy Rev.*, vol. 19, pp. 613–628, Mar. 2013.

[11] J. W. Simpson-Porco, Q. Shafiee, F. Dorfler, J. C. Vasquez, J. M. Guerrero, and F. Bullo, “Secondary Frequency and Voltage Control of Islanded Microgrids via Distributed Averaging,” *IEEE Trans. Ind. Electron.*, vol. 62, no. 11, pp. 7025–7038, Nov. 2015.

[12] Yun Wei Li and Ching-Nan Kao, “An Accurate Power Control Strategy for Power-Electronics-Interfaced Distributed Generation Units Operating in a Low-Voltage

Multibus Microgrid," *IEEE Trans. Power Electron.*, vol. 24, no. 12, pp. 2977–2988, Dec. 2009.

[13] J. M. Guerrero, M. Chandorkar, T.-L. Lee, and P. C. Loh, "Advanced Control Architectures for Intelligent Microgrids—Part I: Decentralized and Hierarchical Control," *IEEE Trans. Ind. Electron.*, vol. 60, no. 4, pp. 1254–1262, Apr. 2013.

[14] T. L. Vandoorn, J. C. Vasquez, J. De Kooning, J. M. Guerrero, and L. Vandevelde, "Microgrids: Hierarchical Control and an Overview of the Control and Reserve Management Strategies," *IEEE Ind. Electron. Mag.*, vol. 7, no. 4, pp. 42–55, Dec. 2013.

[15] J. Kim, J. M. Guerrero, P. Rodriguez, R. Teodorescu, and K. Nam, "Mode Adaptive Droop Control With Virtual Output Impedances for an Inverter-Based Flexible AC Microgrid," *IEEE Trans. Power Electron.*, vol. 26, no. 3, pp. 689–701, Mar. 2011.

[16] Q.-C. Zhong, "Robust Droop Controller for Accurate Proportional Load Sharing Among Inverters Operated in Parallel," *IEEE Trans. Ind. Electron.*, vol. 60, no. 4, pp. 1281–1290, Apr. 2013.

[17] A. Micallef, M. Apap, C. Spiteri-Staines, J. M. Guerrero, and J. C. Vasquez, "Reactive Power Sharing and Voltage Harmonic Distortion Compensation of Droop Controlled Single Phase Islanded Microgrids," *IEEE Trans. Smart Grid*, vol. 5, no. 3, pp. 1149–1158, May 2014.

[18] Q. Shafiee, J. M. Guerrero, and J. C. Vasquez, "Distributed Secondary Control for Islanded Microgrids; A Novel Approach," *IEEE Trans. Power Electron.*, vol. 29, no. 2, pp. 1018–1031, Feb. 2014.

[19] Q. Shafiee, C. Stefanovic, T. Dragicevic, P. Popovski, J. C. Vasquez, and J. M. Guerrero, "Robust Networked Control Scheme for Distributed Secondary Control

of Islanded Microgrids," *IEEE Trans. Ind. Electron.*, vol. 61, no. 10, pp. 5363–5374, Oct. 2014.

2

Reactive Power Sharing in Microgrid Using Virtual Voltage

Abstract: In this chapter, a reactive power control strategy for a low-voltage micro-network is proposed, where the unequal impedance between the distributed generation (DG) units and the location of the load in the microgrid (MG) make not practical the conventional frequency and voltage droop methods. This droop control strategy has been widely used in MGs. Although the shared active power is accurate, the performance of the shared reactive power is not good. This new control strategy proposes the use of virtual voltage to improve the accuracy of reactive power sharing. In the proposed controller, the exchange of reactive power is made through the virtual voltage, whose coefficient is established in relation to the distribution of reactive power; the proposed controller uses only local information. Accuracy in the reactive power sharing and the principle of virtual voltage design are analyzed and its stability is tested through small signal analysis. The proposed control strategy has been tested in simulation through MATLAB-Simulink software.

Keywords: reactive power sharing; microgrid; virtual voltage; power transfer; voltage control.

2.1 Introduction

Microgrids (MGs) help relieve the stress of the main transmission systems, reduce electrical losses, and improve power quality of the systems as it is very effective to integrate renewable energy sources[1]. An MG can combine several renewable energy units, loads and energy storage system [2]. Compared to the conventional distribution system, an MG can be operated connected to the power grid or island mode [3]. This type of features is what makes it very desirable, and it makes a big difference from conventional energy systems.

The islanded mode of MGs brings new challenges because the dynamics are no longer dominated by the main power grid. The island mode requires the implementation of an accurate control and management mechanism to maintain the balance between demand and supply. When the MG operates in autonomous mode, the shunt inverters are enabled by the primary control to achieve a power distribution and the secondary control that is responsible for the deviations. Often the main task of the different methods of secondary control is to calculate a corrective term considering the frequency or voltage error.

Sharing reactive power between generators in high voltage networks is not usually a major concern due to capacitive compensation between loads and transmission lines. However, in low voltage MGs, the low capacity of reagent supply from generation sources and compensators, and small distances between units, does not allow an exact distribution of reactive power to avoid overloads [4], because in a low voltage MG the impedance of the distribution feeder is mainly resistive [5], in this case the droop control method is subject to poor transient stability [5], due to the poor coupling of reactive power between DG units when no additional inductance is present [5]. Line impedances and DG output impedances significantly affect the sharing of reactive power during the operating mode connected to the network and during the island mode, due to voltage drops [5].

Consequently, the concepts of droop control have been widely adopted to provide decentralized power, without relying on communications [6]. Although the frequency droop control technique can be used to achieve accurate real power distribution, voltage droop control commonly results in poor reactive power distribution [7]. This is

due to the lack of coincidence in the voltage drops across the DG, which is induced by the mismatch in the impedance feeder and/or the differences in the powers of the units [8].

At present, the voltage controllers in the MGs are unable to share the reactive power demand among even identical inverters operating in parallel [9]. Some researchers have previously worked on this issue, as in [10], which propose an alternative controller for reactive power sharing between parallel inverters with nominal voltages. The method requires that each unit have a common load voltage measurement, which limits its applicability in more complex MG scenarios with multiple loads.

In [11], the method improves the distribution of reactive power by changing the voltage bias based on conventional slope control, which is activated by a sequence of synchronization events through the communication network. In [12], it is illustrated the control strategy to improve the distribution of reactive power and decrease in a single-phase MG on the island. In [13], a distributed secondary control strategy is proposed, in which each generator uses the measurements of other DGs at each sample time for the control of frequency, voltage and reactive power. In [14], the restoration of frequency and voltage is presented as the secondary control in a hierarchical control of the MG. In these methods the nominal value of the frequency and voltage deviation is determined in the central control and then transmitted to the other DGs of the MG to restore them. Therefore, MG control is assumed centralized in this method.

In [15], a resistive capacitive output impedance (RC-Inverter) is proposed. This equivalent output impedance of the RC inverter is designed by the introduction of capacitive-resistive virtual impedances. This usually provides rapid reactive power for

low MGs voltages and maintains system voltage stability. However, the method works by estimating the voltage drops with the virtual impedance, so the error in the estimate makes the method not work well and accurately. In [16] a voltage source inverter based on servo system is proposed, which is designed as a reference tracker. A new control is proposed to determine the set point of reactive power in each inverter to make its contribution in the distribution of reactive power; but it presents the problem of communication, which makes it very impractical when implemented in industrial cases.

In [17], a new decentralized model is proposed for distribution of reactive power and frequency restoration in an island system. The proposed method does not need communication link between the DG, synchronization between each DG is achieved by detecting load change with the Wavelet transform; but this model is very flawed, since it uses two compensators which act one after the other, after a certain time when a load change occurs a condition is necessary for the second compensator to act and it is necessary that at that time there is no another load change, which would be obsolete in the face of major changes as in real systems. In [18], a novel droop control method for voltage and frequency in autonomous MGs is proposed, by incorporating predictive mechanisms in the DG. However, this method fails to share reactive power between the different DGs.

Therefore, the references consulted show that the previous work has focused on the control of active and reactive power in MGs in island mode and how the virtual voltage has not been considered based on the variable load voltage that is connect to the MG as part of the solution. Therefore, the objective of this work is to show the reactive power sharing in an MG using the concept of virtual voltage and how it improves voltage regulation better than the droop control. Therefore, the contributions in this

article are: the virtual voltage variables that are calculated for each inverter based on the RMS value of the node voltage where the loads are connected. The exchange of reactive power is achieved in several nodes of a network, once there are some variations in loads.

In section 2 the conventional control method and the new control strategy are explained. In section 3, the small signal stability analysis is made to the strategy and in section 4 the results of the Simulations performed in software are shown. MATLAB-Simulink, and in Section 5 the conclusions are presented.

2.2 Materials and Methods

The P-ω and Q-V droop controls have been used successfully in MGs [19]. This method is simple and can perform the 'plug-and-play' feature without communication. Fig. 1 shows the detailed configuration of a DG unit using the proposed control strategy. The P - ω droop control is adopted to regulate the frequency to achieve an accurate sharing of active power, the voltage control loop uses a PI controller to track the voltage reference value, given by the virtual voltage controller, and the current controller loop uses a P controller to adjust the inductance low pass filter current. In the conventional Q-V droop control strategy, the value of the reactive power is fed back to adjust the magnitude of the voltage and the virtual impedance is also generally used to decouple the control of the active power and reactive power in an MG with complex line impedance. It can be seen in Fig. 1 that we add a virtual impedance in proportion to the virtual RMS voltage of the load node, as follows:

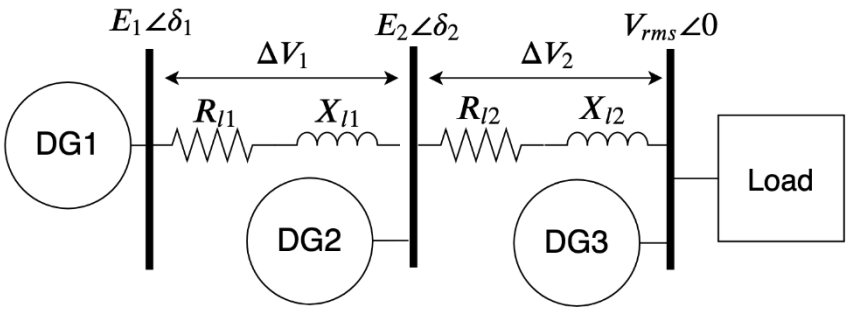

Figure 2.1. Simplified diagram of the MG

Consider a case in Fig. 1, we can calculate active and reactive power flowing to the load from DGs. The active power and the reactive power transferred from the inverter to the load is given by equations (1) and (2), these equations include the active and reactive power that is lost through the inductive reactance associated with the transmission lines.

$$P = \frac{1}{R^2+X^2}(RE^2 - REV\cos\delta + XEV\sin\delta) \quad (1)$$

$$Q = \frac{1}{R^2+X^2}(XE^2 - XEV\cos\delta - REV\sin\delta) \quad (2)$$

The term P is active power, Q is reactive power, E is the voltage at the terminals of the DG, R is the resistive part of the line impedance, X is the inductance of the line impedance, and V is the voltage in the load node.

2.3. Small signal stability analysis

The controlled system has been widely discussed [20]. In this section, a small signal model is derived for the proposed controller, in which the virtual voltage that is based on the RMS voltage of the load node V_{rms} It is considered as the variable controller.

By considering small disturbances around the equilibrium state defined by ($\Delta\delta e, E, V$), the above equations can be linearized around this point, then we have:

$$\Delta p = \left(\frac{\partial p}{\partial E_V}\right)\Delta E_V(s) + \left(\frac{\partial p}{\partial \delta}\right)\Delta\delta(s)$$

$$\Delta p = k_{pe}\Delta E_v(s) + k_{ps}\Delta\delta(s) \quad (3)$$

$$\Delta Q_{(s)} = \left(\frac{\partial Q}{\partial E_V}\right)\Delta X_V(s) + \left(\frac{\partial Q}{\partial \delta}\right)\Delta\delta(s)$$

$$\Delta Q_{(s)} = K_{qe}\Delta E_V(s) + k_{q\delta}\Delta\delta(s) \quad (4)$$

Where Δ indicates the small signal deviation of the variable around the equilibrium point.

$$\Delta W = -k_p\Delta p \quad (5)$$

$$\Delta E = K\Delta V_{rms} \quad (6)$$

Where k_{pe}, k_{ps}, K_{qe} , k_{qs} are calculated around the equilibrium point, which represents the sensitivity of the power flow to the virtual voltage and voltage angle regulation. Making the partial derivative of the active power based on the virtual voltage, we obtain:

$$k_{pe} = \left(\frac{\partial p}{\partial E_V}\right) = \frac{(2RE_V - RV\cos\delta + XV\sin\delta)}{(R^2 + X^2)} \quad (7)$$

Now the partial derivative of the active power with respect to the angle is obtained.

$$k_{p\delta} = \left(\frac{\partial p}{\partial \delta}\right) = \frac{1}{R^2 + X^2}(RE_V V\sin\delta + \mathrm{X}E_V \mathrm{V}\cos\delta) \quad (8)$$

From the partial derivative of the reactive power with respect to the virtual impedance, we obtain.

$$k_{qe} = \left(\frac{\partial Q}{\partial E_V}\right) = \frac{(2XE_V - RV\sin\delta - XV\cos\delta)}{(R^2 + X^2)} \quad (9)$$

From the partial derivative of the reactive power with respect to the virtual impedance, we obtain.

$$k_{q\delta} = \left(\frac{\partial Q}{\partial \delta}\right) = \frac{1}{R^2 + X^2}(XEV\sin\delta - REV\cos\delta) \quad (10)$$

Considering that the real power and the reactive power are normally measured using a first-order low-pass filter, the cut-off frequency W_f of the active power droop controller and the reactive power controller can be linearized around the same point.

$$\Delta P_{med} = \frac{W_f}{S + W_f}\Delta P(s) \quad (11)$$

$$\Delta Q_{med} = \frac{W_f}{S + W_f}\Delta Q(s) \quad (12)$$

Therefore, it follows from the above equations and equation (5)

$$\Delta W(S) = \frac{-K_p W_f}{S + W_f}\Delta P(s) \quad (13)$$

$$\Delta W(S) = \frac{-K_m W_f}{S+W_f}\ (k_{pe}\Delta E_v(s) + k_{ps}\Delta\delta(s))\ \ (14)$$

$$\Delta E(S) = \frac{-K_v W_f}{S+W_f}\ \Delta V_{rms}(S)\ \ (15)$$

Replacing $\Delta E(S)$ of equation (15) in equation (14), we get:

$$\Delta W(S) = \frac{-K_p W_f}{S+W_f}\left[k_{pe}\left(\frac{-K_v W_f}{S+W_f}\ \Delta V_{rms}(S)\right)\ +\ k_{ps}\Delta\delta(s)\right] \quad (16)$$

Using Equations (3), (5) and (6), we can express $\Delta V_{rms}(S)$ as follows:

$$\Delta V_{rms}(S) = \left[\frac{\Delta w(s) - k_p k_{pd}\Delta\delta(s)}{k_p k_{pe} k_v}\right] \qquad (17)$$

Replacing the value of $\Delta V_{rms}(S)$ in equation (16) and reorganizing, we have

$$\Delta w(s) = \frac{-K_p w_f}{S+w_f}\left[k_{pe}\left(\frac{-K_v W_f}{S+W_f}\left[\frac{\Delta w(s) - k_p k_{pd}\Delta\delta(s)}{k_p k_{pe} k_v}\right]\right) +\ k_{ps}\Delta\delta(s)\right] (18)$$

Solving the previous equation we obtain.

$$\Delta W(s) = \frac{-k_p W_f}{S+W_f}\left[\frac{S\Delta\delta(S)k_{p\delta}k_p k_{pe}k_v + \Delta\delta(S)k_{p\delta}k_p k_{pe}k_v w_f - k_{pe}k_v w_f \Delta w(S) +\ \Delta\delta(S)k_{p\delta}k_p k_{pe}k_v w_f}{S k_p k_{pe} k_v + w_f k_p k_{pe} k_v}\right]$$

(19)

Solving equation (19) we get.

$$\Delta W(S) = \frac{-S\Delta\delta(S){k_p}^2 w_f k_{p\delta} k_v k_{pe} - 2\,\Delta\delta(S){k_p}^2 {w_f}^2 k_{p\delta} k_v k_{pe} + k_p k_{pe} k_v {w_f}^2 \Delta w(S)}{S^2 k_p k_{pe} k_v + S w_f k_p k_{pe} k_v + S w_f k_p k_{pe} k_v + {w_f}^2 k_p k_{pe} k_v} \quad (20)$$

$$\Delta W(S) = S\Delta\delta(S) \quad (21)$$

By replacing the equation (21) in equation (20) we obtain the following equation

$$S\Delta\delta(S) = \frac{-S\Delta\delta(S){k_p}^2 w_f k_{p\delta} k_v k_{pe} - 2\,\Delta\delta(S){k_p}^2 {w_f}^2 k_{p\delta} k_v k_{pe} + S\Delta\delta(S) k_p k_{pe} k_v {w_f}^2}{S^2 k_p k_{pe} k_v + S w_f k_p k_{pe} k_v + S w_f k_p k_{pe} k_v + {w_f}^2 k_p k_{pe} k_v} \quad (22)$$

Solving the previous equation, the next expression is obtained:

$$S^3\Delta\delta(S)\left(k_p k_{pe} k_v\right) + S^2\Delta\delta(S)(2 w_f k_p k_{pe} k_v) + S\Delta\delta(S)\left({k_p}^2 k_{p\delta} w_f k_{pe} k_v\right) + \Delta\delta(S)\left(2\,{w_f}^2 {k_p}^2 k_{p\delta} k_{pe} k_v\right) = 0 \quad (23)$$

$$aS^3\Delta\delta(S) + bS^2\Delta\delta(S) + cS\Delta\delta(S) + d\Delta\delta(S) = 0 \quad (24)$$

Where the variable a, b, c and d from the previous equation are:

a = $k_p k_{pe} k_v$

b = $2 w_f k_p k_{pe} k_v$

c = ${k_p}^2 k_{p\delta} w_f k_{pe} k_v$

d = $2\,{w_f}^2 {k_p}^2 k_{p\delta} k_{pe} k_v$

The homogeneous equation (24) describes the free movement of the system for small disturbances around the equilibrium point (δ, E, V). Then, the system response can be analyzed based on the previous characteristic equation.

2.4. Results and Analysis

This section shows the results related to the inverter when considering the proposed control strategy, related to an RMS virtual voltage in the input of the voltage control inverter. This strategy allows to share the reactive power and regulate the voltage in the node where the loads are connected. The simulations were carried out considering a case of rural distribution network where the loads are connected for a period of time.

2.4.1 Active power

The MG used for this investigation is shown in Figure 1. This network is made up of three DGs that deliver active and reactive power to the electrical loads. The load node is made up of five electrical loads related to the domestic consumption of communities that are connected over time. The active power delivered by the DGs must be delivered considering the impedances of the lines, to reach the different loads. In addition, voltage regulation is achieved through the use of the inverter with the RMS virtual voltage control strategy that is changing based on the variable loads that are connected.

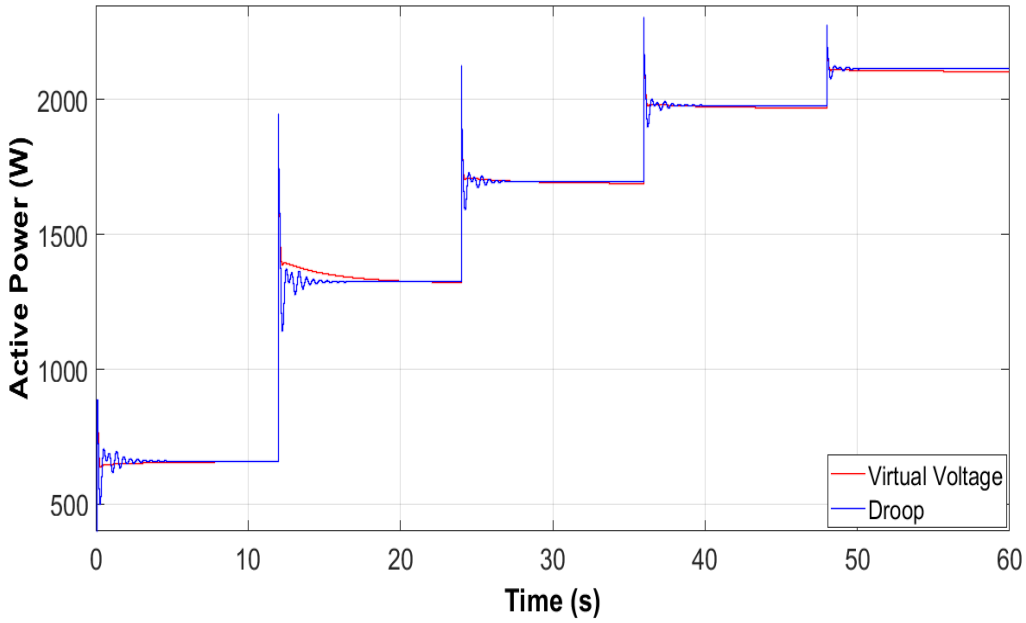
Active Power (W)
2000
1500
1000
500
0
10
20
30
40
50
60
Time (s)
Virtual Voltage
Droop

(a)

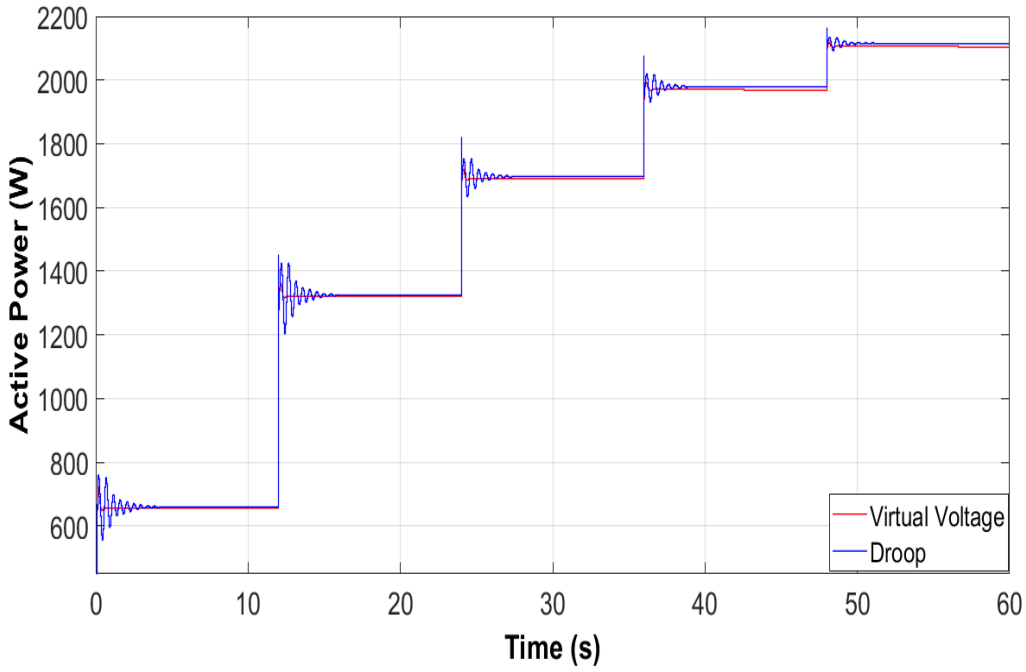
Active Power (W)
2200
2000
1800
1600
1400
1200
1000
800
600
0
10
20
30
40
50
60
Time (s)
Virtual Voltage
Droop

(b)

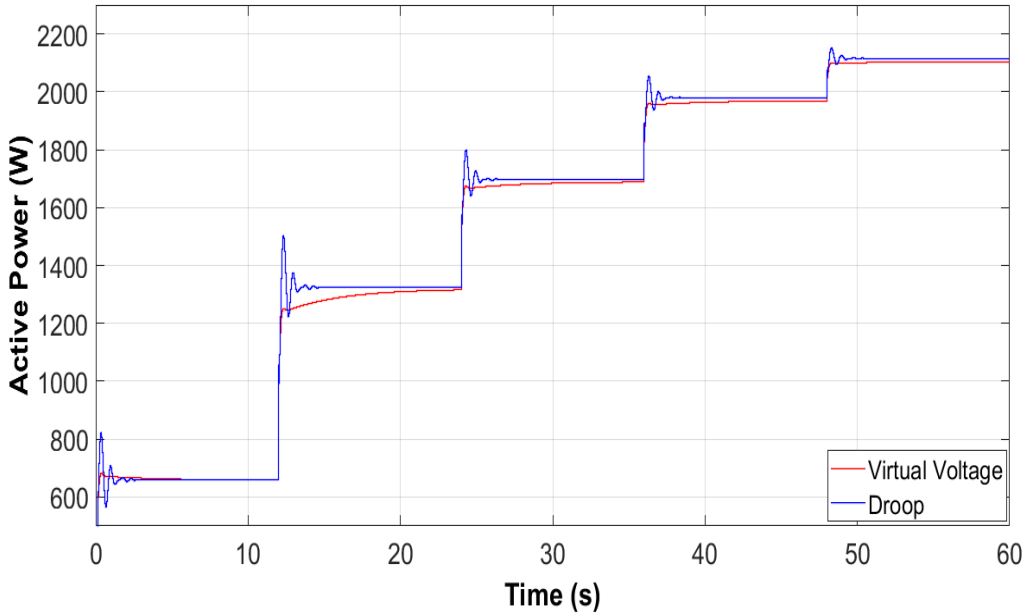

(c)

Figure 2. Active power obtained with the virtual voltage and droop control strategies

Figures 2 (a), 2 (b) and 2 (c) show the active power delivered by each DG, based on the strategy used, which are the strategy of droop control vs the virtual voltage RMS. The graphs show the comparison of the two control strategies and their behavior in the case of a load change in the MG node. Which are connected at different times. The active powers increase depending on the amount of electric load that are connected to the node.

In the previous graphs, we managed to observe the behavior of the controller according to the connection and disconnection of different electrical loads during the simulation time. We can observe how the new proposed controller responds faster and better than the droop controller. It can be seen that both controllers manage to share the active power precisely, according to the connection and disconnection of different loads. We

can also detail that the proposed control strategy manages to stabilize the active power much faster than the fixed value strategy.

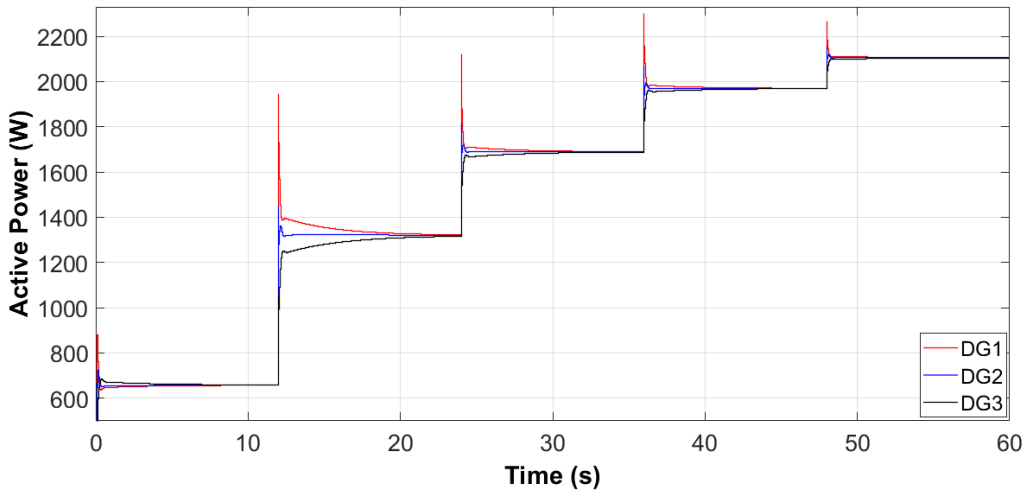

(a)

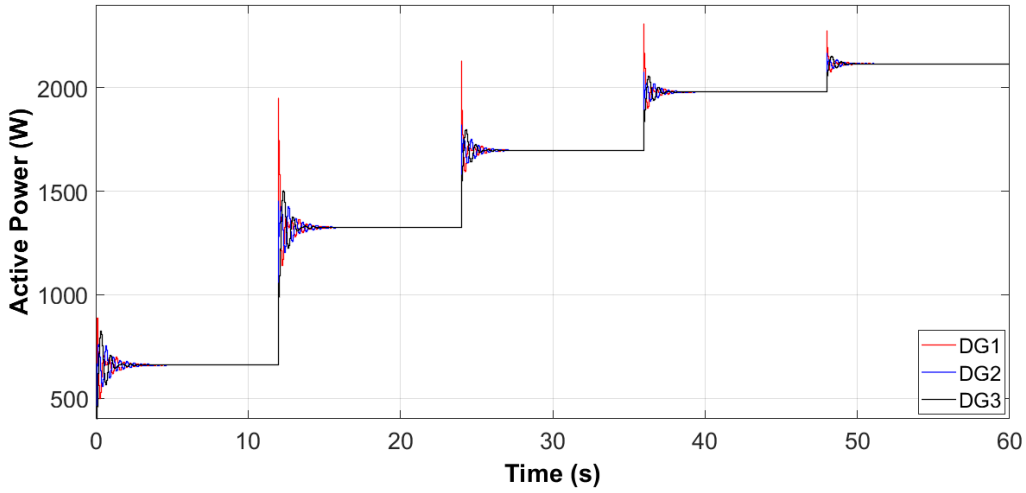

(b)

Figure 3. Active power of DGs obtained with the virtual voltage and droop control strategies

In the previous figures we can see how generators DG1, DG2 and DG3 share the active power, with two different controllers in their inverters, graph a) shows the proposed control strategy of the RMS voltage and the graph b) the droop control strategy.

We see that these strategies manage to share the active power precisely in the face of different load changes. So during the first 12 seconds we observe the active power consumption of approximately 2100 W (watt), as a result of which a load of (10 + J0.05) Ω is connected. In the 12-second period a load of (15 + J0.05) Ω is connected, in this period the active power consumption of the load in the node is increased based on the consumption of the previous period, and it is possible to see that both control strategies respond very well to the connection of the new load, only that the proposed strategy manages to stabilize at a fixed value the active power much faster than the droop.
In the 24-second period a load of (20 + J0.08) Ω is connected to the MG node, in this period an increase in power consumption is generated, but the control strategy acts immediately and recover the active power of the load at a stable value.

In the course of 36 seconds a load (25 + J0.10) Ω is connected, in this period a considerable increase in the active power consumption in the node is generated, but it is possible to see how the control strategy Proposal responds quickly and manages to stabilize the power value at a fixed value.

In the course of 48 seconds, a load of (50 + J0.20) Ω is connected, which causes the active power supplied by the three generators to increase based on the previous period. At this point we observe how both controllers respond exceptionally to the load change.

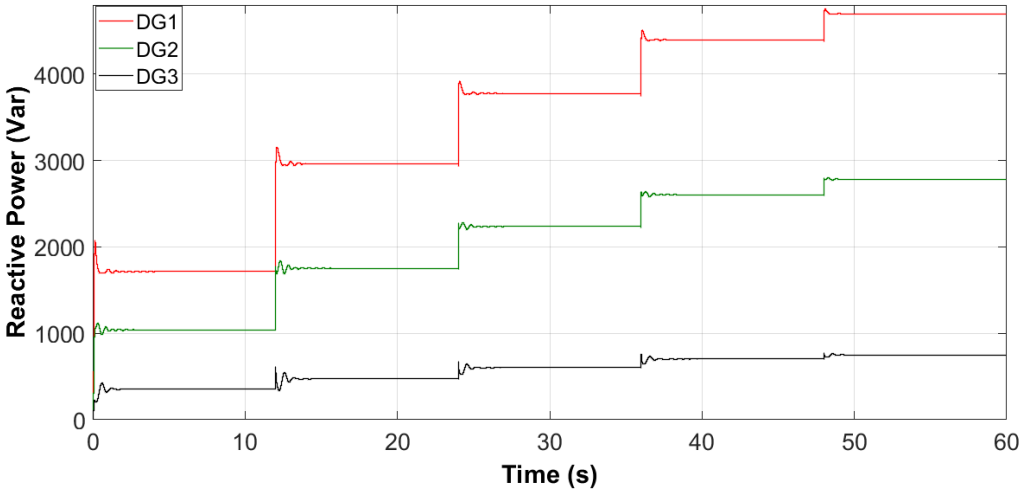

(a)

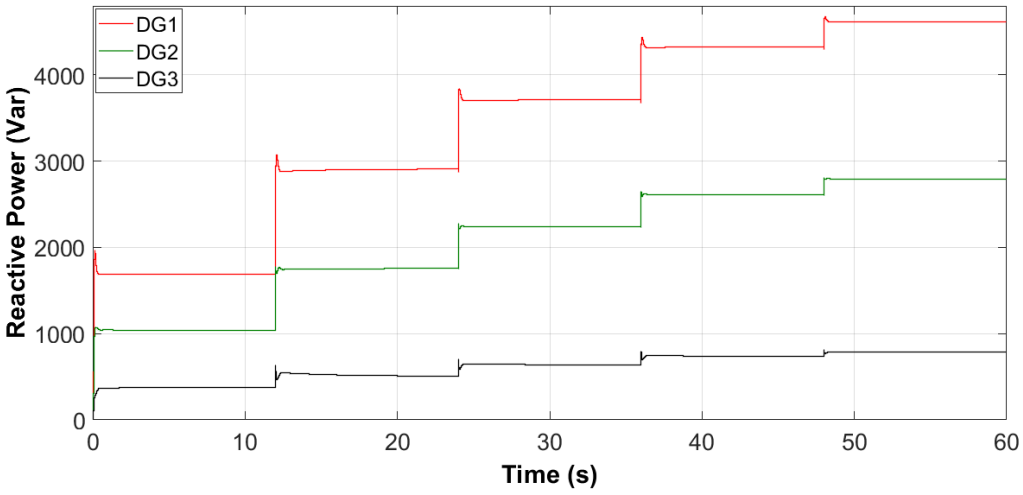

(b)

Figure 4. Reactive power of DGs obtained with the virtual voltage and droop control strategies

In the previous figures we observe how generators DG1, DG2 and DG3 deliver the reactive power to the MG. Besides, two different control strategies in their respective inverters are presented in these figures a) the proposed RMS voltage control strategy and b) the droop control strategy.

We see that only the proposed control strategy manages to share the reactive power quickly and it is stable for different load changes and this is not achieved by the droop control. During the first 12 seconds we can see how a load of (10 + J0.05) Ω is connected in this period of time and the proposed control strategy responds very well to the connection of the load, delivering a reactive power in proportion to the distance. In the period of 12 seconds to 24 seconds a load of (15 + J0.05) Ω is connected, and the reactive power consumption of the load in the node is increased based on the consumption of the previous period. In this period of time DG1, DG2 and DG3 deliver different reactive powers that depend on the distance from the load to each generator.

A load of (20 + J0.08) Ω is connected to the MG node in the period of 24 seconds to 36 seconds. In this period of time it is observed that DG1, DG2 and DG3 increase the reactive power delivered to the MG in different proportions, as a result of the new load on the MG.

Over a period of 36 seconds to 48 seconds a load (25 + J0.10) Ω is connected, which generates an increase in the consumption of reactive power in the MG, showing that the proposed control strategy responds quickly and manages to stabilize the power at a fixed value.

In the course of 48 seconds the load (50 + J0.20) Ω is connected, which causes the reactive power supplied by the three generators to increase based on the previous period. In this period of 48 to 60 seconds, we can observe how the proposed control strategy responds much faster and manages to stabilize at a fixed value much faster than the droop control strategy.

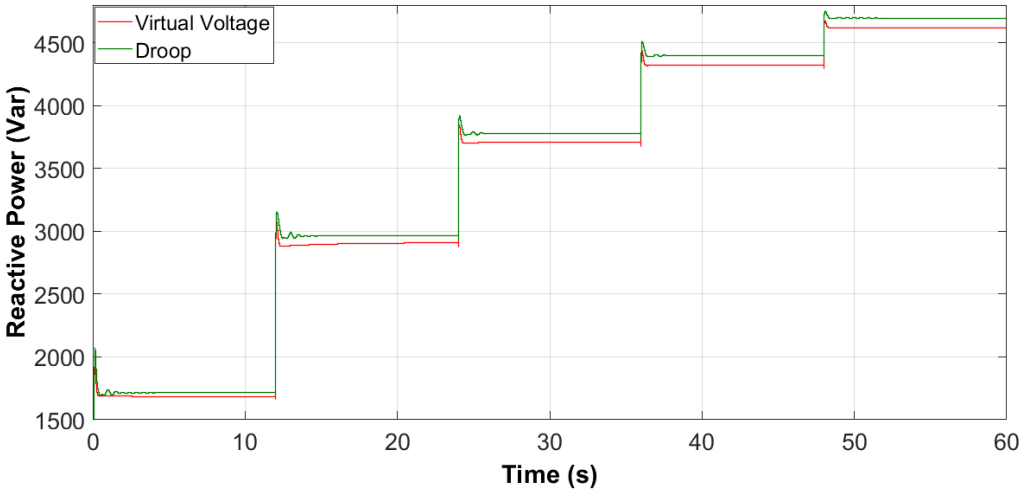
Virtual Voltage
Droop
Reactive Power (Var)
4500
4000
3500
3000
2500
2000
1500
0
10
20
30
40
50
60
Time (s)

(a)

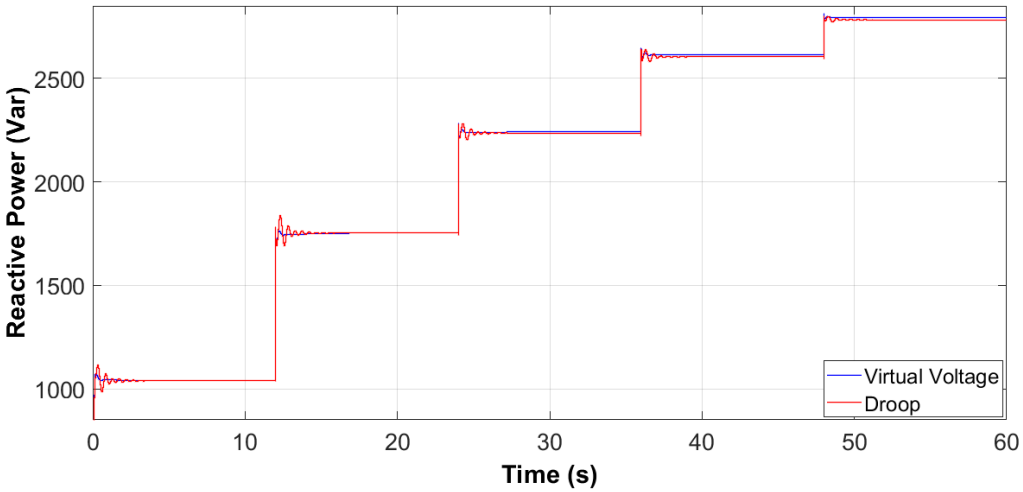
Reactive Power (Var)
2500
2000
1500
1000
0
10
20
30
40
50
60
Time (s)
Virtual Voltage
Droop

(b)

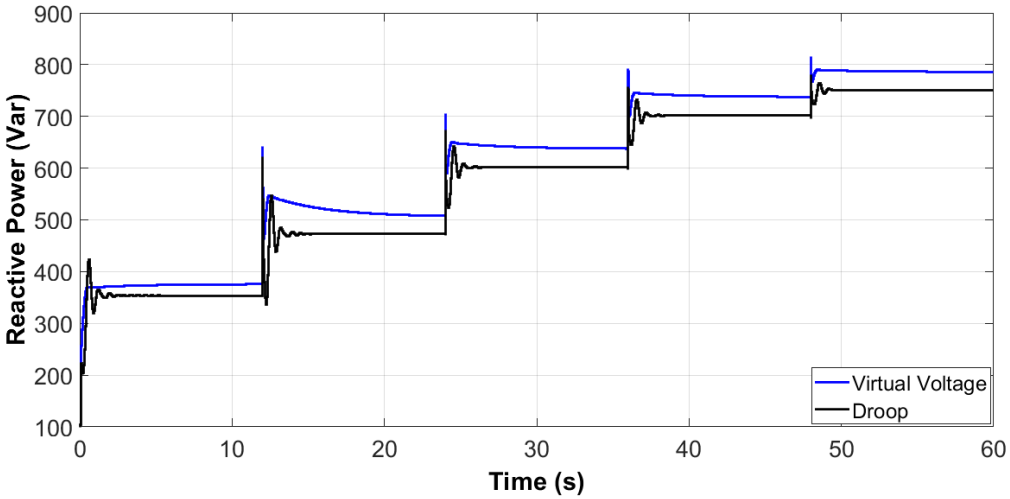

(c)

Figure 5. Reactive power of DGs obtained with the virtual voltage and droop control strategies

In Figures 5a, 5b and 5c, we observe the behavior of the three generators that conform the MG with the proposed controller and the droop controller, when different electrical loads are connected. Over the course of the simulation, we can see that the proposed control responds faster and stabilizes in less time and better than the droop control.

Figure 6 shows the behavior of how the proposed and the droop controls response to the connection of different electrical loads over a period of time. We can observe how the new proposed control responds faster and better than the droop control, to different load changes. The results showed that the proposed control strategy allows the frequency of the three generators to stabilize at a single value, a few seconds after the load changes. In addition, the more different the change in load on the MG connection, the more abrupt is the change in the frequency value. However, no matter how high the change in the variable load (connection of different electrical loads), the controller

maintains the frequency close to 50 Hz, which is the desired value. It is observed that the proposed controller keeps it closer to that value, than the droop controller.

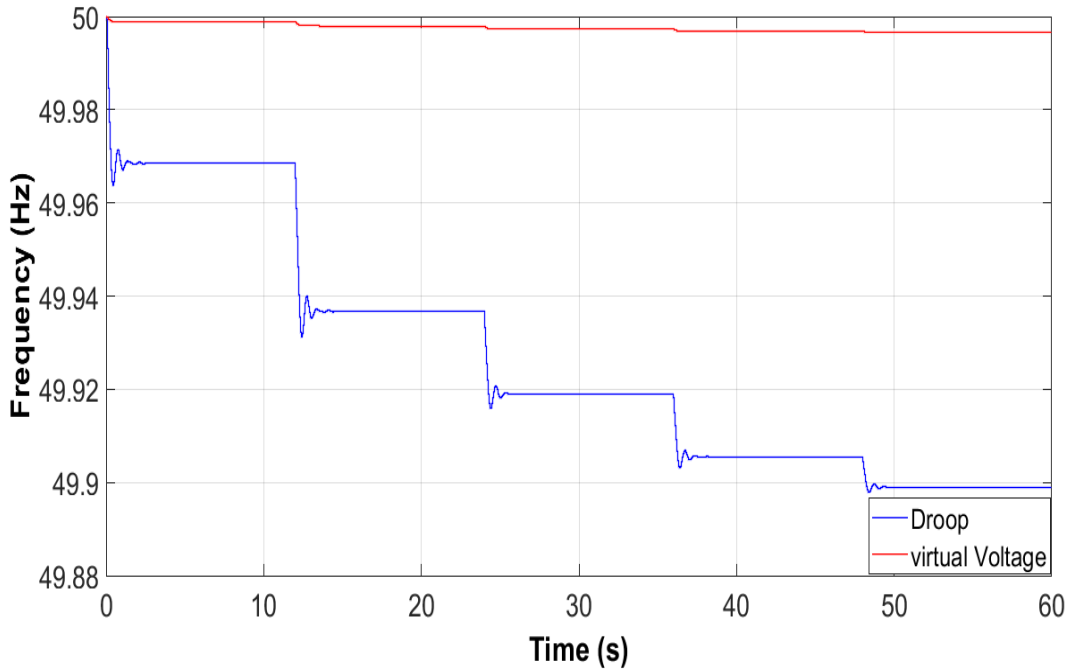

Figure 6. Frequency with the virtual voltage and droop control strategies

Figure 7 shows the behavior of the RMS voltage at the node where the five electrical loads of the MG are connected. The figure shows the RMS voltage of the proposed blue control strategy and the red droop control strategy. These results show that when the connection of the second load is made, the node voltage tends to drop sharply, but immediately the control strategy recovers the voltage to a close original value, Therefore, the proposed control strategy with a voltage virtual RMS, maintains a stable voltage value during all periods in which the electrical loads are connected and disconnected. However, when the droop control strategy is used, the voltage drops below the value obtained with the proposed control strategy, which is why we can conclude according to what has been observed as the proposed new control strategy responds faster and better than the droop controller.

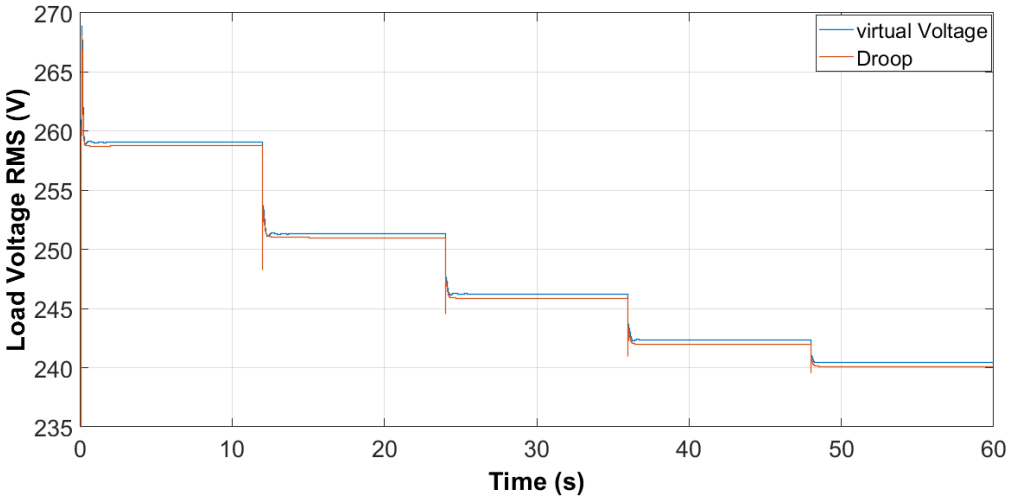

Figure 7. Load voltage with the virtual voltage and droop control strategies

Figures 8 (a), 8 (b), 8 (c) and 8 (d) show the active and reactive power in the MG node , when multiple loads connect and disconnect from the network. The active and reactive powers increase depending on the amount of loads that are connected to the node. We can observe that the active power and reactive power consumed by the loads is the same, independent of the control strategy used to regulate and keep the voltage stable in the node where the loads are connected and disconnected.

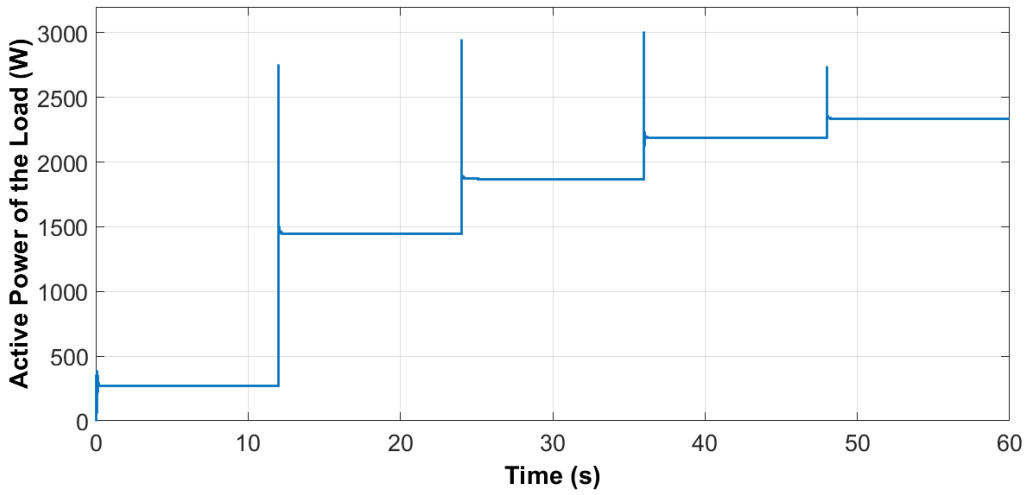

(a)

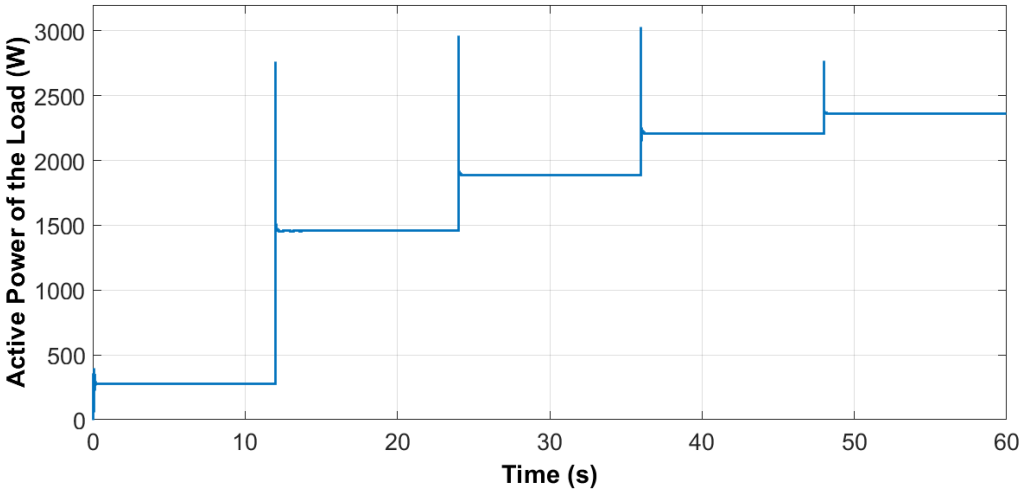
Active Power of the Load (W)
3000
2500
2000
1500
1000
500
0
0
10
20
30
40
50
60
Time (s)

(b)

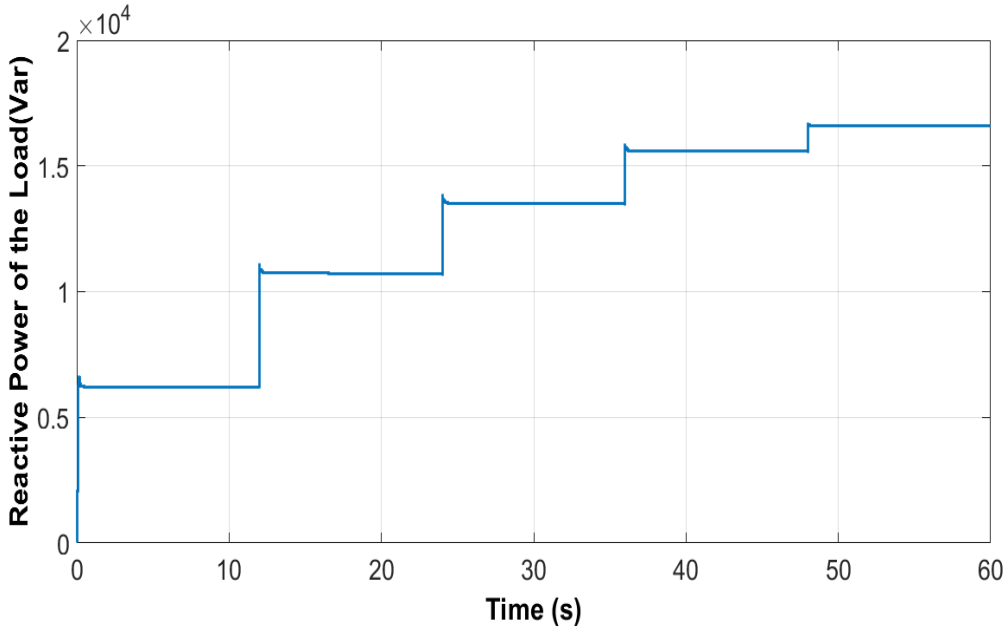
×10^4
2
1.5
1
0.5
0
Reactive Power of the Load(Var)
0
10
20
30
40
50
60
Time (s)

(c)

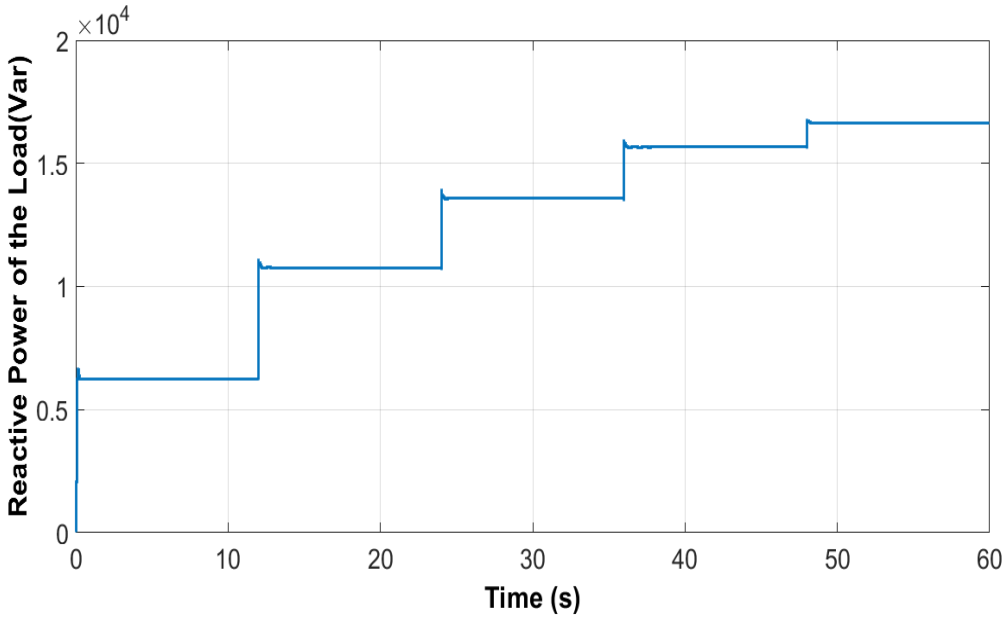

(d)

Figure 8. Active and reactive power in the MG node

2.5 Conclusión

This document presented a new control strategy using a virtual RMS voltage to share the reactive power between different generators distributed in an MG, when electrical loads are connected at different periods of time in a node of the MG. Results were obtained for a system with three DGs, with which it was possible to share reactive power between the DGs of the MG according to the different load changes in a time period. Therefore, at each moment the active power and the reactive power supplied by the DG increase, and this control strategy based on an adaptive virtual RMS voltage related to the RMS voltage of the load node works successfully.

The proposed control strategy effectively regulates the frequency close to 50 Hz and also maintains the active and reactive power to balance the MG. This strategy is useful for the new MG to adapt and share active and reactive power.

2.6 References

[1] R.H.Lasseter, “MicroGrids,” pp. 305–308, 2002.

[2] F. Katiraei and M. R. Iravani, “Power Management Strategies for a Microgrid With Multiple Distributed Generation Units,” *IEEE Trans. Power Syst.*, vol. 21, no. 4, pp. 1821–1831, Nov. 2006.

[3] N. Pogaku, M. Prodanovic, and T. C. Green, “Modeling, Analysis and Testing of Autonomous Operation of an Inverter-Based Microgrid,” *IEEE Trans. Power Electron.*, vol. 22, no. 2, pp. 613–625, Mar. 2007.

[4] J. W. Simpson-Porco, Q. Shafiee, F. Dorfler, J. C. Vasquez, J. M. Guerrero, and F. Bullo, “Secondary Frequency and Voltage Control of Islanded Microgrids via Distributed Averaging,” *IEEE Trans. Ind. Electron.*, vol. 62, no. 11, pp. 7025–7038, Nov. 2015.

[5] Yun Wei Li and Ching-Nan Kao, “An Accurate Power Control Strategy for Power-Electronics-Interfaced Distributed Generation Units Operating in a Low-Voltage Multibus Microgrid,” *IEEE Trans. Power Electron.*, vol. 24, no. 12, pp. 2977–2988, Dec. 2009.

[6] J. Rocabert, A. Luna, F. Blaabjerg, and P. Rodríguez, “Control of Power Converters in AC Microgrids,” *IEEE Trans. Power Electron.*, vol. 27, no. 11, pp. 4734–4749, Nov. 2012.

[7] T. L. Vandoorn, J. C. Vasquez, J. De Kooning, J. M. Guerrero, and L. Vandevelde, “Microgrids: Hierarchical Control and an Overview of the Control and Reserve Management Strategies,” *IEEE Ind. Electron. Mag.*, vol. 7, no. 4, pp. 42–55, Dec. 2013.

[8] J. Kim, J. M. Guerrero, P. Rodriguez, R. Teodorescu, and K. Nam, “Mode Adaptive Droop Control With Virtual Output Impedances for an Inverter-Based Flexible AC Microgrid,” *IEEE Trans. Power Electron.*, vol. 26, no. 3, pp. 689–701, Mar. 2011.

[9] J. A. P. Lopes, C. L. Moreira, and A. G. Madureira, “Defining Control Strategies for MicroGrids Islanded Operation,” *IEEE Trans. Power Syst.*, vol. 21, no. 2, pp. 916–924, May 2006.

[10] Q.-C. Zhong, “Robust Droop Controller for Accurate Proportional Load Sharing Among Inverters Operated in Parallel,” *IEEE Trans. Ind. Electron.*, vol. 60, no. 4, pp. 1281–1290, Apr. 2013.

[11] H. Han, Y. Liu, Y. Sun, M. Su, and J. M. Guerrero, “An Improved Droop Control Strategy for Reactive Power Sharing in Islanded Microgrid,” *IEEE Trans. Power Electron.*, vol. 30, no. 6, pp. 3133–3141, Jun. 2015.

[12] A. Micallef, M. Apap, C. Spiteri-Staines, J. M. Guerrero, and J. C. Vasquez, “Reactive Power Sharing and Voltage Harmonic Distortion Compensation of Droop Controlled Single Phase Islanded Microgrids,” *IEEE Trans. Smart Grid*, vol. 5, no. 3, pp. 1149–1158, May 2014.

[13] Q. Shafiee, J. M. Guerrero, and J. C. Vasquez, “Distributed Secondary Control for Islanded Microgrids—A Novel Approach,” *IEEE Trans. Power Electron.*, vol. 29, no. 2, pp. 1018–1031, Feb. 2014.

[14] J. M. Guerrero, J. C. Vasquez, J. Matas, L. G. de Vicuna, and M. Castilla, “Hierarchical Control of Droop-Controlled AC and DC Microgrids—A General Approach Toward Standardization,” *IEEE Trans. Ind. Electron.*, vol. 58, no. 1,

pp. 158–172, Jan. 2011.

[15] Y. Chen, A. Luo, J. Zhou, L. Bai, and C. Tu, “Rapid reactive power control method for parallel inverters using resistive-capacitive output impedance,” in *2013 1st International Future Energy Electronics Conference (IFEEC)*, 2013, pp. 98–102.

[16] M. Eskandari, L. Li, and M. H. Moradi, “Decentralized Optimal Servo Control System for Implementing Instantaneous Reactive Power Sharing in Microgrids,” *IEEE Trans. Sustain. Energy*, pp. 1–1, 2017.

[17] M. Kosari and S. H. Hosseinian, “Decentralized Reactive Power Sharing and Frequency Restoration in Islanded Microgrid,” *IEEE Trans. Power Syst.*, vol. 32, no. 4, pp. 2901–2912, Jul. 2017.

[18] G. Lou, W. Gu, Y. Xu, M. Cheng, and W. Liu, “Distributed MPC-Based Secondary Voltage Control Scheme for Autonomous Droop-Controlled Microgrids,” *IEEE Trans. Sustain. Energy*, vol. 8, no. 2, pp. 792–804, Apr. 2017.

[19] K. De Brabandere, B. Bolsens, J. Van den Keybus, A. Woyte, J. Driesen, and R. Belmans, “A Voltage and Frequency Droop Control Method for Parallel Inverters,” *IEEE Trans. Power Electron.*, vol. 22, no. 4, pp. 1107–1115, Jul. 2007.

[20] E. A. A. Coelho, P. C. Cortizo, and P. F. D. Garcia, “Small signal stability for single phase inverter connected to stiff AC system,” in *Conference Record of the 1999 IEEE Industry Applications Conference. Thirty-Forth IAS Annual Meeting (Cat. No.99CH36370)*, vol. 4, pp. 2180–2187.

3

Control strategy to regulate voltage and share reactive power using variable virtual impedance for a microgrid

Abstract: This paper presents a control strategy to regulate voltage and share reactive power from distributed generators in a microgrid when electric vehicles (EVs) are connected and disconnected at different nodes and times. The control strategy considers fixed and variable virtual impedances created in the microgrid (MG) when loads change (EVs are connected or disconnected). Fixed virtual impedance is related to the distance from each house to the power inverter and is used as an input of the primary control. Besides, variable virtual impedance is associated with the distance from each EV to the power inverter and is also used as an input of the primary control. Thus, the control of the inverter seeks to regulate the voltage where the EVs create variations in the network. The results show that the control strategy regulates well the voltage of different nodes and the reactive power is distributed to renewable generators based on the distance from the loads to the inverters. By considering fixed and variable virtual impedances in the primary control, voltage can be regulated, assuming various consumptions of EVs in the network. This result is promising for reactive power control and sharing for each distributed generator (DG) in a microgrid where a great number of EVs affect the operation.

Keywords: reactive power sharing; microgrid; virtual impedance; power transfer; voltage control.

3.1 Introduction

Private vehicles are responsible for most of the total transport energy consumption and associated pollutants [1]. Therefore, electric vehicles (EVs) provide a better future by not emitting carbon dioxide (CO2), carbon monoxide (CO), nitrogen oxides (NOx), unburned hydrocarbons (UHCs), lead compounds, sulfur dioxide, and solid particles to the environment, making it a very promising option for transportation [2]. However, the

use of EVs requires the periodic charging of batteries and autonomy must be provided by considering different charging stations operating as nodes in a network that combines the variable loads of home appliances and EVs. Thus, the massive inclusion of EVs will bring issues to the network infrastructure due to branch limits, voltage regulation, and power losses.

A good solution for this problem is the microgrid (MG), which combines several renewable generation units, loads, and storage system [3] to help mitigate the effects of different EVs charging in the network. Thus, houses and buildings could provide small power vehicle stations with distributed generators (DGs) that can supply this variable load in different nodes. The microgrid concept has been introduced as a very effective technology that integrates renewable energy sources [4] and operates either connected to a main network or in isolation [5]. Transport electrification presents several challenges for the smart grid, such as energy quality, reliability, and control [6]. There are three emerging concepts of EVs connected to the network: home-to-vehicle (V2H), vehicle-to-vehicle (V2V), and vehicle-to-power grid (V2G) [7]. V2H refers to the exchange of energy between the EV battery and the domestic power grid, where batteries can function as the power generator to provide the backup power to the electric home [8]. V2V refers to the local exchange between EVs that can charge or discharge battery power between them. V2G uses the power of the local EV community and exchanges it to the power grid through control [9].

Unidirectional V2G is a technology that controls the battery charging speed of EVs in a single direction of power flow between the EV and the network [10,11]. One advantage of unidirectional V2G technology is that is not costly to add the simple controller to manage the charge rate. Unidirectional V2G can provide auxiliary services to the power grid, such as power grid regulation and load reservation [12].

Some papers report trends in the concept of EVs, as well as the key technologies in the development of electric mobility from 2002 to 2012, in three different regions of the world. Some consider different stages in the development of EVs [13]. Original data derived from 257 subject experts surveyed in Denmark, Finland, Iceland, Norway, and Sweden have also been obtained that investigate different expectations and visions associated with a low-carbon form of transport, electric mobility, including the vehicle-to-network scheme [14].

However, in the field of energy systems, there are several new paradigms for the power grid that attempt to address several problems [15–17]. The current EV industry has encountered many technical issues with the connection of EVs to the power grid. For example, charging vehicles introduces negative impacts on the power grid. The smart grid concept was introduced to consider electric transportation, which has modernized the power system with additional communication functions [18], [19]. EV manufacturing technology could provide an opportunity to implement energy stores [20]. The penetration of plug-in electric and hybrid EVs will increase significantly in the coming years. The insertion of EVs in homes that will facilitate the use of renewable sources and possibly generate economic benefits for users, but will also present some challenges, such as how the penetration of EVs affects the power quality of existing electricity networks [11].

Recently, the development of the smart grid concept in power grids has advanced the role of EVs [21]. A control concept for distribution networks with EVs and distributed energy resources has been previously presented. An analysis of the control strategies, market models, and characteristics of existing EVs was performed to take into account the main drawbacks of existing solutions and a new concept of distributed control for the management of the energy system [22]. Another document proposes an allocation planning method for EVs in a multi-agent-based microgrid [23]. Besides, a new scheme

to provide the necessary primary reserve for EVs by controlling multiple agents of each vehicle is proposed in [24] and a new methodology to determine the optimal EV load–discharge strategy based on the uncertainty of the voltage drop is proposed in [25].

The consulted references show that previous works have focused on active and reactive power control, but few have considered virtual impedance as part of the solution. However, they have not worked on using variable virtual impedance to share the reactive power in a microgrid that considers the distances to the connection of EVs. The objective of this paper is to show reactive power sharing and voltage regulation in a microgrid using the concept of variable virtual impedance related to the line distance between the inverter and the consumption of EVs charging in the power grid. Therefore, the contributions in this article are: variable virtual impedances are calculated from each inverter to the possible vehicle connection and disconnection point; a voltage control is applied based on the line distance to the EVs connected; and reactive power sharing from distributed generation is achieved to compensate nodes in a network once some variations in the loads are presented.

The rest of the document is organized as follows. Section 2 explains the new control strategy to share reactive power after each load variation. Section 3 presents the formulation for the small-signal stability analysis applied to the control strategy. Section 4 shows the results of simulations performed with the software MATLAB-Simulink. Finally, Section 5 presents conclusions and future work.

3.2 Control Method

Droop control P–ω and droop control Q–V have been successfully applied to microgrids [26]. These methods are simple but not very effective when the load changes in different nodes in the microgrid. Therefore, this paper proposes a very useful control strategy for this type of problem. Figure 1 shows the diagram of a single

EV and a house connected to a network that uses renewable energies and power inverters.

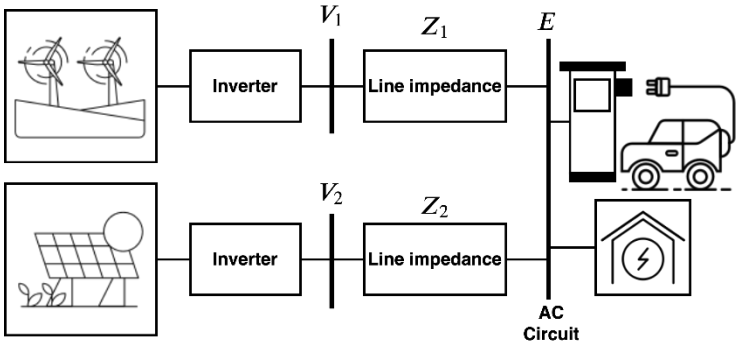

Figure 1. Diagram of an EV connected to the power grid

The active and reactive power transferred from the inverter to the load is given by Equations (1) and (2). These equations express, respectively, the active and reactive power that is lost through the inductive reactance associated with transmission lines. Herein, the term δ represents the phase angle between the voltage generated by the inverters (V) and the voltage of the AC bus (E). Furthermore, the impedance $Z = R + jX$ has an angle θ that can be defined as $R = Z\cos\theta$ and $X = Z\sin\theta$:

$$P = \frac{1}{R^2 + X^2}(RE^2 - REV\cos\delta + XEV\sin\delta) \quad (1)$$

$$Q = \frac{1}{R^2 + X^2}(XE^2 - XEV\,cos\,\delta - REV\,sin\,\delta) \quad (2)$$

A control strategy with virtual impedances is proposed as a method to control the reactive power of the microgrid, considering connections and disconnections of EVs. Figure 2 shows a detailed configuration of a DG unit using the proposed control strategy. The P-ω controller is adopted to regulate the frequency and to achieve accurate reactive power sharing by using virtual impedance.

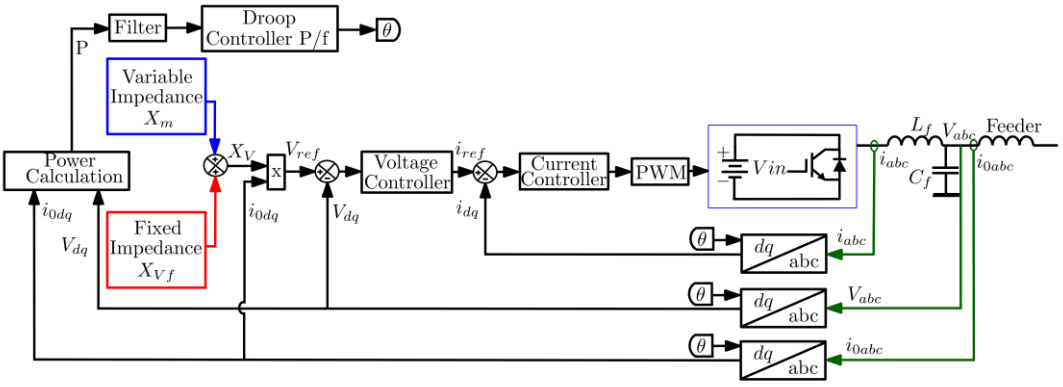

Figure 2. Electrical circuit with the proposed control strategy applied to distributed generation.

The controller used with the electrical circuit starts by measuring the current in the inductance of the filter i_{abc}, the output voltage V_{abc}, and the zero-sequence current i_{0abc}. Using the park-transform method, the three previous values are transformed to obtain the dq values, such as i_{dq}, V_{dq}, and i_{0dq}. Besides, the active power P is calculated by using the output voltage V_{dq} and the current measured in the output of the system i_{0dq}, both in dq coordinates; then, the final signal is passed through the filter and droop controller to obtain. A variable virtual impedance X_m, related to the line and load impedances considered from each EV to inverters, is applied to the control. Then, the total virtual impedance X_V is calculated by summing X_m and a fixed virtual impedance X_{Vf} related to the line and load impedances considered from each house to inverters, as defined in Equation (3). Reactive power sharing is performed by regulating this total virtual impedance according to the location of EVs in the microgrid.

$$X_V = X_{Vf} + X_m \,. \tag{3}$$

Then, the reference voltage V_{ref} is calculated by using the X_V and the i_{0dq}. Next, the reference voltage V_{ref} and the output voltage V_{dq} that is measured and transformed to

dq coordinates are used to obtain the voltage error, which is then converted to the reference current using the voltage controller.

The voltage control loop uses a PR controller to track the voltage reference value, given by the controller. The output of the voltage control gives a reference current that is used to calculate the current error with the i_{odq}. The current control loop uses a P controller to adjust the output current that is sent to the PWM to make the inverter obtain the desired voltage response.

3.3 Small-signal Stability Analysis

The dynamic model of droop control has been widely discussed [27]. In this section, a small-signal model is derived for the proposed controller in which the total virtual impedance X_V is considered. By considering small disturbances around the equilibrium point defined by ($\Delta\delta e,\ E,\ V$), the active power equation can be linearized around this point; thus, the expression shown in Equation (4) is obtained:

$$\Delta P(S) = \left(\frac{\partial p}{\partial X_V}\right)\Delta X_V(S) + \left(\frac{\partial p}{\partial \delta}\right)\Delta\delta(S) \tag{4}$$

This last equation can be expressed in terms of k_{px} and $k_{p\delta}$ as presented in Equation (5):

$$\Delta P(S) = k_{px}\Delta X_V(S) + k_{p\delta}\Delta\delta(S) \tag{5}$$

Similarly, the small disturbances around the equilibrium point are defined by ($\Delta\delta e,\ E,\ V$) and the reactive power equation can be linearized around this point as expressed in Equation (6):

$$\Delta Q(S) = \left(\frac{\partial Q}{\partial X_V}\right)\Delta X_V(S) + \left(\frac{\partial Q}{\partial \delta}\right)\Delta\delta(S) \tag{6}$$

This last equation can be expressed in terms of k_{qx} and $k_{q\delta}$ as shown in Equation (7):

$$\Delta Q(S) = k_{qx}\Delta X_V(S) + k_{q\delta}\Delta\delta(S) \quad (7)$$

where the term Δ indicates the small-signal deviation of the variable around the equilibrium point and theses variations are expressed as shown in Equations (8)–(11). Furthermore, the variations of total virtual impedance ΔX_V in Equation (9) includes the changes in the variable virtual impedance ΔX_m and the changes in the fixed virtual impedance ΔX_{Vf} (considered in this study as zero during the steady-state operation):

$$\Delta W = -k_p\Delta p \quad (8)$$

$$\Delta X_V = \Delta X_{Vf} + \Delta X_m \quad (9)$$

$$\Delta P = k_{px}\Delta X_V + k_{p\delta}\Delta\delta \quad (10)$$

$$\Delta Q = k_{qx}\Delta X_V + k_{q\delta}\Delta\delta \quad (11)$$

The four terms—k_{px}, $k_{p\delta}$, K_{qx}, and $k_{q\delta}$—are calculated around the equilibrium point, which represents the sensitivity of the power flow with the virtual impedance:

$$k_{px} = \left(\frac{\partial p}{\partial X_V}\right) = \frac{(EV\,sin\,\delta)(R^2 + X^2) - (RE^2\,cos\,\delta - XEV\,sin\,\delta)(2X)}{(R^2 + X^2)^2} \quad (12)$$

Then, after the partial derivative of the active power based on virtual impedance, the term in Equation (13) is obtained:

$$k_{px} = \left(\frac{\partial p}{\partial X_V}\right) = \frac{R^2EV\,sin\,\delta - 2XRE^2}{(R^2 + X^2)^2} - \frac{X^2EV\,sin\,\delta - 2XREV\,cos\,\delta}{(R^2 + X^2)^2} \quad (13)$$

Now, by considering the partial derivative of the active power with respect to the angle, the term shown in Equation (10) is obtained:

$$k_{p\delta} = \left(\frac{\partial p}{\partial \delta}\right) = \frac{1}{R^2 + X^2}(REV\ sin\,\delta + XEVcos\,\delta) \tag{14}$$

From the partial derivative of the reactive power with respect to the virtual impedance, the expression shown in Equation (15) is obtained:

$$k_{qx} = \left(\frac{\partial Q}{\partial X_V}\right) = \frac{2XREV\ sin\,\delta - ER^2V\ cos\,\delta}{(R^2 + X^2)^2} + \frac{E^2R^2 - E^2X^2 + EVX^2\ cos\,\delta}{(R^2 + X^2)^2} \tag{15}$$

Furthermore, from the partial derivative of the reactive power with respect to angle, the following expression shown in Equation (16) is obtained:

$$k_{q\delta} = \left(\frac{\partial Q}{\partial \delta}\right) = \frac{1}{R^2 + X^2}(XEV\ sin\,\delta - REV\ cos\,\delta) \tag{16}$$

By considering that active and reactive power are commonly measured using a first-order low-pass filter, the cut-off frequency W_f of the active power controller can be linearized around the same point:

$$\Delta W(S) = \frac{-k_p W_f}{S + W_f}\Delta P(S) \tag{17}$$

$$\Delta P(S) = k_{px}\Delta X_V(S) + k_{p\delta}\Delta\delta(S) \tag{18}$$

After replacing $\Delta P(S)$, defined in Equations (18) and (17), the following equation is obtained:

$$\Delta W(s) = \frac{-k_p W_f}{S + W_f}\left(k_{px}\Delta X_V(S) + k_{ps}\Delta\delta(S)\right) \tag{19}$$

Thus, the virtual impedance is defined by considering (19):

$$\Delta X_V(S) = \frac{w_f}{S + w_f}\left[\frac{S\Delta\delta(S) + k_p k_{p\delta}\Delta\delta(S)}{-k_p k_{px}}\right] \quad (20)$$

After replacing ΔX_V in Equation (20), Equation (21) is obtained and considering that $\Delta P(S) = \frac{S\Delta\delta(S)}{-k_p}$:

$$\Delta W(S) = \frac{-k_p w_f}{S + w_f}\left\{k_{px}\left[\frac{w_f}{S + w_f}\left(\frac{S\Delta\delta(S) + k_p k_{p\delta}\Delta\delta(S)}{-k_p k_{px}}\right)\right] + k_{p\delta}\Delta\delta(S)\right\} \quad (21)$$

By solving Equation (21), the large expression shown in Equation (22) is obtained:

$$\Delta W(S) = \frac{-S\Delta\delta(S)k_{px}{w_f}^2 - \Delta\delta(S)k_{px}k_p k_{p\delta}{w_f}^2 + S\Delta\delta(S)k_{p\delta}k_p k_{px}w_f + \Delta\delta(S)k_{p\delta}k_p k_{px}w}{-S^2 k_{px} - 2Sw_f k_{px} - {w_f}^2 k_{px}} \quad (22)$$

After considering that $\Delta W(S) = S\Delta\delta(S)$ and replacing this in Equation (22), the expression shown in Equation (23) is obtained:

$$S\Delta\delta(S) = \frac{-S\Delta\delta(S)k_{px}{w_f}^2 - \Delta\delta(S)k_{px}k_p k_{p\delta}{w_f}^2 + S\Delta\delta(S)\delta k_p w_f k_{p\delta}k_{px} + \Delta\delta(S)k_{p\delta}k_p k_{px}}{-S^2 k_{px} - 2Sw_f k_{px} - {w_f}^2 k_{px}} \quad (23)$$

Then, after solving Equation (23) and expressing the result in a simplified form, the expression shown in Equation (24) is obtained:

$$S^3\Delta\delta(S) + 2S^2\Delta\delta(S)w_f + S\Delta\delta(S)\left({w_f}^2 + k_{p\delta}k_p w_f - {w_f}^2\right) \quad (24)$$
$$+ \Delta\delta(S)\left(-2\,k_p{w_f}^2 k_{p\delta}\right) = 0$$

This homogeneous equation describes the free movement of the system for small disturbances around the equilibrium point (δ, E, V) and it can be reduced when considering some constant parameters:

$$S^3\Delta\delta(S) + aS^2\Delta\delta(S) + bS\Delta\delta(S) + c\,\Delta\delta(S) = 0 \quad (25)$$

where the parameters a, b, and c are defined in Equations (26)–(28) as follows:

$$a = 2w_f, \quad (26)$$

$$b = ({w_f}^2 + k_{p\delta}k_p w_f - {w_f}^2) \quad (27)$$

$$c = \left(-2\,k_p{w_f}^2 k_{p\delta}\right) \quad (28)$$

Then, the small-signal stability can be studied based on the previous equations. They are implemented in this work for each control system used in the inverters to respond to the load variations at different times and nodes in the network.

3.4 Results

This section shows the results related to the response of the inverter applied at each generator by considering the variable virtual impedances described in Section 3 to be related to the distance to the connection of the EVs in the microgrid. This strategy allows sharing the reactive power and regulating the voltage in the different nodes. Simulations were performed considering a distribution network case where static loads and EVs are connected.

3.4.1 Distribution network case test

The microgrid used for this research is shown in Figure 3. This network is formed by three distributed generators designed to supply six electrical loads. Each load is composed of fixed loads related to home consumption and variable loads related to connected and disconnected EVs. The power must be delivered considering the impedances of lines 1 to 5, to reach the different loads. Besides, voltage regulation is achieved by using the inverter with the total virtual impedance that considers lines, fixed loads, and variable loads of the vehicles connected and disconnected.

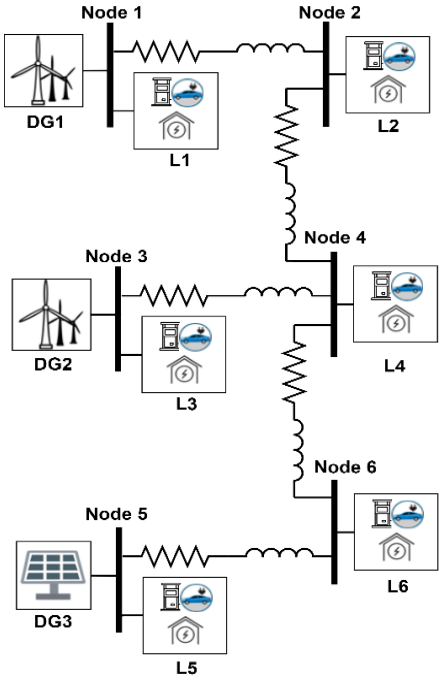

Figure 3. Microgrid used to study the strategy control

3.4.2 Single electric vehicle connection

This test consisted of connecting six EVs at different times and nodes of the microgrid to identify the action of the control strategy with the variable virtual impedance and compare it with the action of the fixed virtual impedance. Thus the six events are presented in Figure 4 and defined as follows:

- Event 1: an EV is connected to Node 1 at 10 seconds, increasing the power consumption of L1 by three times the fixed load (25 + j0.001 Ω).

- Event 2: an EV is connected to Node 2 from 20 seconds, increasing power consumption of L2 about three times the fixed load (10 + j0.03 Ω).
- Event 3: from 30 seconds, an EV is connected to Node 3, increasing the power consumption of L3 by two times the fixed load (20 + j0.01 Ω).
- Event 4: another EV is connected from 40 seconds to Node 4, increasing the power consumption of L4 by two times the value of the fixed load (15 + j0.02 Ω).
- Event 5: the connection of an EV is presented in Node 5 from 50 to 60 seconds, increasing the power consumption of L5 by 12 times the fixed load (25 + j0.09 Ω).
- Event 6: this final event considers that an EV is connected from 60 seconds to Node 6, which generates an additional power consumption of L6 of almost five times the fixed load (18 + j0.05 Ω).

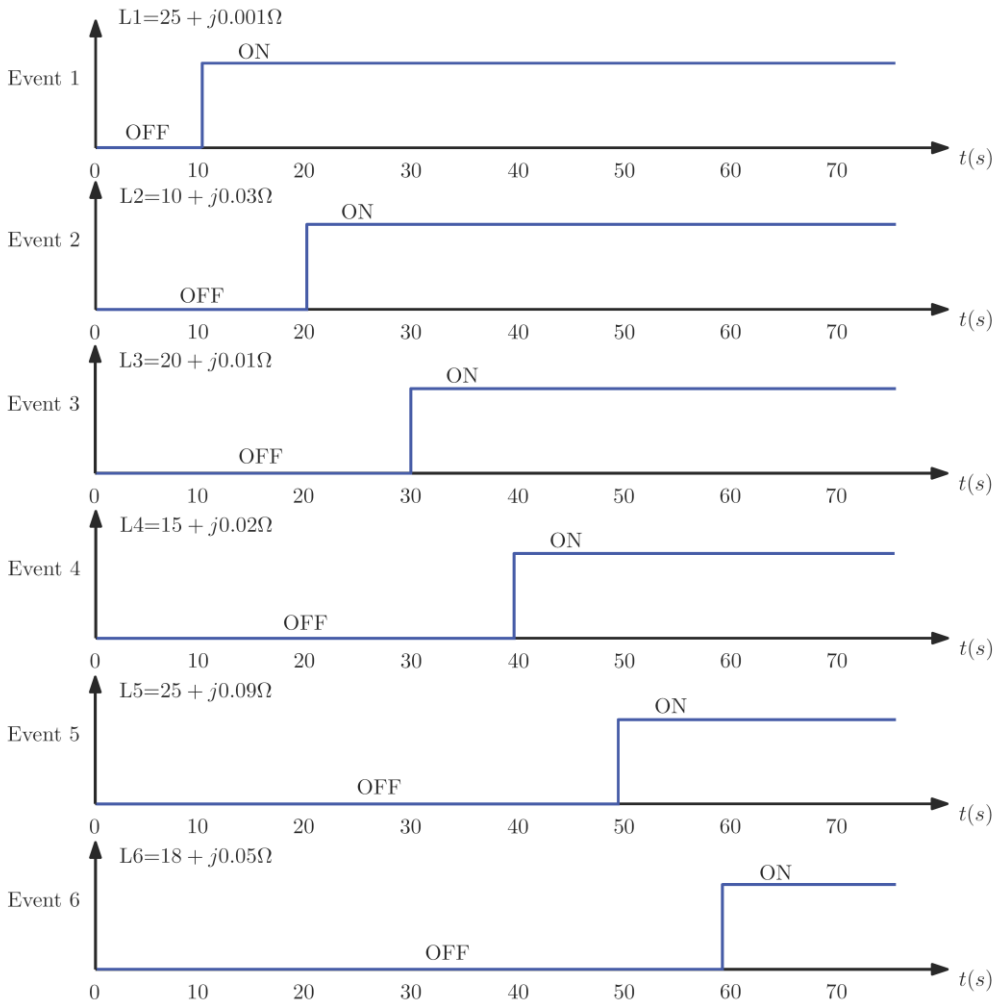

Figure 4. Events considered for the first test related to a single electric vehicle (EV) connection.

3.4.3 Active and reactive power of loads

Figures 5a-5f show the active power consumption versus time of six loads in the microgrid when EVs are connected at different times and nodes considering the six events presented in the previous subsection. All figures compare the active power supplied to loads L1-L6, when using the control strategy based on fixed and variable virtual impedances.

Hence, Figure 5a presents the active power behavior for the Event 1; Figure 5b shows the active power behavior for the Event 2; Figure 5c presents the active power behavior for the Event 3; Figure 5d shows the active power behavior for the Event 4; Figure 5e presents the active power behavior for the Event 5; and Figure 5f shows the active power behavior for the Event 6. These figures show that the system responds to load variations by delivering active power to each load because of the events that occurred in the microgrid. Both control strategies respond to the changes and share the active power from generation to each load.

During the different periods evaluated, each node presents active power variations that are considered by each inverter according to the control strategy applied. However, the control with the fixed virtual impedance has difficulties in sustaining the power delivered to the load with different power variations presented in the same node plotted and power variations of other nodes of the microgrid. On the other side, the control with variable virtual impedance is much more effective in maintaining a sustained active power in all load nodes according to power variations presented in the same node plotted and power variations of other nodes. Therefore, the proposed control strategy that uses a variable virtual impedance allows maintaining the active

power regulated in the different nodes of the microgrid, allowing less power reduction after considering different power variations.

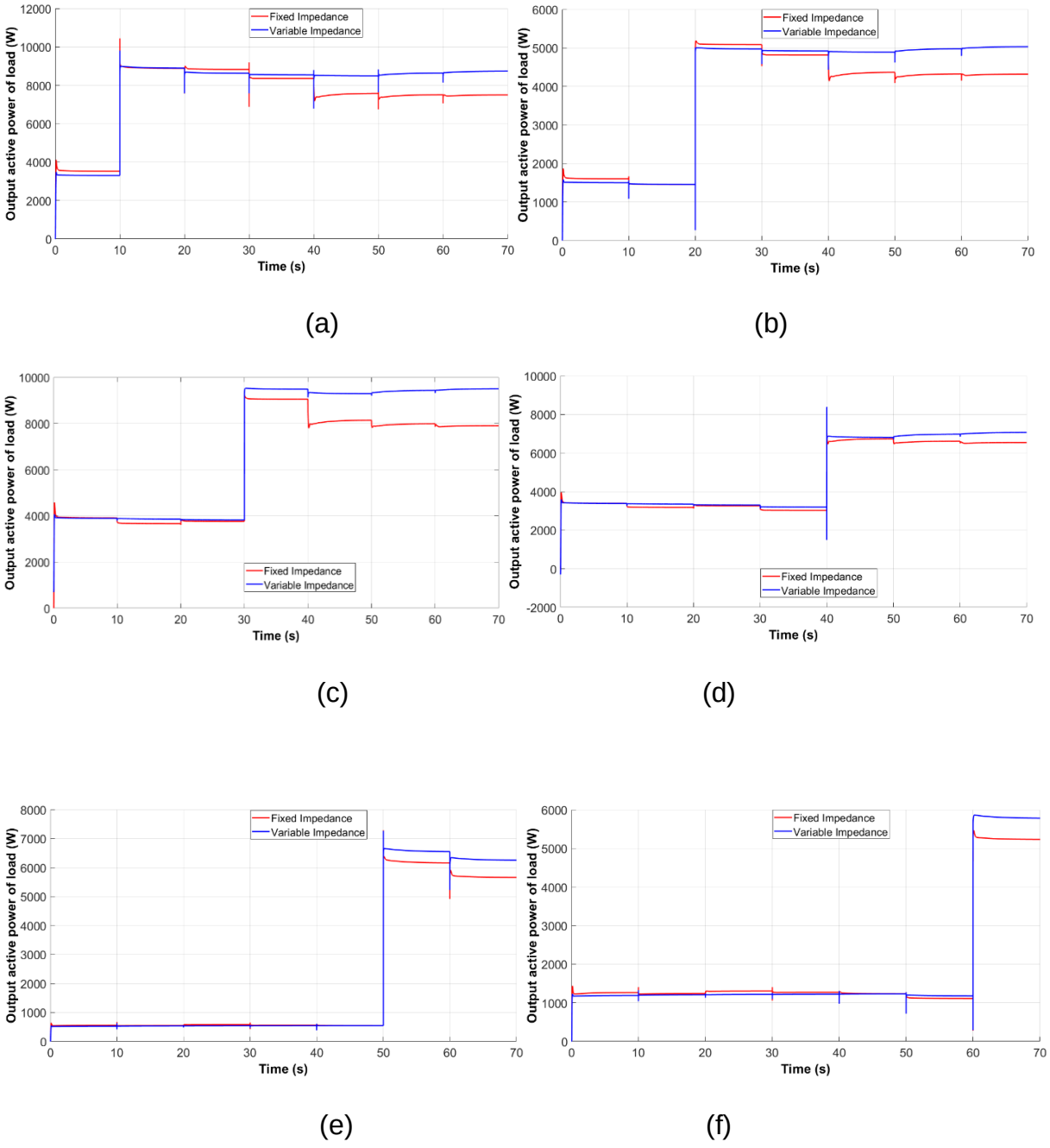

Figure 5. Active power supplied to loads considering a control strategies based on variable and fixed virtual impedances for six power variations: (a) Event 1, (b) Event 2, (c) Event 3, (d) Event 4, (e) Event 5, and (f) Event 6.

Now, as the reactive power is of great interest in this work, the control strategy must also maintain the power supply to the loads during the power variations. Thus,

Figures 6a-6f show the reactive power consumption versus time of the same six loads in the microgrid when the EVs are connected at different times and nodes considering the same six events previously stated. All figures compare the reactive power supplied to loads L1-L6, when using the control strategy based on fixed and variable virtual impedances.

Hence, Figure 6a presents the reactive power supplied to L1 for the Event 1; Figure 6b shows the reactive power behavior of L2 for the Event 2; Figure 6c presents the reactive power behavior for the Event 3; Figure 6d shows the reactive power behavior for the Event 4; Figure 6e displays the reactive power behavior for the Event 5; and Figure 6f shows the reactive power behavior for the Event 6. These figures show that there are variations in the reactive power delivered to each node due to the events that occurred in the microgrid. Both control strategies respond to the changes and share the reactive power from generation to each load.

During the different periods evaluated, each node presents reactive power variations that are considered by each inverter according to the control strategy applied. These six figures show that reactive power increases to supply loads, but the reactive power is better improved when the variable virtual impedance is used. When the reactive power increases in the load, the fixed virtual impedance allows improving the reactive power demanded to the load node to supply power requirements; however, variations of the different loads in the network reduces the effectivity of the control and reduces the power supply in the different periods of time. On the other side, the use of the variable virtual impedance follows variations of the load, increasing the reactive power supply and through the changes of other loads the reactive power supply is better maintained during the different periods. This shows the advantage of using variable virtual impedance in the controller as it allows to improve the reactive

power supplied to the loads in better conditions that the supplied by using a fixed virtual impedance.

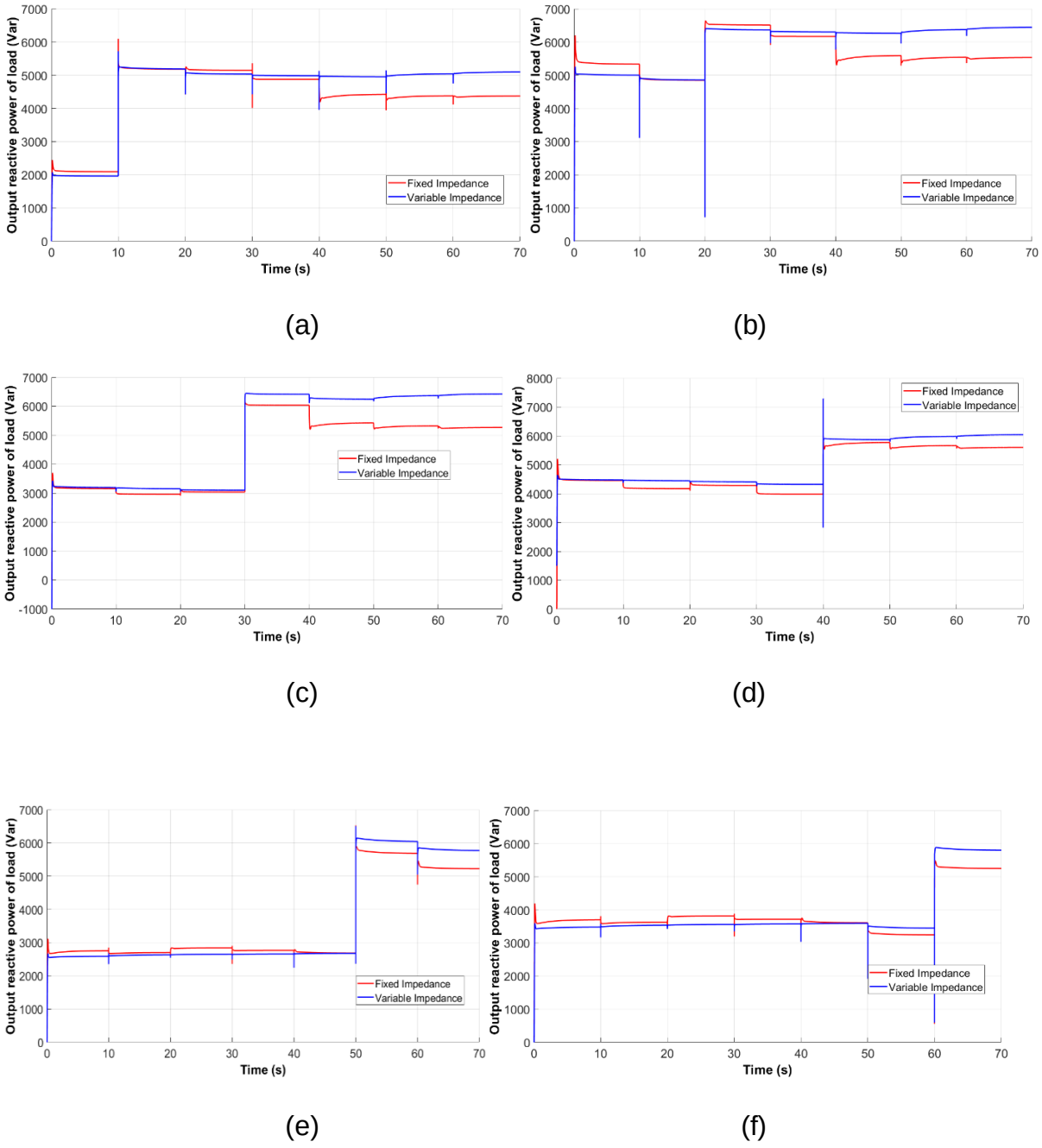

Figure 6. Reactive power supplied to loads considering a control strategies based on variable and fixed virtual impedances for six power variations: (a) Event 1, (b) Event 2, (c) Event 3, (d) Event 4, (e) Event 5, and (f) Event 6.

3.4.4 Voltage in loads

Figures 7a-7f show the voltage behavior in the six nodes of the microgrid when EVs are connected to the network according to the events previously defined. All figures compare the voltage regulated in Nodes 1-6, using the control strategy based on fixed and variable virtual impedances.

Hence, Figure 7a presents the voltage behavior in Node 1 for the Event 1; Figure 7b shows the voltage behavior in Node 2 for the Event 2; Figure 7c presents the voltage behavior in Node 3 for the Event 3; Figure 7d shows the voltage behavior in Node 4 for the Event 4; Figure 7e displays the voltage behavior in Node 5 for the Event 5; and Figure 7f shows the voltage behavior in Node 6 for the Event 6. These figures show that the voltages changes in each node according to the events that occurred in the microgrid. Both control strategies respond to regulate well the voltages of each node and maintain them instead of the different power variations presented in the electrical network.

These results show that at the beginning of the EV connection, the voltage of the node tends to drop sharply, but immediately the control strategy recovers the voltage close to the original value while the EV is charging. Therefore, the control strategy applied with variable virtual impedance maintains a stable voltage value during the different load variation periods when the EVs are connected. On the other side, when the fixed virtual impedance is used, the voltage drops further than the proposed method. The results show that the variable virtual impedance tries to maintain voltage higher than the obtained with fixed virtual impedance and this means the proposed control strategy is better to improve voltages at different nodes after the events tested.

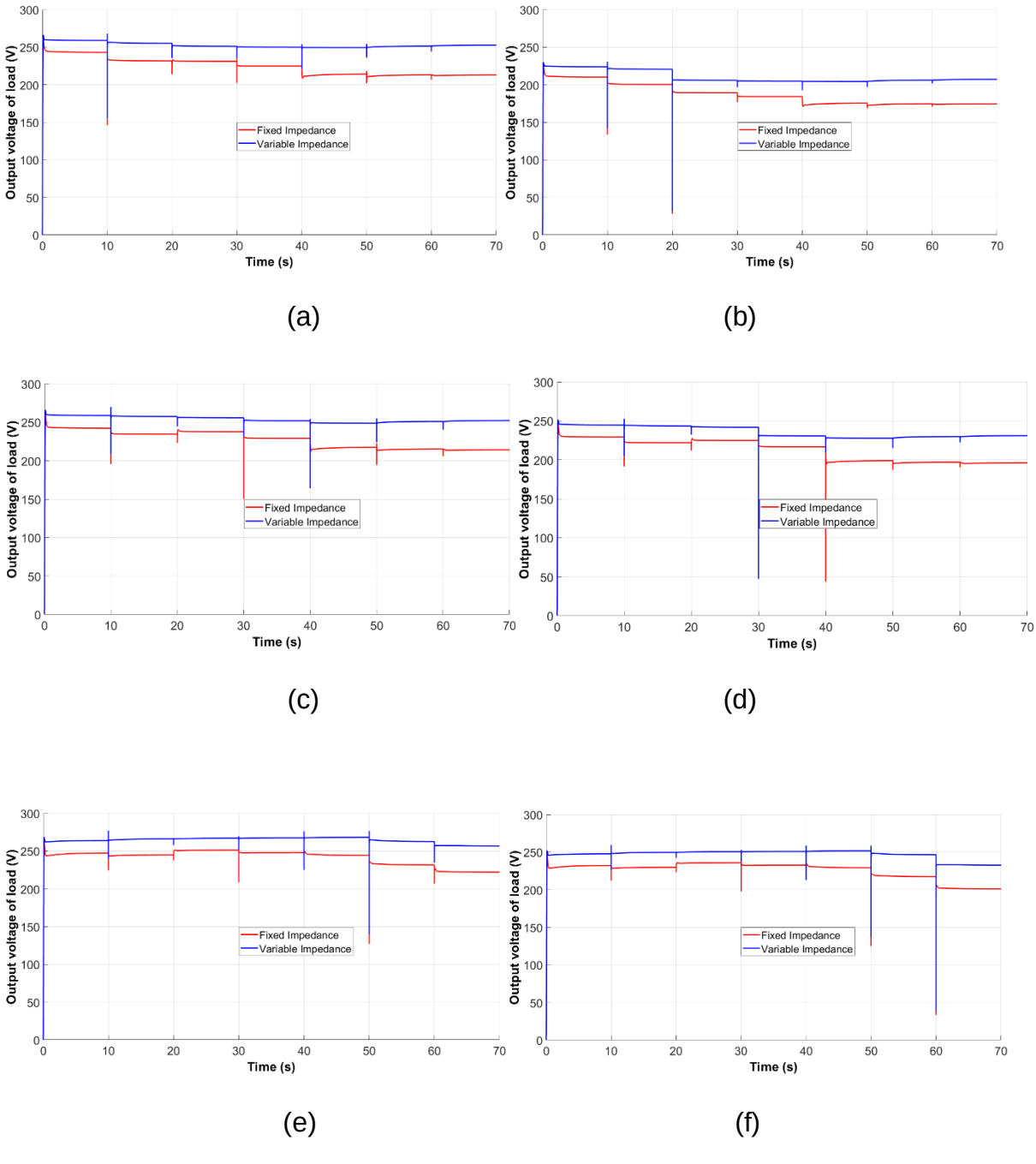

Figure 7. Voltages in the six nodes (Nodes 1-6) considering a control strategies based on variable and fixed virtual impedances for six power variations: (a) Event 1, (b) Event 2, (c) Event 3, (d) Event 4, (e) Event 5, and (f) Event 6.

3.4.5 Responses of DGs

Figure 8 shows the behavior of the power supplied by each DG connected to the microgrid, after the six events tested for single EV connection. Figure 8a shows the

active power supply and Figure 8b shows the response of reactive power supply with the strategy control applied with variable virtual impedance. This test allows identifying the distribution of the active and reactive power supplied among generators in the microgrid.

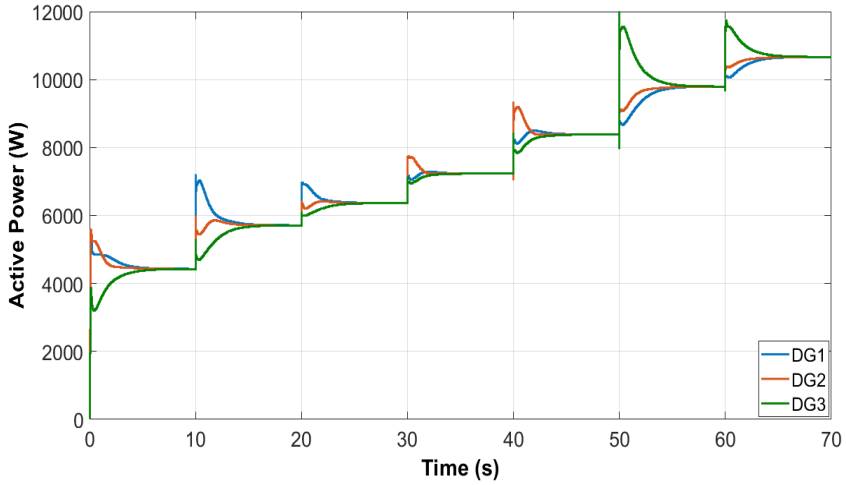

(a)

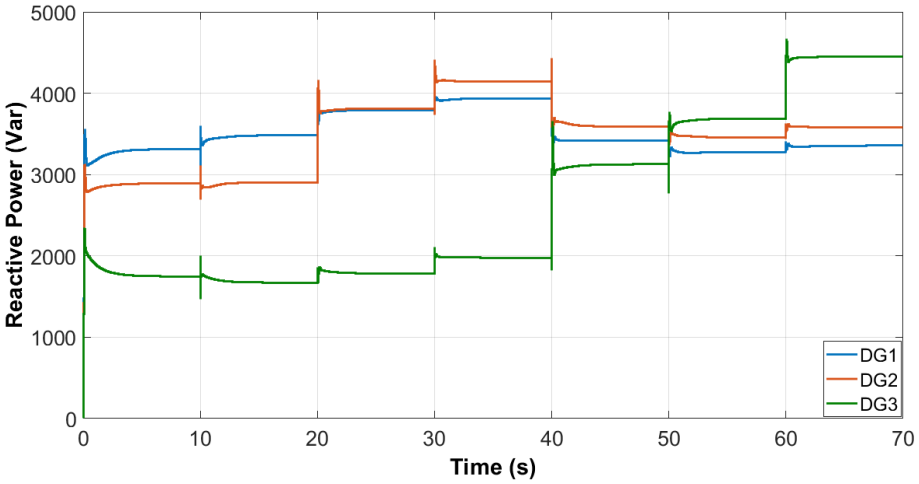

(b)

Figure 8. Power behavior of DGs with the six events (Events 1-6): (a) active power and (b) reactive power.

Figure 8 shows that active power increases with the connection of each EV to the different nodes and each generator stabilizes as quickly as possible to deliver

adequate reactive power to the various connections of EVs. In the two first events (10 and 20 seconds), it is observed that the DG 1 is the one that responds more sharply to the change of load because it is closer to the node where the respective load is located. After 30 seconds, the connection occurs at Node 3, where DG 2 is the one that responds most to this change during the first seconds as it is the generator closest to the load, whereas the control stabilizes the three generators to a same active power value. From 40 seconds, an EV is connected to Node 4 and DG 3 responds more sharply to this type of load change because it is the generator closest to the node where the EV connection occurs.

From 50 seconds, the load of an EV is connected to Node 5 and now DG 3 increases active power because this is the closest generator to the load. From 60 seconds, the load of an EV is connected to Node 6 and DG 3 changes the active power generation because this is the generator that is closest to the load; however, control strategy support is achieved by stabilizing the output power to the same value of the other two DGs.

Figure 9 shows the output frequency of the three DGs and their variation after the different load changes in the nodes that constitute the microgrid. This result considers the control strategy applied with the variable virtual impedance. The frequency of the three generators always stabilizes in a single value a few seconds after the load changes in each of the different nodes. This figure shows that some events create more variations in the frequency, related to the magnitude of power changes and the distance to DGs. However, the controller with the virtual impedance maintains the frequency value close to 50 Hz, which is the desired value.

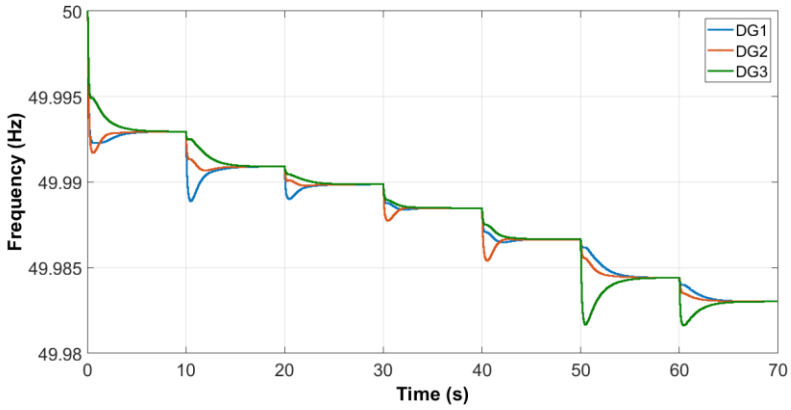

Figure 9. Frequency regulation of the three DGs

3.5 Multiple electric vehicle connection and disconnection

In this second test, various EVs are connected and disconnected at different periods and nodes of the microgrid to simulate the increase and decrease of active and reactive power of loads defined in Figure 3 (L1-L6). Figure 10 shows the events at different periods to identify the controller response under multiple EVs connections and disconnections. The following are the six events considered in the connection and disconnection test of multiple EVs:

- Event 1: at the beginning of the first period (from t_0 to t_1) L1 increases the active power consumption after connecting five EVs to Node 1, changing the power by nine times the fixed load of 25 + j0.001 Ω; at the end of the period, this load is disconnected.
- Event 2: at the beginning of the second period (from t_1 to t_2) the active power increases in L2 when one EV is connected to Node 2, and the power increases by four times its normal value of 10 + j0.03 Ω; at the end of the period, this load is disconnected.
- Event 3: at the beginning of the third period (from t_2 to t_3), the greatest change of active power is presented in Node 3 (L3) with the connection of ten EVs and the

consumption in that node is almost 13 times the fixed load of 20 + j0.01 Ω; at the end of the period, this load is disconnected.

- Event 4: at the beginning of the fourth period (from t_3 to t_4), three EVs are connected to Node 4 (L4), which provides a power consumption of almost five times the average consumption of 15 + j0.02 Ω; at the end of the period, this load is disconnected.
- Event 5: at the beginning of the fifth period (from t_4 to t_5), the connection of two EVs are presented at Node 5 (L5), resulting in an increase in the load of 22 times the normal active power consumption with respect to the fixed load of 25 + j0.09 Ω; at the end of the period, this load is disconnected.
- Event 6: at the beginning of the sixth period (from t_5 to t_6), two EVs are connected to Node 6 (L6), which generates an additional power consumption at the node of almost 8 times the normal consumption of 18 + j0.05 Ω; at the end of the period, this load is disconnected.

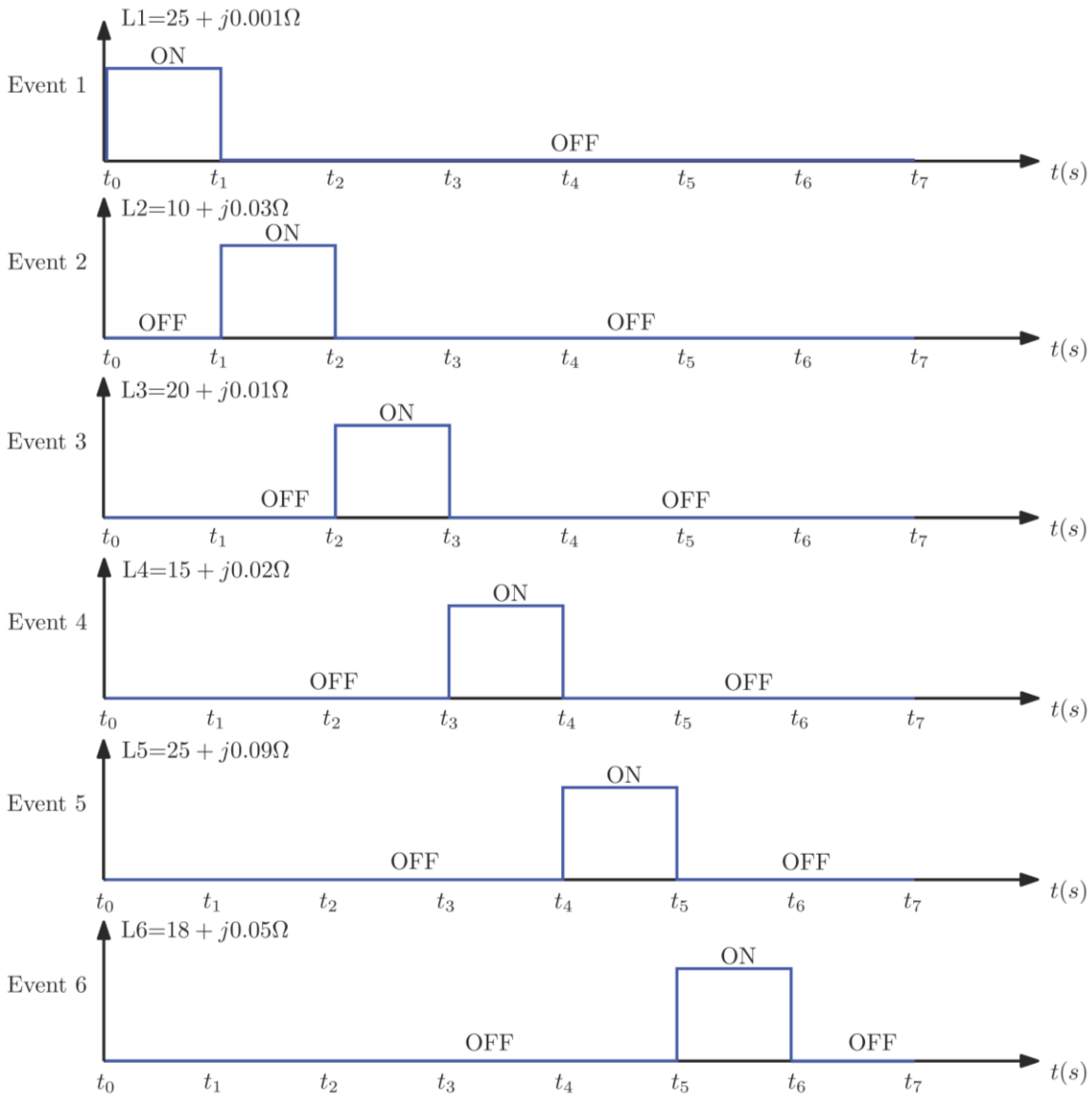

Figure 10. Events considered for the second test related to multiple electric vehicle (EVs) connection.

3.5.1 Active and reactive power

Figures 11a and 11b, respectively, show the active and reactive power supplied to the load when multiple EVs are connected and disconnected in the microgrid. Both active and reactive power increase based on the number of EVs connected to the nodes. It is also observed that powers increase based on the number of EVs connected to the microgrid; i.e., the higher the amount of the vehicles the more significant the

increase of that active and reactive power. In both cases, the control strategy based on variable virtual impedance helps regulate and maintain stability in the power supplied to the load.

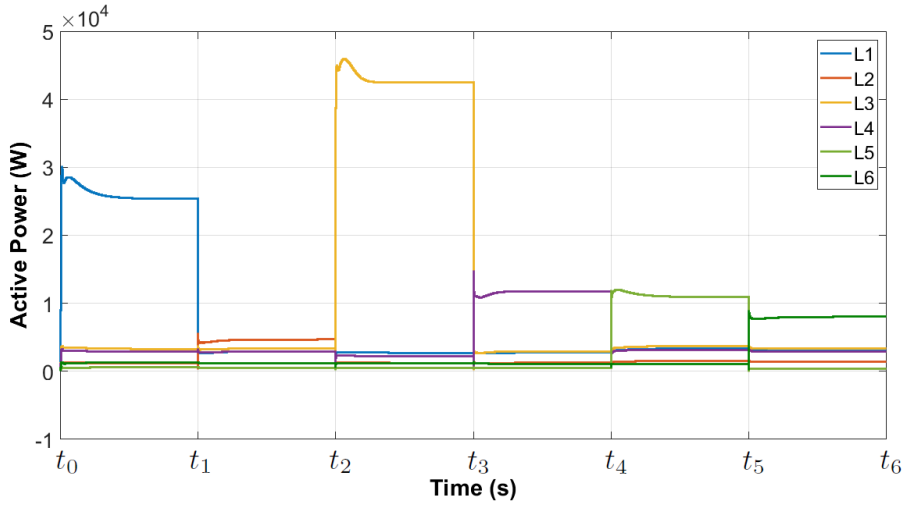

(a)

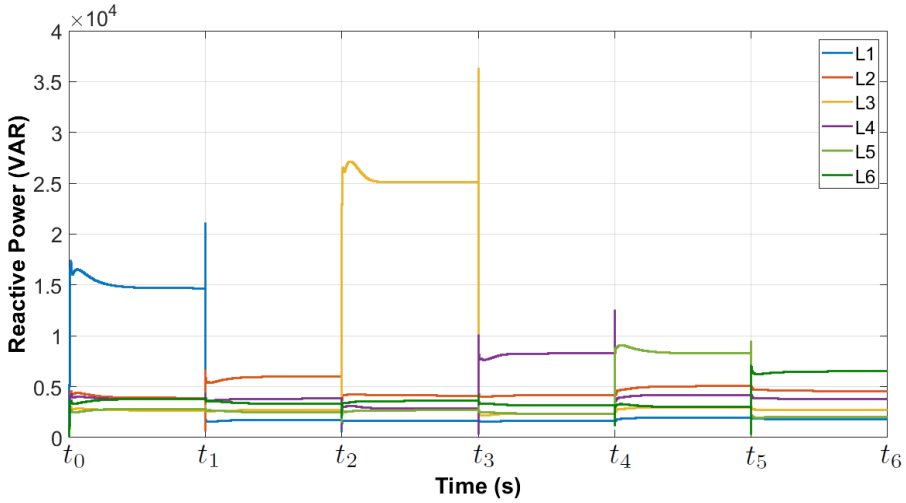

(b)

Figure 11. Load variation with electric vehicles (EVs): (a) active power and (b) reactive power.

3.5.2 Voltage variations

Figure 12 shows the voltages in different nodes of the network when the EVs are connected and disconnected in the network with the defined events (Events 1-6). It is observed that the voltages tend to reduce slightly when the EVs are connected and increase when they are disconnected. However, in the instant that the EVs are connected to the node, the voltage drops and immediately the control strategy recovers the magnitude close to the original value. Therefore, the result shows how the control strategy regulates well the signals at different load nodes by using the variable virtual impedance of the network.

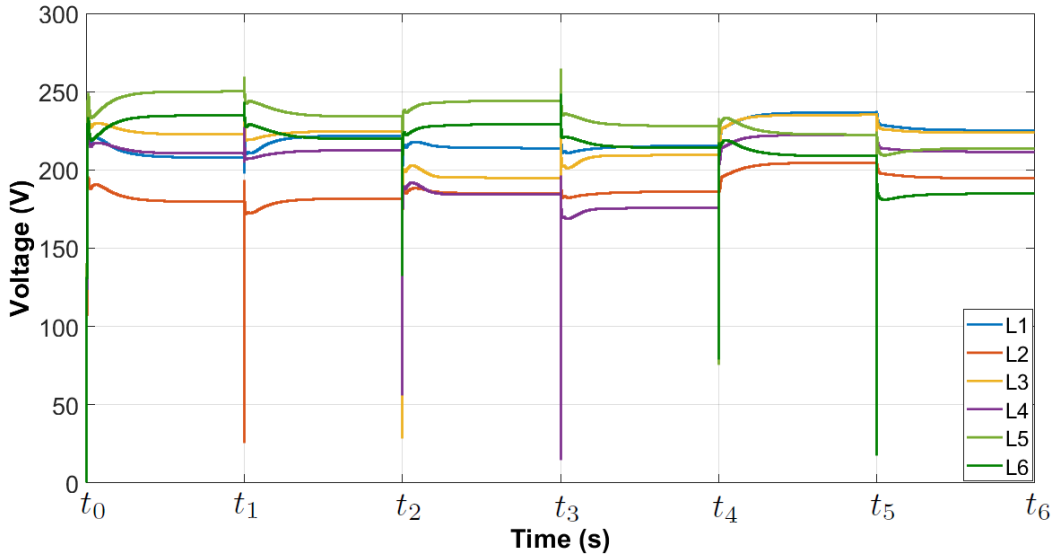

Figure 12. Voltage regulation with variable virtual impedance.

3.5.3 Generation behavior

Figure 13 shows the behavior of the active power in the three DGs when EVs are connected and disconnected. Figure 13a shows the active power and Figure 13b presents the reactive power. In the simulation, active power changes each period, corresponding to the connection and disconnection of EVs along the microgrid according to the events previously defined (Events 1-6).

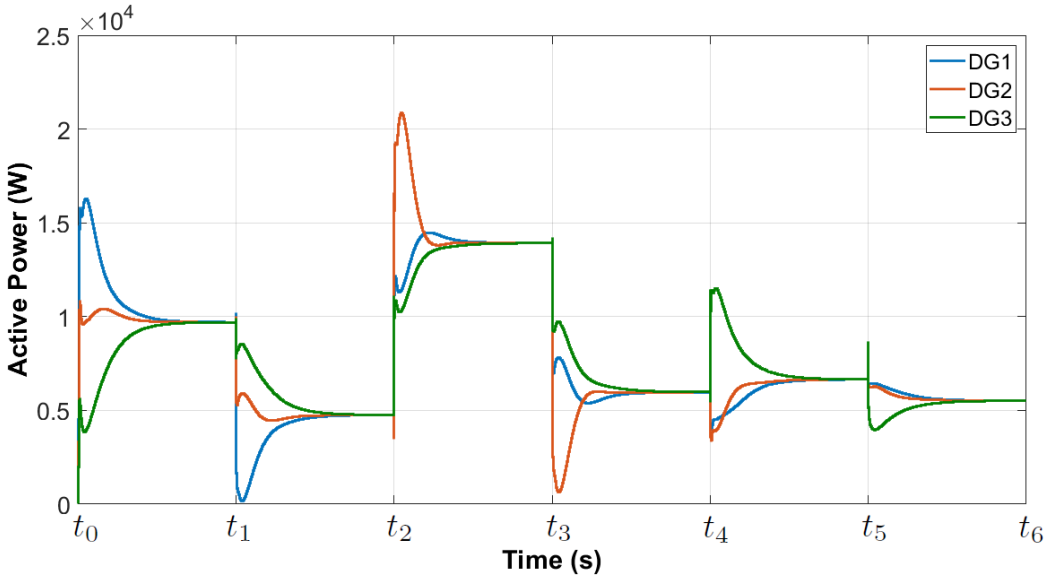

(a)

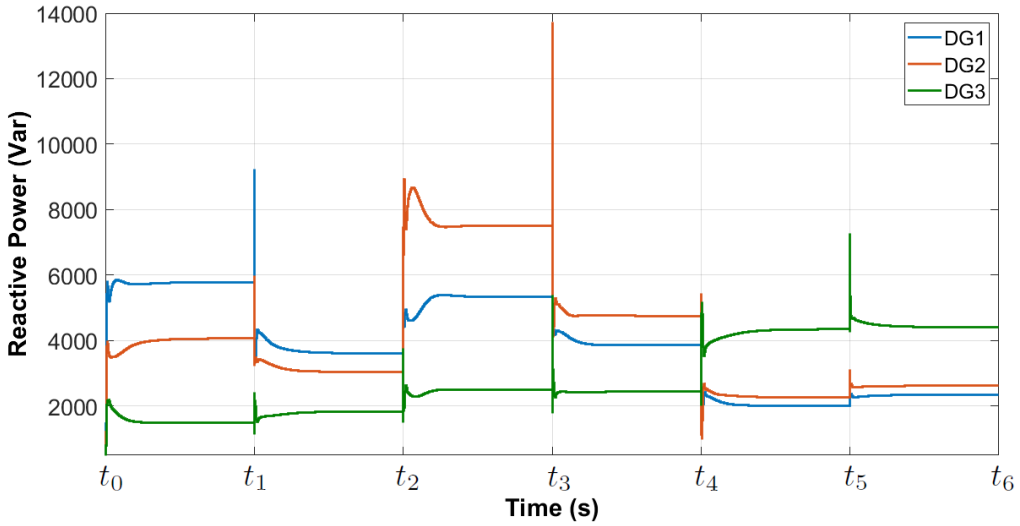

(b)

Figure 13. Behavior of (a) active power and (b) reactive power, when EVs are connected and disconnected at different nodes in the microgrid.

Regarding the active power presented in Figure 13a, the obtained result shows that each distributed generator is stabilized as quickly as possible to deliver adequate active power to the different loads. Thus, the following results are obtained:

- During the first two periods of simulation (Event 1 and Event 2), the microgrid is subjected to the connection and disconnection of five EVs in Node 1 and followed

by one EV connected to Node 2. During these two periods, DGs 1 and 3 are the ones that present most changes in active power and after some seconds, they finish sharing similar values.

- Then, in the third period (Event 3), ten EVs are connected to Node 3 at the beginning of the period and disconnected at the end of the period. During this period, DG 2 responds more abruptly to the load change because this generator is closer than the others to the variable load.
- Later, in the fourth period (Event 4), three EVs are connected to Node 4. In this case, DGs 2 and 3 are the ones that respond most to this load change because they are closest to the load while the control stabilizes the three generators at the same value of active output power.
- In the fifth period (Event 5), two EVs are connected to Node 5. When analyzing the simulation, the DG that responds more to this change is the DG 3 because it is closest to the variations. However, with the help of the control strategy, the output power is stabilized to the same value as the other two DGs.
- Finally, in the sixth period (Event 6), two EVs are connected to Node 6. In this case, DG 3 undergoes the most abrupt change in power generation because it is the closest generator to the load.

Regarding the reactive power presented in Figure 13b, the obtained result shows that each distributed generator is stabilized as quickly as possible to deliver adequate reactive power to the different loads. The following results are obtained:

- DG 1 undergoes the most abrupt change in reactive power during the first period (Event 1) because the connection of EVs is closest to this generator.

- Next, during the second period (Event 2), the same generator undergoes the greatest change in reactive power; however, this time with a negative change because it delivers less reactive power because load decreases 80 % at Node 1 (disconnection of 5 EVs) and Node 2 increases only to one connected EV.
- In the third period (Event 3), DG 3 increases the reactive power because of the load changes from 1 EV to 10 EVs. Then, the load increases 90% and DG 2 delivers more reactive power because the EVs are connected to the same node as the generator. Thus, the proposed control strategy performs regulation according to the closest generator.
- In the fourth period (Event 4), the power reduces in DGs 1 and 2 because of the load change from 10 EVs at Node 3 to only 3 EVs connected at Node 4.
- In the fifth period (Event 5), the powers of DGs 1 and 2 are reduced because three EVs are disconnected from Node 4 and two EVs are connected to Node 5. Besides, if the connection of EVs occurs at a greater distance from these two DGs and much closer to DG 3, then the reactive power in DG 3 increases considerably.
- Finally, in the sixth period (Event 6), it is possible to see a slight increase in reactive power delivered by DGs 1, 2, and 3. Although the connection of two EVs at this Node 6 is equal to those disconnected from Node 5, the power requirement changes and they are separated by a line impedance R = 0.321 Ω and L = 6.23 mH; hence, the reactive power delivered from the DGs in the microgrid is increased.

3.5.4 Frequency regulation

Figure 14 shows the behavior of the output frequency in the three DGs and their variation with load changes. This figure is obtained by considering multiple variations in the power loads as previously described. The results show that the frequency of the

three generators stabilizes in a single value a few seconds after the load changes. The larger the change of load in the EV connection, the more abrupt the change in frequency. However, no matter how high the change in the variable load (connection and disconnection of different EVs), the controller maintains the frequency close to 50 Hz, which is the desired value.

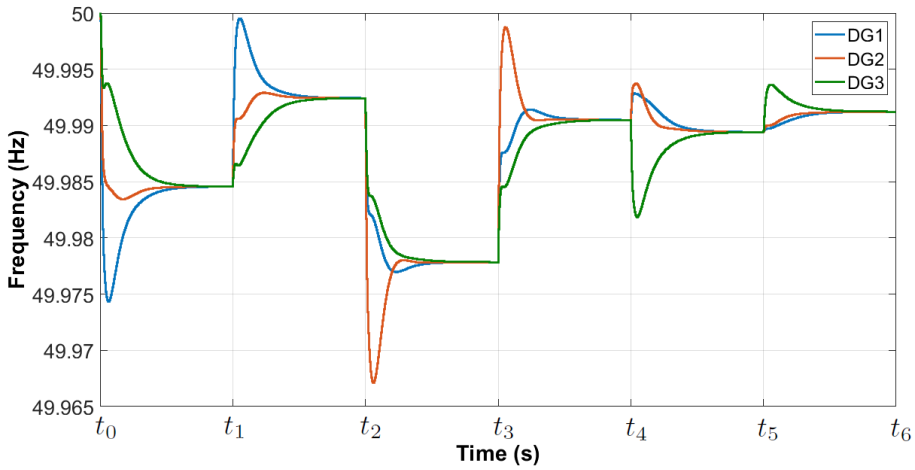

Figure 14. Frequency response by considering different load variations.

3.6 Conclusions

This paper presented a new control strategy to regulate voltage and share reactive power from distributed generators in a microgrid when EVs are connected and disconnected at different nodes and times. The control strategy considered using fixed and variable virtual impedances created in the microgrid (MG) when loads change or when an EV is connected or disconnected. Results were obtained for a system with three generators, which with the control strategy distribute active power regardless of where the vehicles are connected in the microgrid. It was possible to deliver reactive power according to the place where the load variation is presented. Thus, for a few moments, the reactive power supplied by the distributed generators is increased and, in another period, is decreased to regulate voltage in the microgrid. Therefore, this control strategy, based on variable virtual impedance related to the connection

distance of EVs, works properly to control the voltage in the different nodes of the microgrid. The control strategy manages to effectively regulate the frequency close to 50 Hz and the active and reactive power are also maintained to balance the network. This strategy is useful for the new microgrid to adapt and share active and reactive power regardless of the distance where EVs are connected. As in this research, only unidirectional vehicles were considered, in future work, bi-directional vehicles should be tested to provide a power backup to the node where the EV is connected.

Authors' Contributions: Conceptualization, methodology, and software: E.A.M.-V. and J.E.C.-B.; formal analysis, investigation, writing, review, and editing: E.A.M.-V., J.E.C.-B., and F.E.H.-V.

Funding: This research received no external funding.

Acknowledgments**:** The authors thank COLCIENCIAS and the National Doctorate program. The authors also thank Universidad Nacional de Colombia, Sede Manizales and Sede Medellín.

Conflicts of Interest**:** The authors declare no conflict of interest.

3.7 References

1. Neves, S. A.; Marques, A. C.; Fuinhas, J. A. Is energy consumption in the transport sector hampering both economic growth and the reduction of CO 2 emissions? A disaggregated energy consumption analysis. *Transp. Policy* **2017**, *59*, 64–70, doi:10.1016/j.tranpol.2017.07.004.
2. Lirola, J. M.; Castã Neda, E.; Lauret, B.; Khayet, M. A review on experimental research using scale models for buildings: Application and methodologies. *Energy Build.* **2017**, *142*, 72–110, doi:10.1016/j.enbuild.2017.02.060.
3. Katiraei, F.; Iravani, M. R. Power Management Strategies for a Microgrid With

Multiple Distributed Generation Units. *IEEE Trans. Power Syst.* **2006**, *21*, 1821–1831, doi:10.1109/TPWRS.2006.879260.

4. Lasseter, R. H. MicroGrids. In *2002 IEEE Power Engineering Society Winter Meeting. Conference Proceedings (Cat. No.02CH37309)*; IEEE; Vol. 1, pp. 305–308.
5. Pogaku, N.; Prodanovic, M.; Green, T. C. Modeling, Analysis and Testing of Autonomous Operation of an Inverter-Based Microgrid. *IEEE Trans. Power Electron.* **2007**, *22*, 613–625, doi:10.1109/TPEL.2006.890003.
6. Shaukat, N.; Khan, B.; Ali, S. M.; Mehmood, C. A.; Khan, J.; Farid, U.; Majid, M.; Anwar, S. M.; Jawad, M.; Ullah, Z. A survey on electric vehicle transportation within smart grid system. *Renew. Sustain. Energy Rev.* **2018**, *81*, 1329–1349, doi:10.1016/J.RSER.2017.05.092.
7. Liu, C.; Chau, K. T.; Wu, D.; Gao, S. Opportunities and Challenges of Vehicle-to-Home, Vehicle-to-Vehicle, and Vehicle-to-Grid Technologies. *Proc. IEEE* **2013**, *101*, 2409–2427, doi:10.1109/JPROC.2013.2271951.
8. Pode, R. Battery charging stations for home lighting in Mekong region countries. *Renew. Sustain. Energy Rev.* **2015**, *44*, 543–560, doi:10.1016/j.rser.2015.01.003.
9. Diyun Wu; Chau, K. T.; Shuang Gao Multilayer framework for vehicle-to-grid operation. In *2010 IEEE Vehicle Power and Propulsion Conference*; IEEE, 2010; pp. 1–6.
10. Yilmaz, M.; Krein, P. T. Review of the Impact of Vehicle-to-Grid Technologies on Distribution Systems and Utility Interfaces. *IEEE Trans. Power Electron.* **2013**, *28*, 5673–5689, doi:10.1109/TPEL.2012.2227500.
11. Romo, R.; Micheloud, O. Power quality of actual grids with plug-in electric vehicles in presence of renewables and micro-grids. *Renew. Sustain. Energy*

Rev. **2015**, *46*, 189–200, doi:10.1016/J.RSER.2015.02.014.

12. Guille, C.; Gross, G. A conceptual framework for the vehicle-to-grid (V2G) implementation. *Energy Policy* **2009**, *37*, 4379–4390, doi:10.1016/J.ENPOL.2009.05.053.
13. Frieske, B.; Kloetzke, M.; Mauser, F. Trends in vehicle concept and key technology development for hybrid and battery electric vehicles. In *2013 World Electric Vehicle Symposium and Exhibition (EVS27)*; IEEE, 2013; pp. 1–12.
14. Sovacool, B. K.; Kester, J.; Noel, L.; de Rubens, G. Z. Contested visions and sociotechnical expectations of electric mobility and vehicle-to-grid innovation in five Nordic countries. *Environ. Innov. Soc. Transitions* **2019**, *31*, 170–183, doi:10.1016/J.EIST.2018.11.006.
15. Ilo, A. "Link"—The smart grid paradigm for a secure decentralized operation architecture. *Electr. Power Syst. Res.* **2016**, *131*, 116–125, doi:10.1016/j.epsr.2015.10.001.
16. Green, J.; Newman, P. Citizen utilities: The emerging power paradigm. *Energy Policy* **2017**, *105*, 283–293, doi:10.1016/j.enpol.2017.02.004.
17. Matko, V.; Brezovec, B. Improved Data Center Energy Efficiency and Availability with Multilayer Node Event Processing. *Energies* **2018**, *11*, 2478, doi:10.3390/en11092478.
18. De Ridder, F.; D'Hulst, R.; Knapen, L.; Janssens, D. Applying an Activity based Model to Explore the Potential of Electrical Vehicles in the Smart Grid. *Procedia Comput. Sci.* **2013**, *19*, 847–853, doi:10.1016/J.PROCS.2013.06.113.
19. Lei Shi; Haiping Xu; Dongxu Li; Zuzhi Zhang; Yuchen Han The photovoltaic charging station for electric vehicle to grid application in Smart Grids. In *2012 IEEE 6th International Conference on Information and Automation for Sustainability*; IEEE, 2012; pp. 279–284.

20. Aliasghari, P.; Mohammadi-Ivatloo, B.; Alipour, M.; Abapour, M.; Zare, K. Optimal scheduling of plug-in electric vehicles and renewable micro-grid in energy and reserve markets considering demand response program. *J. Clean. Prod.* **2018**, *186*, 293–303, doi:10.1016/J.JCLEPRO.2018.03.058.

21. Tan, K. M.; Ramachandaramurthy, V. K.; Yong, J. Y. Integration of electric vehicles in smart grid: A review on vehicle to grid technologies and optimization techniques. *Renew. Sustain. Energy Rev.* **2016**, *53*, 720–732, doi:10.1016/J.RSER.2015.09.012.

22. Stanev, R. A control strategy and operation paradigm for electrical power systems with electric vehicles and distributed energy ressources. In *2016 19th International Symposium on Electrical Apparatus and Technologies (SIELA)*; IEEE, 2016; pp. 1–4.

23. Hapsari, A. P. N.; Kato, T.; Takahashi, H.; Sasai, K.; Kitagata, G.; Kinoshita, T. Multiagent-based microgrid with electric vehicle allocation planning. In *2013 IEEE 2nd Global Conference on Consumer Electronics, GCCE 2013*; IEEE, 2013; pp. 436–437.

24. Haes Alhelou, H. S.; Golshan, M. E. H.; Fini, M. H. Multi agent electric vehicle control based primary frequency support for future smart micro-grid. In *2015 Smart Grid Conference (SGC)*; IEEE, 2015; pp. 22–27.

25. Zhuang Yang; Bin Duan; Mingjie Chen; Zhiyong Zhu A proactive operation strategy of electric vehicle charging-discharging in Photovoltaic micro-grid. In *2016 IEEE Power & Energy Society Innovative Smart Grid Technologies Conference (ISGT)*; IEEE, 2016; pp. 1–5.

26. De Brabandere, K.; Bolsens, B.; Van den Keybus, J.; Woyte, A.; Driesen, J.; Belmans, R. A Voltage and Frequency Droop Control Method for Parallel Inverters. *IEEE Trans. Power Electron.* **2007**, *22*, 1107–1115,

doi:10.1109/TPEL.2007.900456.

27. Coelho, E. A. A.; Cortizo, P. C.; Garcia, P. F. D. Small signal stability for single phase inverter connected to stiff AC system. **2003**, 2180–2187, doi:10.1109/ias.1999.798756.

4

Reactive power sharing among distributed generators in a microgrid by using virtual current

Abstract: This paper presents a new autonomous effective power distribution control strategy for three-phase parallel inverters. The proposal uses a controller that can provide the system with an accurate power sharing among distributed generators (DGs) installed in the microgrid (MG) once some load variations are presented in the network. The methodology uses virtual current loop introduced into the current controller of the inverter to optimize the output signal, which goes directly to the PWM. This virtual current is obtained by using a virtual impedance loop. Furthermore, a small-signal model of the system is used to check stability of the proposed control strategy, which was developed for island-mode operation of the MG. Simulations were performed for a system with MG with two generators and a load with five households and it was implemented in Matlab-Simulink software. The results show that the model developed, allows a great margin of stability and a rapid response of the system when electrical loads change, fulfilling the reactive power sharing among generators. The proposed method shows a large margin of stability and a rapid transient response of the system.

Keywords: reactive power sharing; microgrid; distributed generation; virtual impedance; virtual current.

4.1 Introduction

In recent years, towards the decentralization of electricity generation, the penetration of distributed generation (DG) has significantly increased and microgrids (MGs) are becoming an important concept to integrate these generation units [1]. Thus, the concept of MG has been introduced as a very effective technology to integrate renewable energy sources in the network [2] and when compared to the conventional

distribution system, new partial system can operate connected to the main power grid or isolated [3]. By paralleling multiple inverters a droop control scheme is generally used [4–6], in which the voltage and frequency of each inverter are adjusted in order to control the active and reactive power.

In an MG in island operation mode, power must be properly shared to loads by the multiple DG units that conform the network. Conventionally, the frequency and voltage magnitude droop control is adopted, whose objective is to share active and reactive power in an MG performed in a decentralized manner without using any communication between DG units, [1,7–9]. In this control category, the active and reactive power are calculated using low pass filters [10]; consequently, the main focus of droop control is the exchange of average active and reactive power.

Active power sharing is accurate, while reactive power sharing depends on line impedances [11,12]. To improve MG performance some modified droop control methods have been presented in literature. In [13], an interesting method of dropping Q-V points is proposed, where the authors show a new cooperative harmonic filtering strategy for the interface converters of distributed generation sources. A droop control method based on the reactive volt-ampere consumption of harmonics of each interface converter is designed and implemented. However, the shared reactive power errors can hardly be completely eliminated using this method, especially in weak MGs.

Furthermore, the island operation can be considered as one of the most attractive features of an MG, as it guarantees service continuity in case of network interruption [14]. When the MG is in island operation mode, the DG units must be able to cooperatively regulate the voltage and frequency, and maintain the balance between

power generation and the power consumed by the load within the MG. Consequently, the concepts of droop control have been widely adopted in [9,15,16] to provide decentralized control of power sharing without relying on communications.

As the MG allows DG units to work in an island operation mode, the system can improve reliability and power quality for customers [14]. However, when operating in island mode some challenging issues appears such as the difficulty of maintaining the power balance between generation and loads and reactive power sharing [15,17]. When an MG operates in island mode, the droop control technique provides a decentralized control capability that does not depend on external communication links in the control strategy; although the frequency droop technique can manage active power sharing accurately, the voltage droop technique generally results in a poor reactive power sharing, due to the mismatch in the impedances of the DG unit feeders and, also, due to the different values of DG units [18]. Consequently, the reactive power sharing problem in an MG working in island operation mode has received considerable attention in the literature and many control techniques have been developed to address this problem [5,19–22].

Commonly, in high voltage networks the reactive power sharing among generators is not usually a major concern due to capacitive compensation between loads and transmission lines. However, in low-voltage MGs, the low capacity to supply reactive power from generation sources and compensators, and small distances between units, does not allow an exact distribution of reactive power to avoid overloads [23]. Line impedances and DG impedances significantly affect the reactive power sharing during the operating mode connected to the network and during the island mode, due to voltage drops [20]. At present, the voltage controllers in the MGs are unable to share

the demand for reactive power among even identical inverters operating in parallel [24]. Some researchers have previously worked on this issue, as in [21], which propose an alternative controller for reactive power sharing between parallel inverters with nominal voltages. The method requires that each unit have a common load voltage measurement, which limits its applicability in more complex MG scenarios with multiple loads.

The references consulted in this research show that the previous documents have focused more on performing an active power control and reactive power sharing still require better applications to improve accuracy. Therefore, the objective of this work is to show that the reactive power can be shared between generators in an MG more accurate by using virtual current injected to the current controller of the inverter to optimize the output signal. The main contribution in this paper is related to the virtual currents that calculated from each inverter based on the active output power of the inverter. This new current control achieves an accurate exchange of reactive power between generators of the MG when load variations are presented. Thus, Section 2 explains the new control strategy for sharing reactive power after each load variation. Furthermore, Section 3 presents the mathematical formulation of the control method, small-signal model, current loop controller, three-phase half-bridge circuit, output LC filter, line impedance, and the inverter used in the control strategy. Even more, Section 4 shows the results of the simulations performed in a distribution system test case by using the MATLAB-Simulink software. Finally, Section 5 presents the conclusions and future work.

4.2 Materials and Methods

4.2.1 Control Method

A strategy with a virtual current is proposed as a method to control the reactive power and voltage in the MG, when load changes in certain periods of time. Figure 1 shows a detailed configuration of a DG unit using the proposed control strategy. The P-ω controller is adopted to regulate the frequency and achieve an accurate exchange of active power between the different DGs that conform the MG. The virtual current is obtained from the active power divided by a virtual impedance and used as a current input for the controller. To subtract from the value that comes out of the voltage controller which is a proportional resonant (PR) and the measured current. This current controller works with a P (proportional) which increases the signal that is sent to the PWM to make the switch in the inverter to obtain the desired current and voltage values.

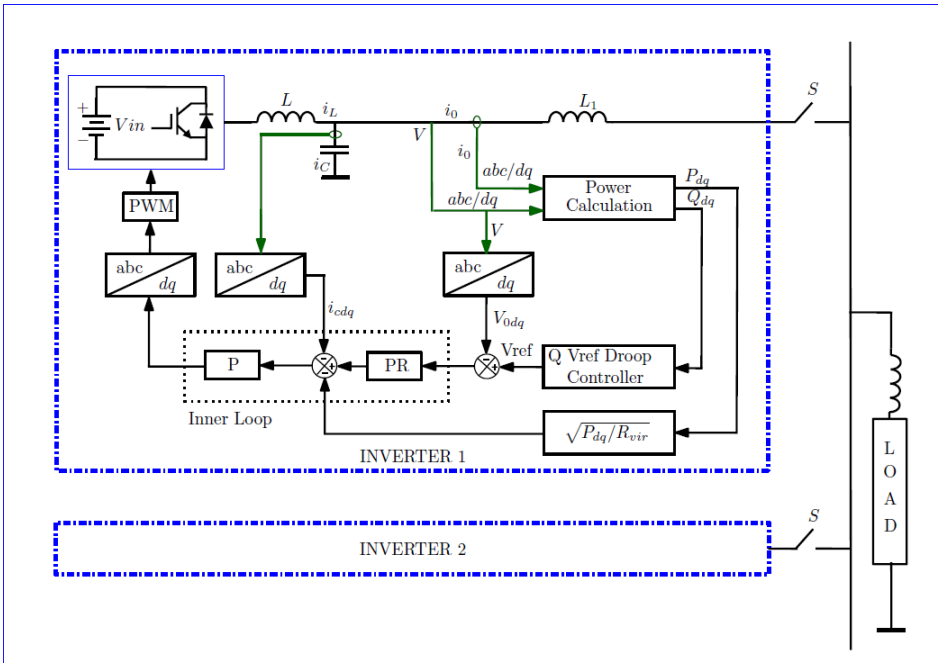

Figure 1. Droop controller with the virtual current.

4.2.2 Small-signal model

To analyze the stability of the controller, a small-signal model of the inverters with the proposed control strategy is included. Each inverter is modeled with individual reference and includes the dynamics of the voltage and current controller, LC filter, and line impedance, to reach the equilibrium point. The internal voltage controller is based on a PR structure in the steady-state reference, where generalized integrators are used to achieve a zero steady-state error. Based on the abc/dq coordinated transformation principle, a three-phase system can be modeled in two independent single-phase systems. Thus, the block diagram of Figure 2 shows the voltage controller in a synchronous reference frame that includes all feedback terms and the four states A_{dq} and B_{dq}.

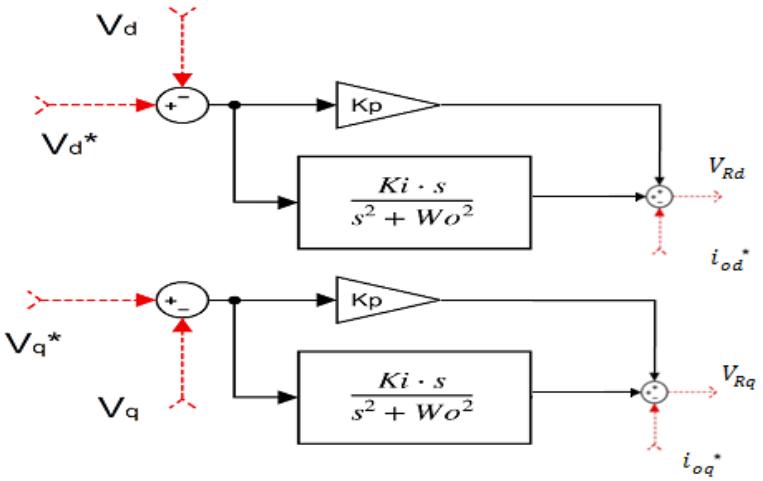

Figure 2. Droop controller with the virtual current.

The corresponding state equations can be expressed as in Equations (1) and (2):

$$\frac{dA_d}{dt} = (V_d^* - V_d) - w_0{}^2 B_q + w_0 A_q, \quad (1)$$

$$\frac{dA_q}{dt} = \left(V_q^* - V_q\right) - w_0{}^2 B_q - w_0 A_d. \quad (2)$$

Thus, the algebraic equations are expressed as in Equations (3) and (4):

$$i_{id}{}^{*} = k_{pv}(V_d{}^{*} - V_d) + k_{iv}B_d + I_{Rd}, \quad (3)$$

$$i_{iq}{}^{*} = k_{pv}\left(V_q{}^{*} - V_q{}^{*}\right) + k_{iv}B_q + \ I_{Rq}. \quad (4)$$

The linearized small-signal state space models of the voltage controller are presented in Equation (5).

$$\begin{bmatrix}\Delta\dot{A}_{dq}\\ \Delta B_{dq}\end{bmatrix} = A_{vol}\begin{bmatrix}\Delta A_{dq}\\ \Delta B_{dq}\end{bmatrix} + B_{vol1}\left[\Delta V_{odq}{}^{*}\right] + B_{vol2}\begin{bmatrix}\Delta i_{idq}\\ \Delta V_{odq}\end{bmatrix}, \quad (5)$$

where, the terms A_{vol} is the system matrix. B_{vol1}, and B_{vol2} are the input matrices as shown in Equations (6), (7), and (8).

$$A_{vol} = \begin{bmatrix} 0 & w_0 & -w_0{}^2 & 0 \\ -w_0 & 0 & 0 & -w_0{}^2 \\ 1 & 0 & 0 & w_0 \\ 0 & 1 & -w_0 & 0 \end{bmatrix}, \quad (6)$$

$$B_{vol1} = \begin{bmatrix} 1 & 0 \\ 0 & 1 \\ 0 & 0 \\ 0 & 0 \end{bmatrix}, \quad (7)$$

$$B_{vol2} = \begin{bmatrix} 0 & 0 & 0 & 0 \\ 0 & 0 & 0 & 0 \\ -1 & 0 & 0 & 0 \\ 0 & -1 & 0 & 0 \end{bmatrix}, \quad (8)$$

The linearized small-signal state space models of the voltage controller are presented in Equation (9).

$$\left[\Delta i_{dq}{}^{*}\right] = C_{vol}\begin{bmatrix}\Delta A_{dq}\\ \Delta B_{dq}\end{bmatrix} + D_{vol1}[\Delta V_{od}{}^{*}] + D_{vol2}\begin{bmatrix}\Delta i_{idq}\\ \Delta V_{odq}\end{bmatrix} + D_{vol3}[\Delta I_{Rdq}] \quad (9)$$

where, the terms C_{vol} is the output matrix, and the terms D_{vol1}, D_{vol2}, and D_{vol3} are the feed-forward matrices as shown in Equations (10)-(13).

$$C_{vol} = \begin{bmatrix} 0 & 0 & k_{iv} & 0 \\ 0 & 0 & 0 & K_{iv} \end{bmatrix}, \quad (10)$$

$$D_{vol1} = \begin{bmatrix} k_{pv} & 0 \\ 0 & k_{pv} \end{bmatrix}, \quad (11)$$

$$D_{vol2} = \begin{bmatrix} 0 & 0 & -k_{pv} & 0 \\ 0 & 0 & 0 & -k_{pv} \end{bmatrix}, \quad (12)$$

$$D_{vol3} = \begin{bmatrix} 1 & 0 \\ 0 & 1 \end{bmatrix}; \quad (13)$$

4.2.3 Current loop controller

The internal current controller is based on a stationary frame structure as shown in Figure 3.

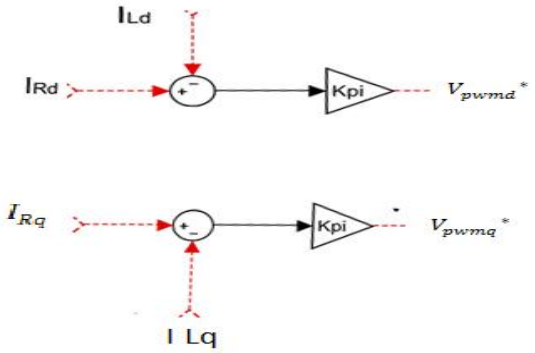

Figure 3. Internal current controller.

The input currents on the d and q axis for the controller are I_{Rd} and I_{Rq}, which are the result of the algebraic sum of the output current of the voltage controller ${i_{od}}^*$ and ${i_{oq}}^*$, minus the virtual current as expressed in Equations (14) and (15):

$$I_{Rd} = {i_{od}}^* - {i_{od}}^{**}, \quad (14)$$

$$I_{Rq} = {i_{oq}}^{*} - {i_{oq}}^{**}. \quad (15)$$

Next, the previous equations related to the d and q axes are obtained by replacing the value of the virtual current ${i_{od}}^{**}$ and ${i_{oq}}^{**}$, with its equivalent $\left(\frac{P_{odq}}{R_{vir}}\right)^{\frac{1}{2}}$.

The algebraic equations for the reference current can be expressed as in Equations (16) and (17):

$$I_{Rd} = {i_{od}}^{*} - \left(\frac{P_{od}}{R_{vir}}\right)^{\frac{1}{2}}, \quad (16)$$

$$I_{Rq} = {i_{oq}}^{*} - \left(\frac{P_{oq}}{R_{vir}}\right)^{\frac{1}{2}}, \quad (17)$$

The linearized small-signal state space models of the above equations can be represented in a simple way as shown in Equation (18):

$$\left[I_{Rdq}\right] = C\left[\Delta {i_{odq}}^{*}\right] - D\left[\Delta P_{odq}\right]^{\frac{1}{2}}, \quad (18)$$

where the terms C and D are matrices that can be represented as in Equations (19) and (20):

$$C = \begin{bmatrix} 1 & 0 \\ 0 & 1 \end{bmatrix}, \quad (19)$$

$$D = \begin{bmatrix} \left(\frac{1}{R_{vir}}\right)^{\frac{1}{2}} & 0 \\ 0 & \left(\frac{1}{R_{vir}}\right)^{\frac{1}{2}} \end{bmatrix}. \quad (20)$$

From Figure 3 we can observe and obtain the algebraic equation of the internal loop current control, which can be expressed in Equations (21) and (22):

$$V_{pwmd}{}^{*} = k_{pi}(I_{Rd} - i_{ld}), \tag{21}$$

$$V_{pwmq}{}^{*} = k_{pi}(I_{Rq} - i_{lq}). \tag{22}$$

The linearized small-signal state space models of the current controller loop are presented in Equations (23)-(25).

$$[\Delta V_{pwmdq}{}^{*}] = D_{cor1}[\Delta I_{Rdq}] + D_{cor2}\begin{bmatrix}\Delta i_{idq}\\ \Delta V_{odq}\end{bmatrix}, \tag{23}$$

where, the terms D_{cor1} and D_{cor2} are matrices that contains the control parameters k_{pi} as shown in Equations (24) and (25):

$$D_{cor1} = \begin{bmatrix}k_{pi} & 0\\ 0 & k_{pi}\end{bmatrix}, \tag{24}$$

$$D_{cor2} = \begin{bmatrix}-k_{pi} & 0 & 0 & 0\\ 0 & -k_{pi} & 0 & 0\end{bmatrix}. \tag{25}$$

Based on Equations (11)-(14), the output of the current controller $\Delta V_{pwmdq}{}^{*}$ can be derivated as in Equation (26):

$$[\Delta V_{pwmdq}{}^{*}] = D_{cor1}C_{vol}\begin{bmatrix}\Delta A_{dq}\\ \Delta B_{dq}\end{bmatrix} + D_{cor1}D_{vol1}[\Delta V_{od}{}^{*}] + (D_{cor1}D_{vol2} + D_{cor2})\begin{bmatrix}\Delta i_{idq}\\ \Delta V_{odq}\end{bmatrix} + (D_{cor1}D_{vol3})[\Delta I_{Rdq}]. \tag{26}$$

4.2.4 Three-phase half-bridge circuit and output LC filter

The corresponding state equations are expressed as shown in Equations (27)-(29):

$$\frac{di_{id}}{dt} = \frac{-r}{L} i_{id} + w_0 i_{lq} + \frac{k_{pwm}}{L} V_{pwmd}{}^{*} - \frac{1}{L} V_{od}, \quad (27)$$

$$\frac{di_{iq}}{dt} = \frac{-r}{L} i_{iq} + w_0 i_{ld} + \frac{k_{pwm}}{L} V_{pwmq}{}^{*} - \frac{1}{L} V_{oq}, \quad (28)$$

$$\frac{dV_{od}}{dt} = w_0 V_{oq} + \frac{1}{c} i_{Ld} - \frac{1}{c} i_{od}, \quad (29)$$

$$\frac{dV_{oq}}{dt} = -w_0 V_{od} + \frac{1}{c} i_{Lq} - \frac{1}{c} i_{oq}. \quad (30)$$

The output variables of the LC filter are the state variables V_{odq}. Thus, Equation (31) represents the linearized small-signal state space:

$$\begin{bmatrix} \Delta \dot{\imath}_{idq} \\ \Delta V_{odq} \end{bmatrix} = A_{LC} \begin{bmatrix} \Delta i_{idq} \\ \Delta V_{odq} \end{bmatrix} + B_{LC1} \left[\Delta V_{pwmdq}{}^{*} \right] + B_{LC2} \left[\Delta i_{odq} \right], \quad (31)$$

where the terms A_{LC}, B_{LC1}, and B_{LC2} are matrices that consider the parameters of the system as presented in Equations (32)-(34):

$$A_{LC} = \begin{bmatrix} \frac{-r}{L} & w_0 & \frac{-1}{L} & 0 \\ -w_0 & \frac{-r}{L} & 0 & \frac{-1}{L} \\ \frac{1}{c} & 0 & 0 & w_0 \\ 0 & \frac{1}{c} & -w_0 & 0 \end{bmatrix}, \quad (32)$$

$$B_{LC1} = \begin{bmatrix} \frac{k_{pwm}}{L} & 0 \\ 0 & \frac{k_{pwm}}{L} \\ 0 & 0 \\ 0 & 0 \end{bmatrix}, \quad (33)$$

$$B_{LC2} = \begin{bmatrix} 0 & 0 \\ 0 & 0 \\ \frac{-1}{c} & 0 \\ 0 & \frac{-1}{c} \end{bmatrix}. \quad (34)$$

In Equation (19), the output of the controller in the current loop $\Delta V_{pwmdq}{}^{*}$ can be replaced by Equation (26), then Equation (31) can be expressed as in Equation (35):

$$\begin{bmatrix} \Delta \dot{i}_{idq} \\ \Delta V_{odq} \end{bmatrix} = A_{LC} \begin{bmatrix} \Delta i_{idq} \\ \Delta V_{odq} \end{bmatrix} + B_{LC1} D_{cor1} C_{vol} \begin{bmatrix} \Delta A_{dq} \\ \Delta B_{dq} \end{bmatrix} + B_{LC1} D_{cor1} D_{vol1} \left[\Delta V_{odq}{}^{*}\right] +$$

$$B_{LC1}(D_{cor1} D_{vol2} + D_{cor2}) \begin{bmatrix} \Delta i_{idq} \\ \Delta V_{odq} \end{bmatrix} + B_{LC1} D_{cor1} D_{vol3} \left[\Delta i_{Rdq}\right] + B_{LC2} \left[\Delta i_{odq}\right] \quad (35)$$

4.2.5 Line impedance

Line impedances are considered in the MG to connect each inverter and the load; thus, real line impedance must be considered in the model to identify the power losses of the circuit. The corresponding state equations can be expressed as in Equations (36) and (37):

$$\frac{d_{iod}}{dt} = \frac{-r_L}{L_i} i_{od} + w_0 i_{oq} + \frac{1}{L_i} V_{od} - \frac{1}{L_i} V_{bus\ d}, \quad (36)$$

$$\frac{d_{ioq}}{dt} = \frac{-r_L}{L_i} i_{oq} + w_0 i_{od} + \frac{1}{L_i} V_{oq} - \frac{1}{L_i} V_{bus\ q}. \quad (37)$$

The output variables of the line impedance are the state variables i_{odq}. Linearized models of small-signal state space are as in Equation (38):

$$\left[\Delta \dot{\imath}_{idq}\right] = A_L\left[\Delta i_{odq}\right] + B_{L1}\begin{bmatrix}\Delta i_{idq}\\ \Delta V_{odq}\end{bmatrix} + B_{L2}\left[\Delta V_{bus\ dq}\right], \quad (38)$$

where the terms A_L, B_{L1}, and B_{L2} are matrices that consider the parameters of the system as presented in Equations (39)-(41).

$$A_L = \begin{bmatrix}\frac{-r_L}{L_i} & w_0\\ -w_0 & \frac{-r_L}{L_i}\end{bmatrix}; \quad (39)$$

$$B_{L1} = \begin{bmatrix}\frac{1}{L_i} & 0\\ 0 & \frac{1}{L_i}\end{bmatrix}; \quad (40)$$

$$B_{L2} = \begin{bmatrix}-\frac{1}{L_i} & 0\\ 0 & -\frac{1}{L_i}\end{bmatrix}. \quad (41)$$

4.2.6 Complete model of the inverter

A complete small-signal state space model of the inverter, as expressed in Equations (42) and (43), can be obtained by combining the status space models of the voltage controller, current controller, LC output filter, and line impedance, given by Equations (5), (18), (35) and (38), respectively.

$$[\Delta \dot{X}] = A[\Delta X] + B_1[\Delta V_{odq}{}^*] + B_2\left[\Delta V_{bus\ dq}\right] \quad (42)$$

$$\Delta X = [\ \ \Delta A_{dq}\ \ \Delta B_{dq}\ \ \Delta i_{idq}\ \ \Delta V_{odq}\ \ \Delta i_{odq}\ \ \Delta P_{odq}{}^{\frac{1}{2}}\ \ ] \qquad (43)$$

Next, the complete small-signal state space model of the inverter is obtained with the proposed of applying the control strategy that modifies the current controller by combining the different state space models. Herein, the terms A, B_1, and B_2 correspond to the matrices shown in Equations (44)-(46):

$$A = \begin{bmatrix} A_{vol} & B_{vol2} & 0 & 0 \\ 0 & 0 & C & -D \\ B_{LC1}D_{cor1}C_{vol} & A_{LC} + B_{LC1}(D_{cor1}D_{vol2} + D_{cor2}) & B_{LC2} + B_{LC1}(D_{cor1}D_{vol3}\,C) & 0 \\ 0 & B_{l1} & A_l & 0 \end{bmatrix}, \qquad (44)$$

$$B_1 = \begin{bmatrix} B_{vol1} \\ 0 \\ B_{LC1}D_{cor1}D_{vol1} \\ 0 \end{bmatrix}, \qquad (45)$$

$$B_2 = \begin{bmatrix} 0 \\ 0 \\ 0 \\ B_{L2} \end{bmatrix}. \qquad (46)$$

4.3 Results

This section shows the results related to the response of the power inverter applied to each generator when the control strategy presented in Section 2 is considered. This control strategy is related to the virtual current considered as an input for the current control of the inverter. This strategy allows to share the reactive power with precision and regulate the voltage in the nodes. The simulations were carried out by considering

a distribution network test case where the loads are connected and disconnected at different periods of time.

4.3.1 System test case

The MG used for this investigation is shown in Figure 4. This network is formed by two DGs designed to supply one load. Load considers five household consumptions that are connected and disconnected over time. The power of the DGs must be delivered considering the impedances of the lines, to supply the power of the changing load. In addition, voltage regulation is achieved by using the inverter with the virtual current that changes based on the connected and disconnected loads.

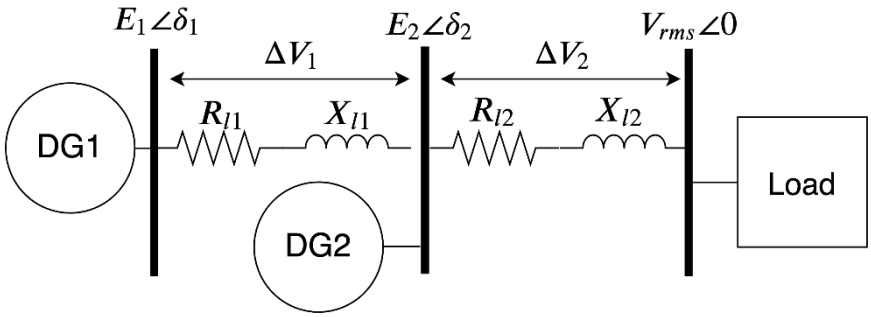

Figure 4. MG test case with two DGs and a load

4.3.2 Active power supplied by DG

Figures 5(a) and 5(b) show the active power delivered by DG1 and DG2, respectively, which consider the droop control versus the virtual current control strategies. The figure shows in red the active power supplied by DGs with the proposed control strategy and in blue the active power supplied by DGs with the droop control strategy. These figures

compare the control strategies and behaviors when the loads are connected and disconnected at different times. The active power increases depending on the amount of power load connected to the node. It is observed that the greater the number of loads connected to the node, the greater the active power consumption.

During the first 12 seconds a load of 10+j0.05 Ω is connected to the load node and both control strategies respond very well to the connection of the load with approximately 1000 W. In the 12-second period a load of 15+j0.05 Ω is connected for a few seconds and the active power consumption of the load in the node is increased by more than 100% based on the consumption of the previous period. The same load is disconnected from the MG at 24 seconds and at the same period a load of 20+j0.60 Ω is connected, where the power consumption is reduced. At 36 seconds a load 25+j0.10 Ω is connected, which generates an active power consumption increase of almost 50% of the initial load. Finally, at 48 seconds the load 10+j0.05 Ω is disconnected, and a load 50+j0.20 Ω is connected, which causes the active power supplied by the two generators to decrease, which allows the system to deliver less active power.

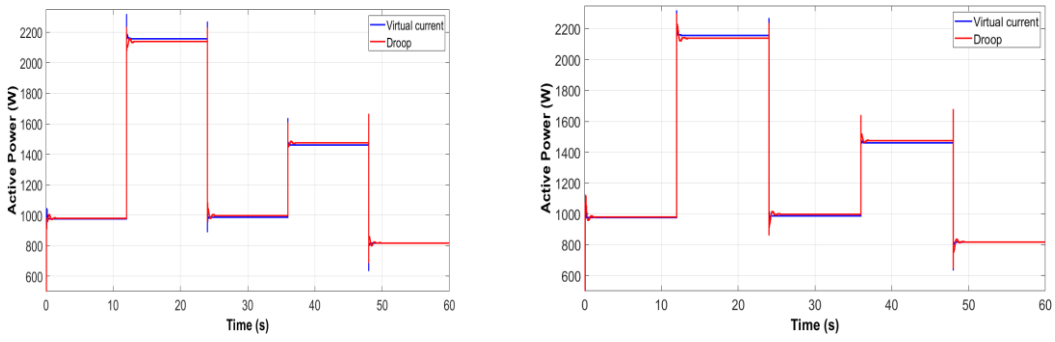

(a) (b)

Figure 5. Active power supplied by (a) DG1 and (b) DG2; when the systems uses virtual current and droop controls

The previous figures show that the new proposed controller responds faster and better than the droop controller when load is connected and disconnected. Besides, both controllers share the active power accurately for the changes. However, the proposed control strategy manages to stabilize the active power much faster than the droop control strategy.

4.3.3 Reactive power supplied by DG

Figures 6(a) and 6(b) show the active power delivered by DG1 and DG2, respectively, which consider the droop control versus the virtual current control strategies. The figure shows in red the reactive power supplied by DGs with the proposed control strategy and in blue the reactive power supplied by DGs with the droop control strategy. These figures compare the control strategies and behaviors when the loads are connected and disconnected at different times. Reactive power increases depending on the amount of power load connected to the node. It is observed that the greater the number of loads connected to the node, the greater the reactive power consumption.

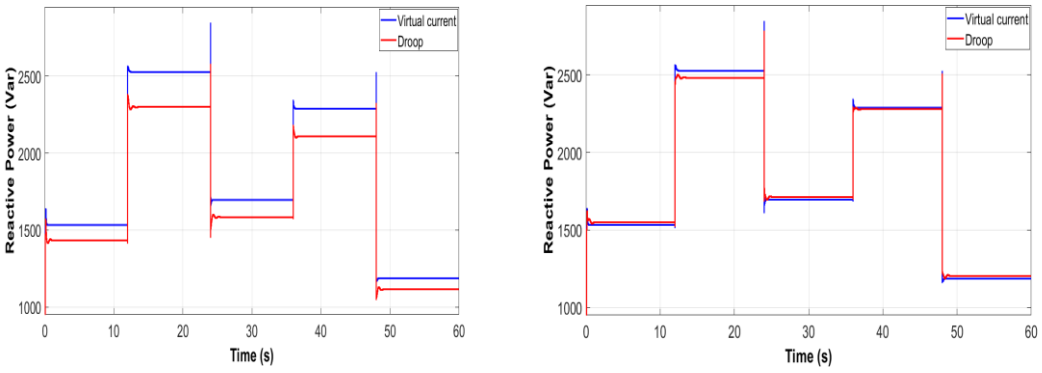

Figure 6. Reactive power supplied by (a) DG1 and (b) DG2; when the systems uses virtual current and droop controls

The results show that the proposed virtual current control strategy manages better the reactive power sharing with different load changes than the droop control. During the first 12 seconds, the load of 10+j0.05 Ω is connected to identify the response of the control strategy and around 1500 VAR of power consumption is observed. Later, after the 12-second period, a load of 15+j0.05 Ω is connected for a few seconds and the reactive power increases and based on the consumption of the previous period, this load is disconnected from the MG at 24 seconds. Then, at the same period a load of 20+j0.60 Ω is connected to the node of the MG and the reactive power is reduced as the load 15+j0.05 Ω has been disconnected and the new connected load is not as large as the previous one. Over a period of 36 seconds a load of 25+j0.10 Ω is connected to the network, which generates a reactive power consumption increase and the control strategy responds quickly to stabilize the power and to share the reactive power with the same amount between the two generators. At 48 seconds a load of 10+j0.05 Ω is disconnected, and a load of 50+j0.20 Ω is connected, which causes a reactive power decrease in the two generators approximately 50% of previous load.

The results show that the droop control strategy does not allow reactive power to be shared with accuracy between the generation units than the new proposed control strategy. The proposed control strategy manages to share with precision the reactive power between two DGs in the MG. Besides, the proposed new controller responds faster and better than the droop controller when load is connected and disconnected at different times and power.

4.3.4 Frequency

Figure 7 shows the frequency of the system using both the droop and the virtual current

controllers, when considering different load variations. The figure shows in red the system frequency with the proposed control strategy and in blue the system frequency with the droop control strategy. These figure is obtained by considering multiple variations in power loads as described above for the active and reactive power.

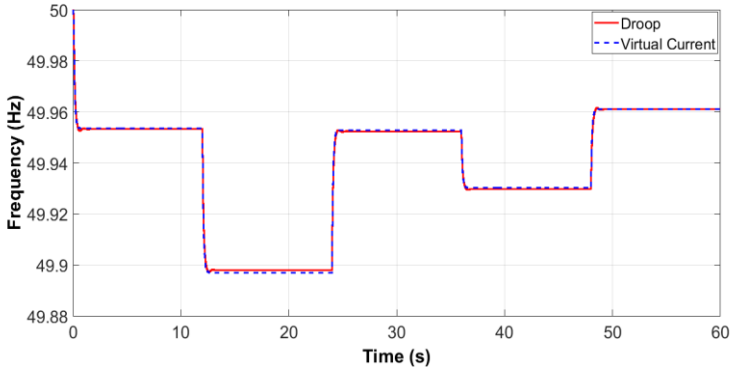

Figure 7. Frequency of the system when using virtual current and droop controls

The previous figures show how both control strategies act when the load changes during different periods of time and the results show that the new proposed controller responds faster and better than the droop controller. Furthermore, the results show that the proposed control strategy ensures that the frequency of the two generators stabilizes at a single value, a few seconds after the load changes. In addition, the more different the change in load on the MG connection, the more abrupt is the change in the frequency value. However, no matter how large the load changes (connection and disconnection of different electrical loads), the controller maintains the frequency close to 50 Hz, which is the desired value.

4.3.5 Voltage and currents

Figure 8 shows the behavior of the RMS voltage at the node where the five electrical loads of the MG are connected. The figure shows in red the voltage in the load with the proposed control strategy and in blue the voltage in the load with the droop control strategy. These results show that at the beginning of the first load connection, the node voltage tends to drop sharply, but immediately the control strategy recovers the voltage to a close original value. Therefore, the proposed control strategy with a virtual current maintains a stable voltage value during the period in which the electrical loads are connected and disconnected. However, when the droop control strategy is used, the voltage drops beyond the proposed method, as the proposed new control strategy responds faster and better than the droop controller.

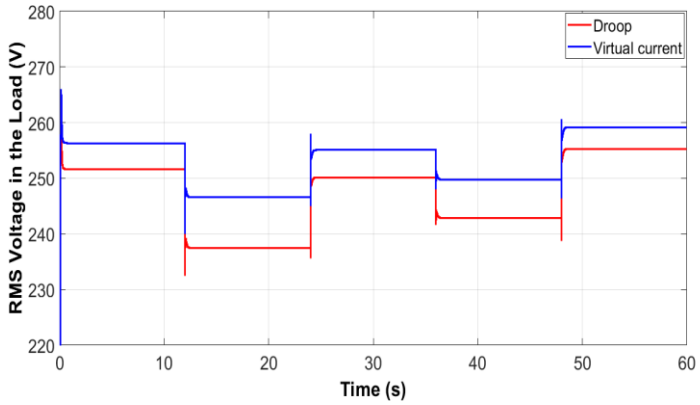

Figure 8. Voltage in the load when using virtual current and droop controls

Figure 9 shows the current consumed in the node where the loads are connected. The figure shows in red the current in the load with the proposed control strategy and in blue the current in the load with the droop control strategy. The current is lower with the proposed current control strategy compared to the droop control strategy, which brings much benefit since there is less loss in the conductors and winding of the inductive load due to joule effect.

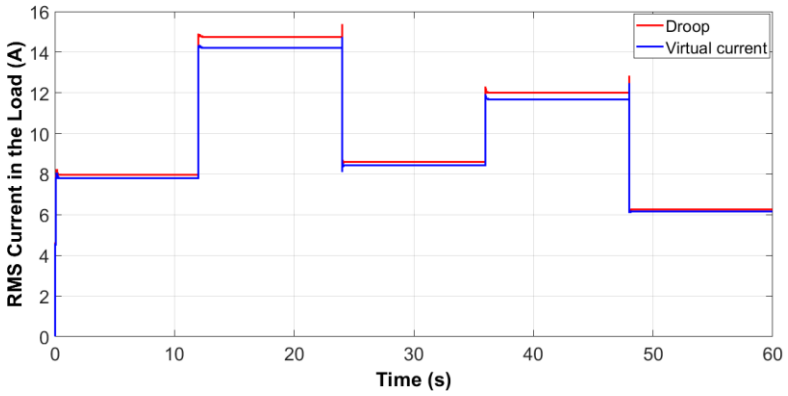

Figure 9. Current in the load when using virtual current and droop controls

4.4 Conclusions

The paper presented a new control strategy that uses a virtual current to share reactive power accurately between two DGs in an MG, when electrical loads are connected and disconnected at different time periods. Results were obtained for a system with two DGs and a load with five different power consumptions, in which the reactive power shared was correctly distributed between the two generators of the MG, according to the time period that corresponds to the variation of the load. Therefore, in a few moments the reactive power supplied by the DGs increases and in another time period it decreases to regulate the voltage in the MG. Therefore, the control strategy based on an adaptive virtual current related to the output power of the inverters works successfully. The proposed control strategy effectively regulates the frequency close to 50 Hz and also maintains the active and reactive power balance. The strategy can be easily adapted to the MG to share accurately the active and reactive power.

4.5 References

1. Guerrero, J.M.; Vasquez, J.C.; Matas, J.; de Vicuna, L.G.; Castilla, M. Hierarchical Control of Droop-Controlled AC and DC Microgrids—A General Approach Toward

Standardization. *IEEE Trans. Ind. Electron.* **2011**, *58*, 158–172.

2. Lasseter, R.H. MicroGrids. In Proceedings of the 2002 IEEE Power Engineering Society Winter Meeting. Conference Proceedings (Cat. No.02CH37309); IEEE; Vol. 1, pp. 305–308.
3. Pogaku, N.; Prodanovic, M.; Green, T.C. Modeling, Analysis and Testing of Autonomous Operation of an Inverter-Based Microgrid. *IEEE Trans. Power Electron.* **2007**, *22*, 613–625.
4. Guerrero, J.M.; Hang, L.; Uceda, J. Control of distributed uninterruptible power supply systems. *IEEE Trans. Ind. Electron.* **2008**, *55*, 2845–2859.
5. Tuladhar, A.; Hua Jin; Unger, T.; Mauch, K. Control of parallel inverters in distributed AC power systems with consideration of line impedance effect. *IEEE Trans. Ind. Appl.* **2000**, *36*, 131–138.
6. Lopes, J.A.P.; Moreira, C.L.; Madureira, A.G. Defining control strategies for microgrids islanded operation. *IEEE Trans. Power Syst.* **2006**, *21*, 916–924.
7. Guerrero, J.M.; GarciadeVicuna, L.; Matas, J.; Castilla, M.; Miret, J. Output Impedance Design of Parallel-Connected UPS Inverters With Wireless Load-Sharing Control. *IEEE Trans. Ind. Electron.* **2005**, *52*, 1126–1135.
8. Pogaku, N.; Prodanovic, M.; Green, T.C. Modeling, Analysis and Testing of Autonomous Operation of an Inverter-Based Microgrid. *IEEE Trans. Power Electron.* **2007**, *22*, 613–625.
9. De, D.; Ramanarayanan, V. Decentralized Parallel Operation of Inverters Sharing Unbalanced and Nonlinear Loads. *IEEE Trans. Power Electron.* **2010**, *25*, 3015–3025.
10. Coelho, E.A.A.; Cortizo, P.C.; Garcia, P.F.D. Small signal stability for single phase inverter connected to stiff AC system. **2003**, 2180–2187.
11. He, J.; Li, Y.W. Analysis, design, and implementation of virtual impedance for

power electronics interfaced distributed generation. *IEEE Trans. Ind. Appl.* **2011**, *47*, 2525–2538.

12. Li, Y.W. Control and resonance damping of voltage-source and current-source converters with LC filters. *IEEE Trans. Ind. Electron.* **2009**, *56*, 1511–1521.
13. Lee, T.L.; Cheng, P.T. Design of a new cooperative harmonic filtering strategy for distributed generation interface converters in an islanding network. *IEEE Trans. Power Electron.* **2007**, *22*, 1919–1927.
14. Zamani, M.A.; Sidhu, T.S.; Yazdani, A. Investigations Into the Control and Protection of an Existing Distribution Network to Operate as a Microgrid: A Case Study. *IEEE Trans. Ind. Electron.* **2014**, *61*, 1904–1915.
15. Rocabert, J.; Luna, A.; Blaabjerg, F.; Rodríguez, P. Control of Power Converters in AC Microgrids. *IEEE Trans. Power Electron.* **2012**, *27*, 4734–4749.
16. Nutkani, I.U.; Loh, P.C.; Blaabjerg, F. Droop Scheme With Consideration of Operating Costs. *IEEE Trans. Power Electron.* **2014**, *29*, 1047–1052.
17. Lee, C.K.; Chaudhuri, B.; Hui, S.Y. Hardware and Control Implementation of Electric Springs for Stabilizing Future Smart Grid With Intermittent Renewable Energy Sources. *IEEE J. Emerg. Sel. Top. Power Electron.* **2013**, *1*, 18–27.
18. Kim, J.; Guerrero, J.M.; Rodriguez, P.; Teodorescu, R.; Nam, K. Mode Adaptive Droop Control With Virtual Output Impedances for an Inverter-Based Flexible AC Microgrid. *IEEE Trans. Power Electron.* **2011**, *26*, 689–701.
19. Guerrero, J.M.; Matas, J.; Garcia de Vicuna, L.; Castilla, M.; Miret, J. Decentralized Control for Parallel Operation of Distributed Generation Inverters Using Resistive Output Impedance. *IEEE Trans. Ind. Electron.* **2007**, *54*, 994–1004.
20. Yun Wei Li; Ching-Nan Kao An Accurate Power Control Strategy for Power-Electronics-Interfaced Distributed Generation Units Operating in a Low-Voltage Multibus Microgrid. *IEEE Trans. Power Electron.* **2009**, *24*, 2977–2988.

21. Zhong, Q.-C. Robust Droop Controller for Accurate Proportional Load Sharing Among Inverters Operated in Parallel. *IEEE Trans. Ind. Electron.* **2013**, *60*, 1281–1290.

22. Lee, C.-T.; Chu, C.-C.; Cheng, P.-T. A New Droop Control Method for the Autonomous Operation of Distributed Energy Resource Interface Converters. *IEEE Trans. Power Electron.* **2013**, *28*, 1980–1993.

23. Simpson-Porco, J.W.; Shafiee, Q.; Dorfler, F.; Vasquez, J.C.; Guerrero, J.M.; Bullo, F. Secondary Frequency and Voltage Control of Islanded Microgrids via Distributed Averaging. *IEEE Trans. Ind. Electron.* **2015**, *62*, 7025–7038.

24. Lopes, J.A.P.; Moreira, C.L.; Madureira, A.G. Defining Control Strategies for MicroGrids Islanded Operation. *IEEE Trans. Power Syst.* **2006**, *21*, 916–924.

5

Control strategy to share reactive power between generators distributed in a microgrid, using a virtual voltage.

Abstract

This research uses a new autonomous effective distribution control strategy for parallel three-phase inverters. In contrast to the conventional droop control, the new controller is capable of giving a high-speed response and accurate to the reactive power sharing because it uses a virtual impedance loop to get a virtual voltage. The virtual impedance is introduced in the inverter's current controller to optimize the result. The small-signal model of the system was developed for the autonomous operation of the inverter-based microgrid with the proposed controller. The model developed shows great stability and a rapid transient response of the system.

5.1 Introduction

With the increased concerns on environment and cost of energy, the power industry is experiencing fundamental changes with more renewable energy sources (RESs) or microsources such as photovoltaic cells, small wind turbines, and microturbines being integrated into the power grid in the form of distributed generation (DG). These RES-based DG systems are normally interfaced to the grid through power electronics [1], distributed generation (DG) has advantages of pollution reduction, high-energy utilization rate, flexible installation location, and low-power transmission losses. DG units also present a higher degree of controllability and operability compared to the conventional generators [2]. which will allow microgrids (MGs) to play a major and critical role in maintaining the stability of electrical networks [3],[4]. So, MGs will gradually be a strong and effective support for the main power grid and potentially one of the future trends of power system [5]. In an islanded MG, the loads must be properly shared by multiple DG units. Conventionally, the frequency and voltage magnitude

droop control is adopted, which aims to achieve MG power sharing in a decentralized manner [6]-[10]. However, the droop control governed MG is prone to have some power control stability problems when the DG feeders are mainly resistive [11].

Islanded operation can be considered as one of the most attractive features of an MG, since it ensures service continuity in the event of a grid interruption [12]. When islanded, distributed generation (DG) units must be able to cooperatively regulate the voltage and frequency, and maintain the generation/load power balance within the MG. Accordingly, droop control concepts have been widely adopted in [13]-[15]. to provide decentralized power sharing control without relying on communications. However, MG always faces challenging problems, such as control stability and power sharing issues [16],[13]. In an islanded MG, the load demand must be properly shared by multiple DG units. That means each DG unit should output power in proportion to its power rating. Commonly, the frequency and voltage magnitude droop control is adopted, which mimics the behavior of synchronous machines in the power systems [17]-[20].

Although the frequency droop technique can achieve accurate real power sharing, the voltage droop technique always results in poor reactive power sharing due to the mismatch in feeder impedances, and also to the different local loads[21]. As a great improvement in droop control application, virtual impedance method can be used to improve the power control stability and power sharing accuracy at the same time In [22]-[24].Configurations often further aggravate reactive power sharing problems [25]. To solve the power control issues, a few improved methods have been proposed. In [[26],[27] the virtual frequency–voltage frame and virtual real and reactive power concept were developed, which improve the stability of the MG system. However, these methods cannot suppress the reactive power sharing errors at the same

time.Islanded MGs have been used in applications like avionic, automotive, marine, or rural areas [28]-[30]. In the case of paralleling inverters, the droop method consists of subtracting proportional parts of the output average active and reactive powers to the frequency and amplitude of each module to emulate virtual inertias. These control loops, also called P − f and Q − E droops, have been applied to parallel connected uninterruptible power systems (UPSs) in order to avoid mutual control wires while obtaining good power sharing [31],[11]. However, although this technique achieves high reliability and flexibility, it has several drawbacks that limit its application.

An MG also allows the DG units to work in an islanded configuration, and therefore improves the availability and quality of power supplied to customers [12]. However, islanded MGs exhibit challenging control problems, such as the difficulty of maintaining generation/load power balance and reactive power sharing. The reason for the popularity of the droop control technique is that it provides a decentralized control capability that does not depend on external communication links Although the frequency droop technique can achieve accurate real power sharing, the voltage droop technique typically results in poor reactive power sharing due to the mismatch in the impedances of the DG unit feeders and, also, due to the different ratings of the DG units [21]. Consequently, the problem of reactive power sharing in islanded MGs has received considerable attention in the literature and many control techniques have been developed to address this issue [32]-[36].

The references consulted in this research show that previous studies have focused more on performing active power control and that reactive power sharing still requires better applications to improve accuracy. Therefore, the objective of this work is to show that the reactive power can be shared between generators in a microgrid (MG) more

accurately by using virtual voltage injected to the voltage controller of the inverter to optimize the output signal.

The main contribution in this paper is related to the virtual voltages calculated from each inverter based on the active output power of the inverter. This new voltage control achieves an accurate exchange of reactive power between generators of the MG when load variations are presented.

Thus, Section 2 explains the new control strategy for sharing reactive power after each load variation. Furthermore, Section 3 presents the mathematical formulation of the control method, small-signal model, voltage loop controller, three-phase half-bridge circuit, output LC filter, line impedance, and the inverter used in the control strategy. In addition, Section 4 shows the results of the simulations performed in a distribution system test case by using the MATLAB-Simulink software. Finally, Section 5 presents the conclusions and future work.

5.2 Materials and Methods

5.2.1 Control Method

voltage in the MG when the load changes during certain periods. Figure 1 shows a detailed configuration of a DG unit using the proposed control strategy. The P-ω controller is adopted to regulate the frequency and achieve an accurate exchange of active power between the different DGs that comprise the MG. The virtual voltage is obtained from the active power multiplied by a virtual impedance and used as a voltage input for the controller, which is a proportional resonant (PR). The output signal is sent

to the current controller that works with a P (proportional), which increases the signal that is sent to the PWM to make the switch in the inverter obtain the desired current and voltage values.

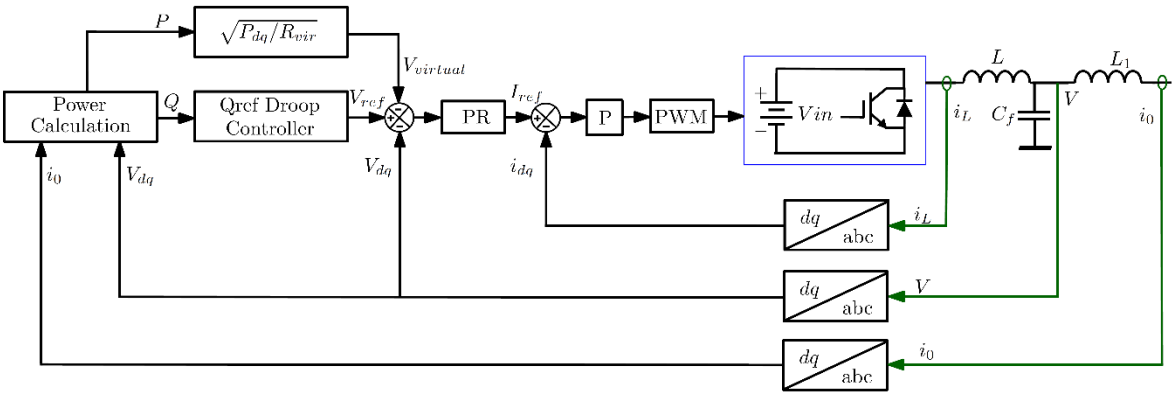

Figure 1. Configuration of a DG unit with the control strategy

5.3 Small-signal Model

A small-signal model was developed to analyze the stability of the system. Simulation is achieved and results are presented to assess the feasibility of the novel approach. The power controller is governed by the behavior of the inverter output currents and voltages, which are measured to obtain the active power that is being generated as shown in Equation (1):

$$\left[\Delta \dot{\mathrm{P}}_{odq}\right] = A_P[\Delta \mathrm{P}_{odq}] + B_P\left[\Delta {V_{odq}}^*\right]. \qquad (1)$$

The modified voltage references that are generated in a stationary reference frame can be easily transferred to the synchronous reference frame and expressed in *dq* coordinates as follows:

$$V_{od}{}^{**} = V_{od}{}^{*} - \sqrt{R_{vir}P_{od}} \qquad (2)$$

$$V_{oq}{}^{**} = V_{oq}{}^{*} - \sqrt{R_{vir}P_{oq}}. \qquad (3)$$

The equations can be rewritten as follows:

$$V_{od}{}^{**} = V_{od}{}^{*} - (R_{vir}P_{od})^{\frac{1}{2}}, \qquad (4)$$

$$V_{oq}{}^{**} = V_{oq}{}^{*} - \left(R_{vir}P_{oq}\right)^{\frac{1}{2}}. \qquad (5)$$

The algebraic equations of voltage reference generation can be expressed as:

$$\left[\Delta V_{odq}{}^{**}\right] = C\left[\Delta V_{odq}{}^{*}\right] - D\left[\Delta P_{odq}\right]^{\frac{1}{2}}, \qquad (6)$$

where

$$C = \begin{bmatrix} 1 & 0 \\ 0 & 1 \end{bmatrix} \quad , \quad D = \begin{bmatrix} R_{vir}{}^{\frac{1}{2}} & 0 \\ 0 & R_{vir}{}^{\frac{1}{2}} \end{bmatrix}. \qquad (7)$$

5.3.1 Voltage loop controller

The inner voltage loop controller is based on a PR structure in the stationary reference frame, where generalized integrators are used to achieve a zero steady-state error. Based on the *abc*/αβ of the coordinated transformation principle, a three-phase system can be modeled in two independent single-phase systems.

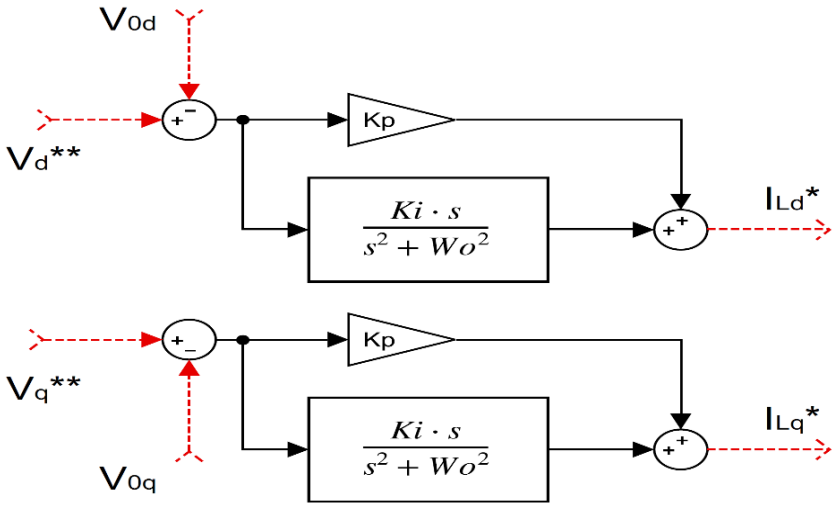

Figure 2. Block diagram of the voltage controller

Figure 2 shows the block diagram of the voltage controller in a synchronous reference frame that includes all feedback and feedback terms. You can see that there are four states, A_{dq} and B_{dq} in Fig. 2. The corresponding state equations can be expressed as:

$$\frac{dA_d}{dt} = (V_d{}^{**} - V_{od}) - w_0{}^2 B_q + w_0 A_q, \qquad (8)$$

$$\frac{dA_q}{dt} = \left(V_q{}^{**} - V_{oq}\right) - w_0{}^2 B_q - w_0 A_d. \qquad (9)$$

The variables A_{dq} and B_{dq} do not have any particular physical meanings but they are states to develop the state–space model:

$$\frac{dB_d}{dt} = A_d + w_0 B_q, \qquad (10)$$

$$\frac{dB_q}{dt} = A_q - w_0 B_d, \qquad (11)$$

as well as the algebraic equations:

$$i_{id}{}^* = k_{pv}(V_d{}^{**} - V_{od}) + k_{iv} B_d, \qquad (12)$$

$$i_{iq}{}^{*} = k_{pv}\left(V_q{}^{**} - V_{oq}\right) + k_{iv}B_q. \qquad (13)$$

The linearized small-signal state–space models of the voltage loop controller are presented in Eqs. (14)–(17):

$$\begin{bmatrix}\Delta\dot{A}_{dq}\\ \Delta B_{dq}\end{bmatrix} = A_{vol}\begin{bmatrix}\Delta A_{dq}\\ \Delta B_{dq}\end{bmatrix} + B_{vol1}\left[\Delta V_{odq}{}^{**}\right] + B_{vol2}\begin{bmatrix}\Delta i_{idq}\\ \Delta V_{odq}\end{bmatrix}, \qquad (14)$$

where

$$A_{vol} = \begin{bmatrix} 0 & w_0 & -w_0{}^2 & 0\\ -w_0 & 0 & 0 & -w_0{}^2\\ 1 & 0 & 0 & w_0\\ 0 & 1 & -w_0 & 0\end{bmatrix}, B_{vol1} = \begin{bmatrix}1 & 0\\ 0 & 1\\ 0 & 0\\ 0 & 0\end{bmatrix}, \quad B_{vol2} = \begin{bmatrix}0 & 0 & 0 & 0\\ 0 & 0 & 0 & 0\\ -1 & 0 & 0 & 0\\ 0 & -1 & 0 & 0\end{bmatrix}, \quad (15)$$

$$\left[\Delta i_{dq}{}^{*}\right] = C_{vol}\begin{bmatrix}\Delta A_{dq}\\ \Delta B_{dq}\end{bmatrix} + D_{vol1}\left[\Delta V_{od}{}^{**}\right] + D_{vol2}\begin{bmatrix}\Delta i_{idq}\\ \Delta V_{odq}\end{bmatrix}, \quad (16)$$

where

$$C_{vol} = \begin{bmatrix}0 & 0 & k_{iv} & 0\\ 0 & 0 & 0 & K_{iv}\end{bmatrix}; \quad D_{vol1} = \begin{bmatrix}k_{pv} & 0\\ 0 & k_{pv}\end{bmatrix}; \quad D_{vol2} = \begin{bmatrix}0 & 0 & -k_{pv} & 0\\ 0 & 0 & 0 & -k_{pv}\end{bmatrix}. \quad (17)$$

5.3.2 Current loop controller

The inner current loop controller in based on a proportional structure in a stationary reference frame. The algebraic equations of current loop controller can be expressed as:

$$V_{pwmd}{}^{*} = k_{pi}(i_{id}{}^{*} - i_{id}), \qquad (18)$$

$$V_{pwmd}{}^{*} = k_{pi}\left(i_{iq}{}^{*} - i_{iq}\right). \qquad (19)$$

The linearized small-signal state–space models of the current loop controller are presented in Eqs. (20)–(22):

$$\left[\Delta V_{pwmdq}{}^{*}\right] = D_{cor1}\left[\Delta i_{idq}{}^{*}\right] + D_{cor2}\begin{bmatrix}\Delta i_{idq}\\ \Delta V_{odq}\end{bmatrix}, \qquad (20)$$

where

$$D_{cor1} = \begin{bmatrix} k_{pi} & 0 \\ 0 & k_{pi} \end{bmatrix} \; ; \quad D_{cor2} = \begin{bmatrix} -k_{pi} & 0 & 0 & 0 \\ 0 & -k_{pi} & 0 & 0 \end{bmatrix}. \tag{21}$$

Based on Eqs. (16) and (20), $\Delta V_{pwmdq}{}^{*}$ can be derived as follows:

$$\left[\Delta V_{pwmdq}{}^{*}\right] = D_{cor1} C_{vol} \begin{bmatrix} \Delta A_{dq} \\ \Delta B_{dq} \end{bmatrix} + D_{cor1} D_{vol1} \left[\Delta V_{odq}{}^{**}\right] + (D_{cor1} D_{vol2} + D_{cor2}) \begin{bmatrix} \Delta i_{idq} \\ \Delta V_{odq} \end{bmatrix}.$$

(22)

5.3.3 Three-phase half-bridge circuit and output LC filter

The corresponding state equations can be expressed as:

$$\frac{di_{id}}{dt} = \frac{-r}{L} i_{id} + w_0 i_{lq} + \frac{k_{pwm}}{L} V_{pwmd}{}^{*} - \frac{1}{L} V_{od}, \tag{23}$$

$$\frac{di_{iq}}{dt} = \frac{-r}{L} i_{iq} + w_0 i_{ld} + \frac{k_{pwm}}{L} V_{pwmq}{}^{*} - \frac{1}{L} V_{oq}, \tag{24}$$

$$\frac{dV_{od}}{dt} = w_0 V_{oq} + \frac{1}{c} i_{Ld} - \frac{1}{c} i_{od}, \tag{25}$$

$$\frac{dV_{oq}}{dt} = -w_0 V_{od} + \frac{1}{c} i_{Lq} - \frac{1}{c} i_{oq}. \tag{26}$$

The output variables of the LC filter are the state variables V_{odq}. The following equations represent the linearized small-signal state–space models:

$$\begin{bmatrix} \Delta \dot{\imath}_{idq} \\ \Delta V_{odq} \end{bmatrix} = A_{LC} \begin{bmatrix} \Delta i_{idq} \\ \Delta V_{odq} \end{bmatrix} + B_{LC1} \left[\Delta V_{pwmdq}{}^{*}\right] + B_{LC2} \left[\Delta i_{odq}\right], \tag{27}$$

$$A_{LC} = \begin{bmatrix} \frac{-r}{L} & w_0 & \frac{-1}{L} & 0 \\ -w_0 & \frac{-r}{L} & 0 & \frac{-1}{L} \\ \frac{1}{c} & 0 & 0 & w_0 \\ 0 & \frac{1}{c} & -w_0 & 0 \end{bmatrix} \quad ; \; B_{LC1} = \begin{bmatrix} \frac{k_{pwm}}{L} & 0 \\ 0 & \frac{k_{pwm}}{L} \\ 0 & 0 \\ 0 & 0 \end{bmatrix} \; ; \; B_{LC2} = \begin{bmatrix} 0 & 0 \\ 0 & 0 \\ \frac{-1}{c} & 0 \\ 0 & \frac{-1}{c} \end{bmatrix}. \qquad (28)$$

In Eq. (27), the output of current loop controller $\Delta V_{pwmdq}{}^{*}$ can be substituted by (22); then, Eq. (27) can be expressed as:

$$\begin{bmatrix} \Delta \dot{\imath}_{idq} \\ \Delta V_{odq} \end{bmatrix} = A_{LC} \begin{bmatrix} \Delta i_{idq} \\ \Delta V_{odq} \end{bmatrix} + B_{LC1} D_{cor1} C_{vol} \begin{bmatrix} \Delta A_{dq} \\ \Delta B_{dq} \end{bmatrix} + B_{LC1} D_{cor1} D_{vol1} \left[\Delta V_{odq}{}^{**}\right] \; +$$

$$B_{LC1}(D_{cor1} D_{vol2} + D_{cor2}) \begin{bmatrix} \Delta i_{idq} \\ \Delta V_{odq} \end{bmatrix} + B_{LC2}\left[\Delta i_{odq}\right]. \qquad (29)$$

Line impedance

Only the real line impedance is considered here because the virtual impedance is already modeled above. The corresponding state equations can be expressed as:

$$\frac{d_{iod}}{dt} = \frac{-r_L}{L_i} i_{od} + w_0 i_{oq} + \frac{1}{L_i} V_{od} - \frac{1}{L_i} V_{bus\,d}, \qquad (30)$$

$$\frac{d_{ioq}}{dt} = \frac{-r_L}{L_i} i_{oq} + w_0 i_{od} + \frac{1}{L_i} V_{oq} - \frac{1}{L_i} V_{bus\,q}. \qquad (31)$$

The output variables of the line impedance are the state variables i_{odq}. The linearized small-signal state–space models are as follows:

$$\left[\Delta \dot{\imath}_{odq}\right] = A_L\left[\Delta i_{odq}\right] + B_{L1} \begin{bmatrix} \Delta i_{idq} \\ \Delta V_{odq} \end{bmatrix} + B_{L2}\left[\Delta V_{bus\,dq}\right], \qquad (32)$$

$$A_L = \begin{bmatrix} \frac{-r_L}{L_i} & w_0 \\ -w_0 & \frac{-r_L}{L_i} \end{bmatrix} \quad ; \quad B_{L1} = \begin{bmatrix} \frac{1}{L_i} & 0 \\ 0 & \frac{1}{L_i} \end{bmatrix} \; ; \quad B_{L2} = \begin{bmatrix} -\frac{1}{L_i} & 0 \\ 0 & -\frac{1}{L_i} \end{bmatrix}. \qquad (33)$$

5.3.4 Complete model of the inverter

A complete small-signal state–space model of the inverter, as expressed in Eqs. (34) and (35), can be obtained by combining the state–space models of the voltage controller, current controller, LC output filter, and line impedance as given by Eqs. (6), (14), (29), and (32), respectively:

5.4 Results

This section shows the results related to the inverter response applied to each generator when considering the control strategy described in Section 2 as related to the virtual voltage that enters the inverter's voltage control. This strategy allows the reactive power to be shared with more accurate results and the voltage to be regulated in the node where the loads are connected. The simulations were conducted considering the case of a distribution grid where the loads are connected and disconnected for a specific period.

5.4.1 System test case

The MG used for this investigation is shown in Figure 3. This network is formed by two DGs designed to supply one load. Load considers five household consumptions that are connected and disconnected over time.

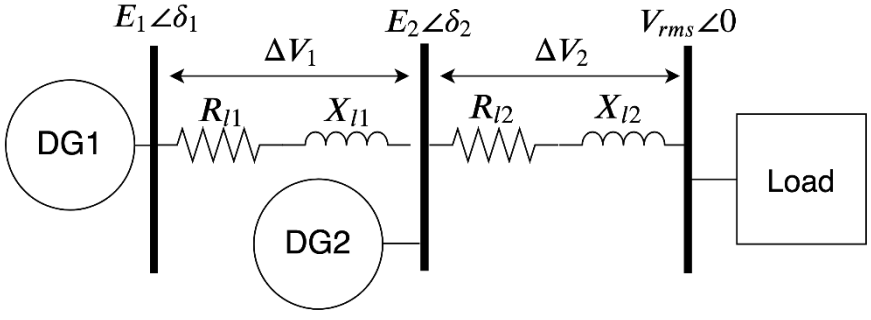

Figure 3. Microgrid test case with two DGs and loads

5.4.2 Active power

The MG used for this research is formed by two DGs designed to supply an electric load. The charging node comprises five electrical loads related to household consumption and connected and disconnected over time. The power of the DGs must be delivered considering the line impedances in order to reach the different loads. In addition, voltage regulation is achieved by using the inverter with a virtual voltage control strategy that changes depending on the variable loads being connected and disconnected.

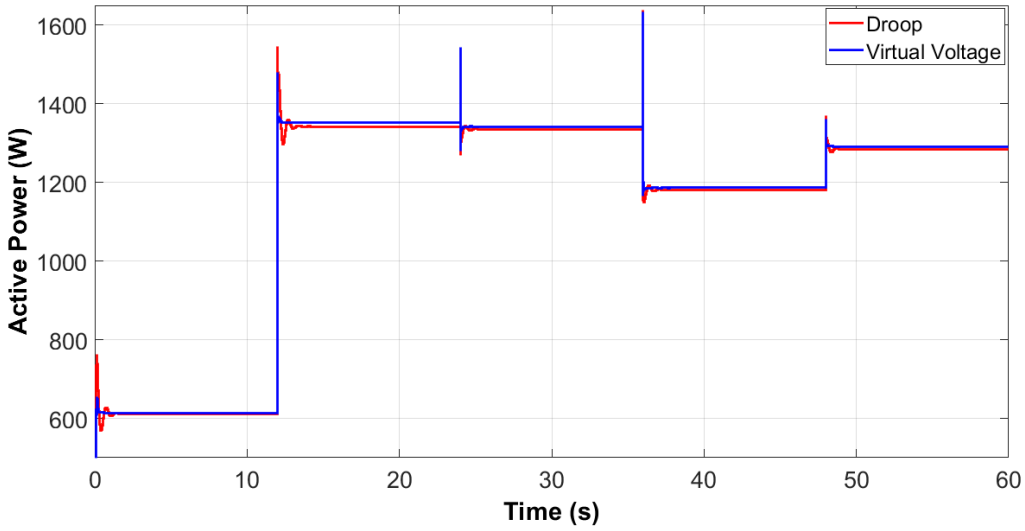

(a)

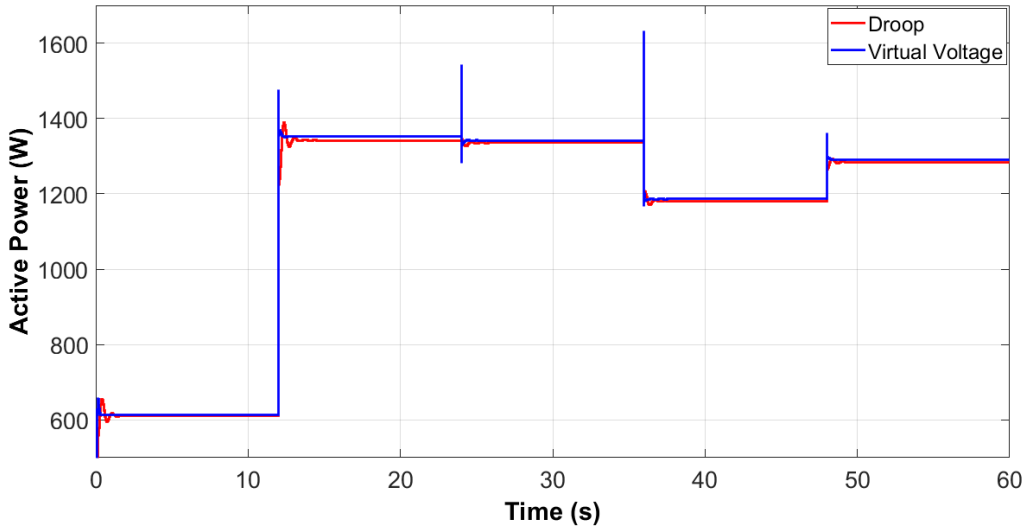

(b)

Figure 3. Active power a) DG1 (virtual voltage control vs. droop control, and b) DG2 (virtual voltage control vs. droop)

Figures 3(a) and 3(b) show the active power delivered by each DG based on the strategy used; i.e., the droop and virtual voltage control strategies. The graphs compare the two control strategies and their reaction to periodic load changes in the MG node. The active power increases depending on the amount of electric load connected to the node; i.e., the greater the number of loads connected to the node, the greater the active power consumption.

Figs. 3(a) and 3(b) show the behavior of the controller with the connection and disconnection of different electrical loads. Furthermore, this figures show how the new proposed controller responds faster and better than the droop controller. It can be seen that both controllers manage to share the active power accurately with the connection and disconnection of different loads. Thus, the proposed control strategy stabilizes the active power much faster than the droop control strategy.

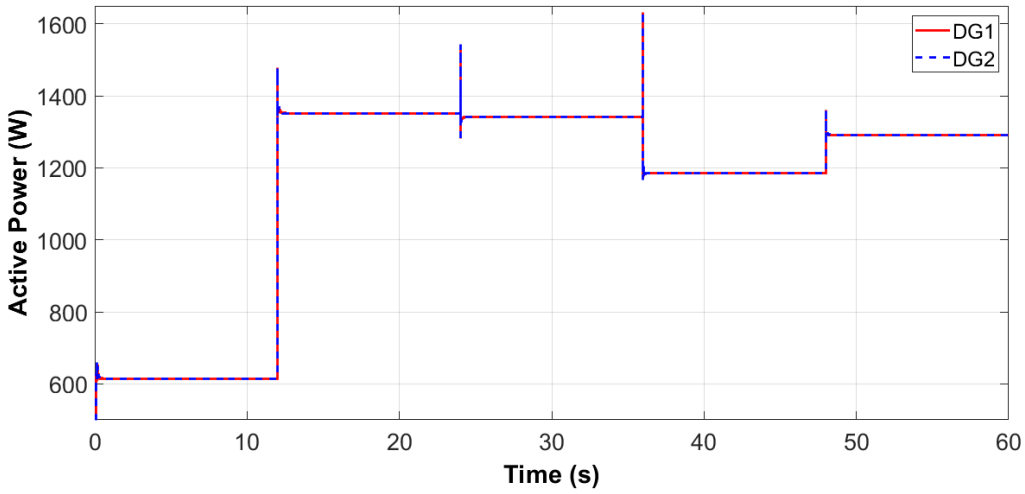

(a)

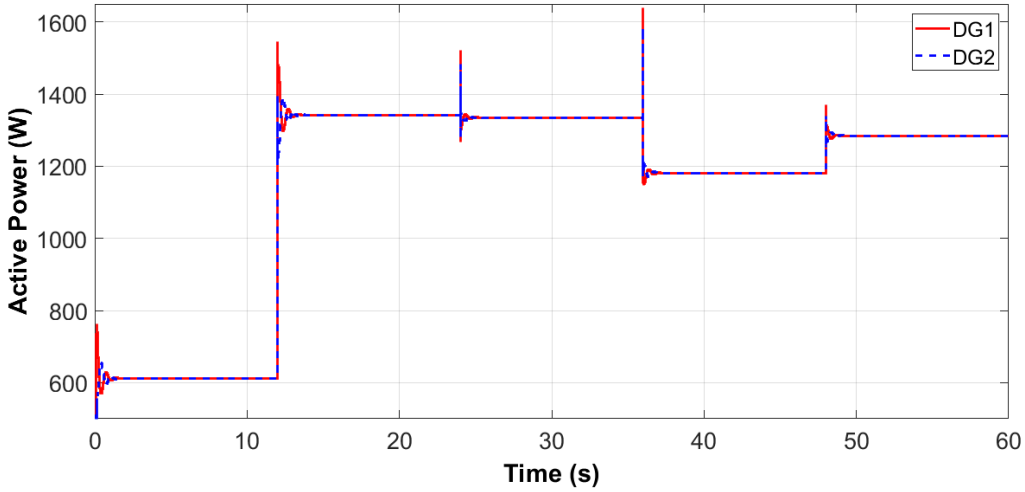

b)

Figure 4. Active power a) virtual voltage and b) droop control

Figs. 4(a) and 4(b) show how the generators DG1 and DG2 share the active power with two different controllers in their inverters. Fig. 4(a) shows the proposed virtual voltage control strategy and Fig. 4(b) shows the droop control strategy. These strategies share the active power accurately in the presence of different load changes. Thus, during the first 12 seconds, the active power consumption of approximately 600 W is presented when a load of (12 + J0.06) Ω is connected. In the 12-second period a load of (17 + J0.05) Ω is connected; in this period, the active power consumption of the

load in the node is increased based on the consumption of the previous period and it is possible to see that both control strategies respond very well to the connection of the new load. In the 24-second period, the load of (12 + J0.06) Ω of the MG is disconnected; in that same period, a load of (22 + J0.07) Ω is connected to the node of the MG. In this period, a slight drop in power consumption is observed but the control strategy acts immediately and recovers the active power of the load at a stable value as the load has been disconnected (12 + J0.05) Ω and the connected load is very similar.

A load of (30 + J0.10) Ω is connected during 36 seconds; in this period, a considerable decrease in the active power consumption in the node is generated. As a consequence, the load 22 + J0.07) Ω is disconnected, which causes the generators to deliver less active power in this period because the connected load is lower than the load that was disconnected in that same instant; however, it is possible to see how the proposed control strategy responds quickly and manages to stabilize the value of the power at a fixed value.

During 48 seconds, a load of (60 + J0.30) Ω is connected, which causes the active power supplied by the two generators to increase based on the previous period. At this point, both controllers respond acceptably to the load change.

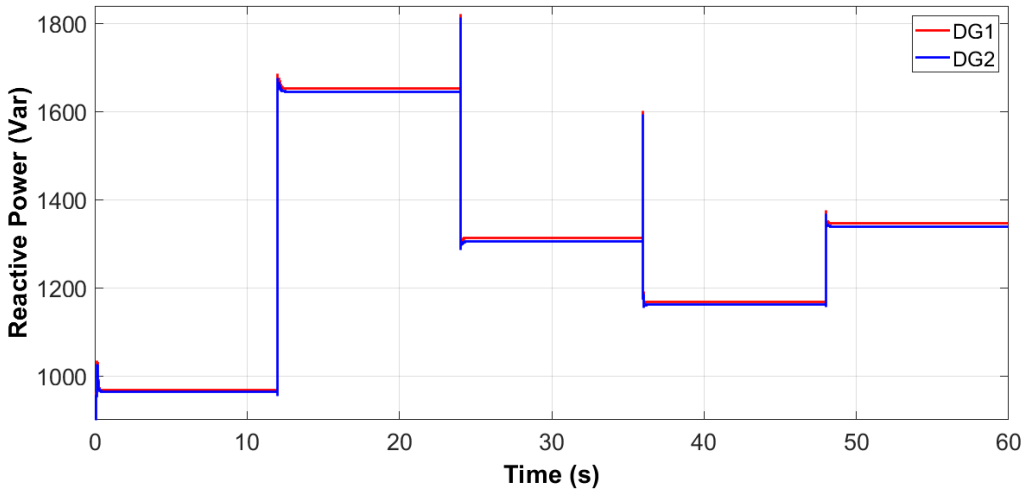

(a)

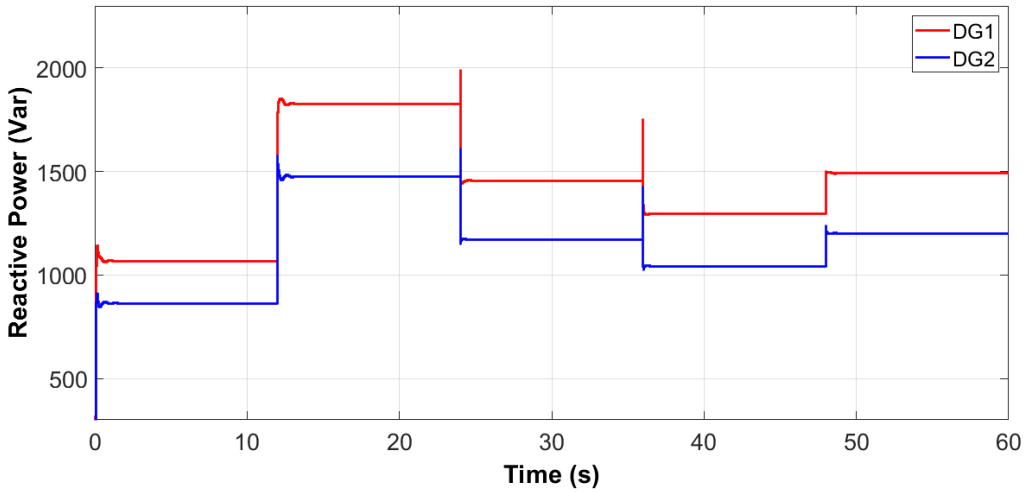

(b)

Figure 5a) Reactive power (virtual voltage) Figure 5b) Reactive power (droop)

Figs. 5(a) and 5(b) shows how the generators DG1 and DG2 share the reactive power, each with two different controller types in their inverters: Fig. 5(a) shows the proposed virtual voltage control strategy and Fig. 5(b) shows the droop control strategy.

The proposed control strategy (virtual voltage) manages to share reactive power

accurately in the presence of different load changes, which is not achieved with the droop control during the first 12 seconds. When a load of (12 + J0.06) Ω is connected, then it is possible to see that the control strategy responds very well to the connection of the load and it is observed that each DG delivers the same reactive power 965 VAR, something that does not happen with the droop control strategy, which does not perform an accurate distribution of the reactive power and where the first DG delivers 1067 VAR and the second generator delivers 863 VAR. In the 12-second period, a load of (17 + J0.05) Ω is connected; in this period, the reactive power consumption of the load in the node is increased based on the consumption of the previous period. In this period, DG1 and DG2 deliver a reactive power of 3300 VAR, where each distributed generator delivers a reactive power of 1650 VAR using the proposed control strategy, whereas with the droop control strategy DG1 delivers a reactive power of 1826 VAR and DG2 delivers 1474 VAR.

In the period of 24 seconds a load of (22 + J0.07) Ω is connected to the MG node. In this period, a drop in reactive power consumption is generated because the load is disconnected (12 + J0.06) Ω and the connected load is not as robust as the previous one. In this period, it is observed that DG1 and DG2 deliver a reactive power of 2620 VAR to the MG where each delivers 1310 VAR with the proposed control strategy. By using the droop control strategy, 2620 VAR is also delivered but is distributed in the following way: DG1 delivers a reactive power of 1450 VAR and DG2 delivers a power of 1170 VAR to the MG.

Over a period of 36 seconds, a load (30 + J0.10) Ω is connected that generates an increase in the consumption of reactive power in the MG to see how quickly the proposed control strategy responds and stabilizes the value of the power at a fixed

value. In this period, the delivery of reactive power of the two generators to the MG is 2336 VAR where each generator delivers 1168 VAR, which achieves an accurate reactive power sharing, unlike the droop control strategy where the distributed generators deliver the same total reactive power but distributed as follows: DG1 delivers 1295 VAR and DG2 delivers 1041 VAR. Between 36 and 48 seconds, the delivery of the reactive power by the generators decreases as a result of the electrical load of (22 + J0.07) Ω being disconnected in that period, which causes lower consumption in the node.

During the 48 seconds, the load (60 + J0.30) Ω is connected, which causes the reactive power supplied by the two generators to increase approximately 15% based on the previous load. From 48 to 60 seconds, the distributed generators deliver a reactive power of 2690 VAR to the MG regardless which control strategy is used. When the proposed control strategy is used, an accurate reactive power sharing is achieved by each DG, where each one delivers 1345 VAR to the MG, whereas when the droop control strategy is used the DG1 delivers a reactive power of 1490 VAR and the DG2 delivers a power of 1200 VAR.

Figures 5(a) and 5(b) show how DG1 and DG2 share the reactive power accurately when they use the proposed control strategy (virtual voltage) instead of the droop control strategy.

Figs. 6(a) and 6(b) show the behavior of the proposed controller (virtual voltage) and the droop controller in the two generators that form the MG and how it responds with the connection and disconnection of different electrical loads. Over the course of the simulation, it is observed that the proposed new controller responds faster and better

than the droop controller; as noted in Figs. 6(a) and 6(b), the Droop controller cannot share accurately the reactive power among the distributed generators that conform the MG.

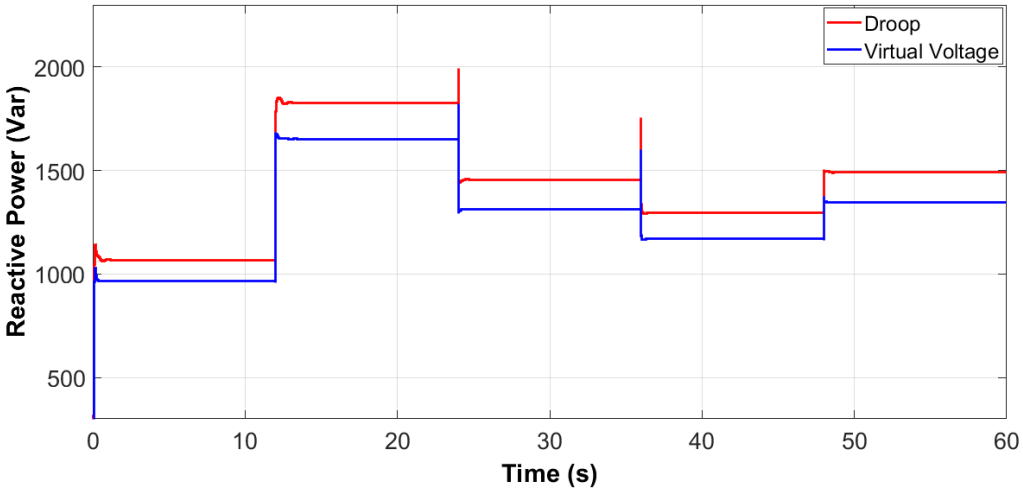

(a)

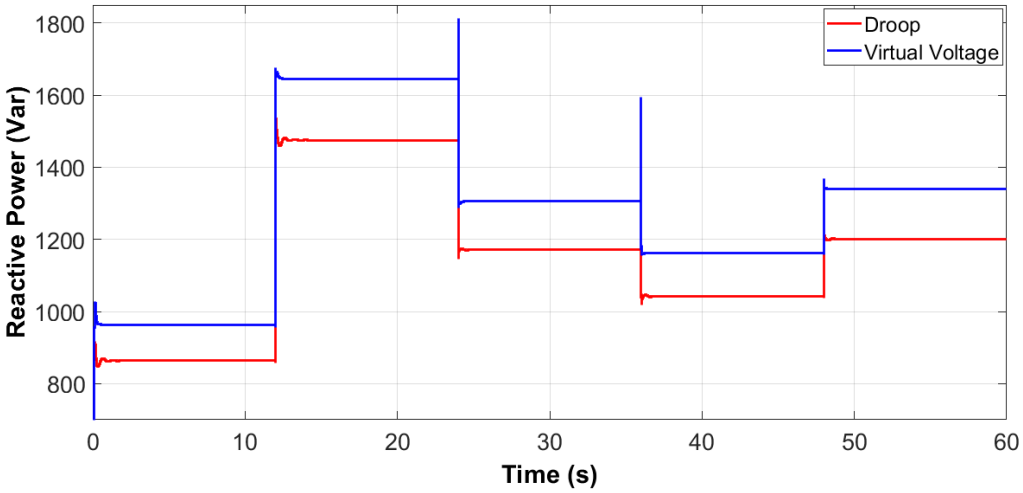

(b)

Figure 6. Reactive power a) virtual voltage vs. droop control in DG1 and b) virtual voltage vs. droop in DG2

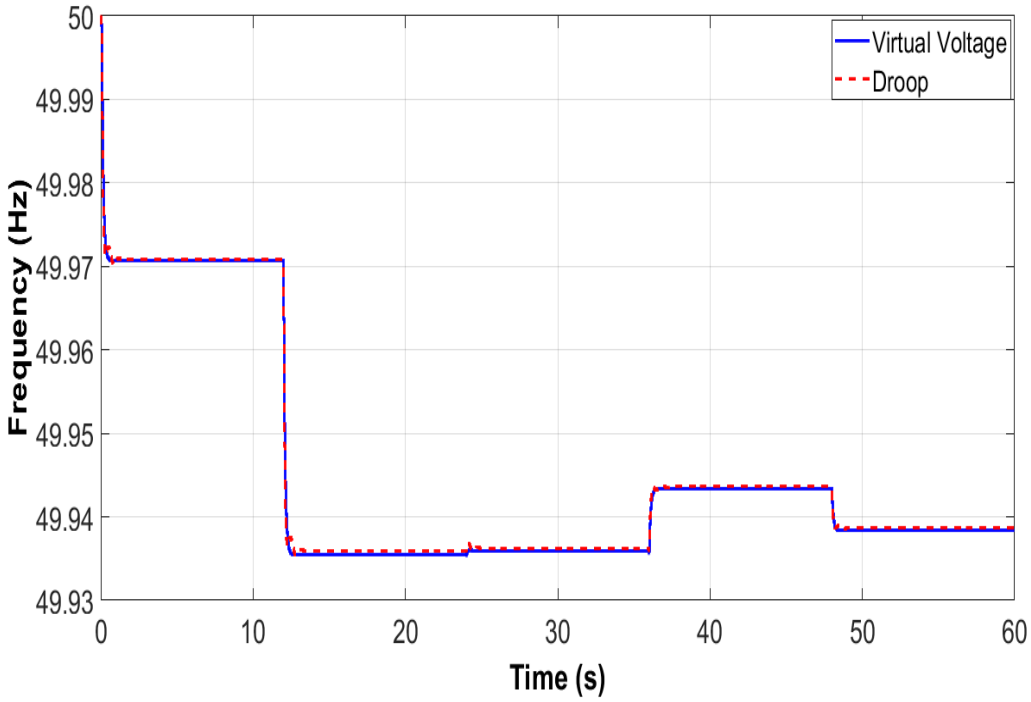

Figure 7. Frequency (virtual voltage vs. droop)

Figs. 7 show how both control strategies (virtual voltage and droop) respond to the connection of different electrical loads during a period in a node of the MG. The proposed new controller of a virtual voltage responds faster and better than the droop controller, given the different load change. It was also possible to observe the behavior of the output frequency in the two distributed generators and their variation with the load changes. These graphs are obtained considering multiple variations in power loads as described above. The results show that the proposed control strategy ensures that the frequency of the two generators is stabilized at a single value a few seconds after the load changes. In addition, the more varied the change in the load on the MG connection, the more abrupt the change in the frequency value. However, no matter how high the change in the variable load (connection and disconnection of different electrical loads), the controller maintains a frequency close to 50 Hz, which is the desired value.

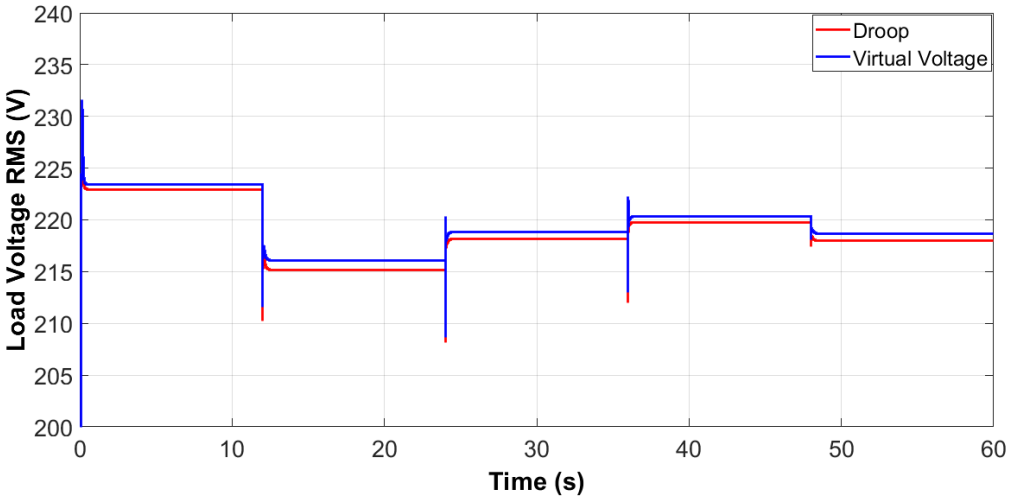

Figure 8 Voltage RMS the load (droop vs. virtual voltage)

Figure 8 shows the behavior of the RMS voltage at the node where the five electrical loads of the MG are connected. The figure shows in red the RMS voltage of the proposed control strategy and, in blue, the droop control strategy. These results show that when the connection of the second load is made, the node voltage tends to drop sharply, but immediately the control strategy recovers the voltage to a close original value. Therefore, the proposed control strategy with a virtual voltage maintains a stable voltage value during all periods when electrical loads are connected and disconnected. However, when the droop control strategy is used, the voltage drops below the value obtained with the proposed control strategy. Therefore, the proposed new control strategy responds faster and better than the droop controller.

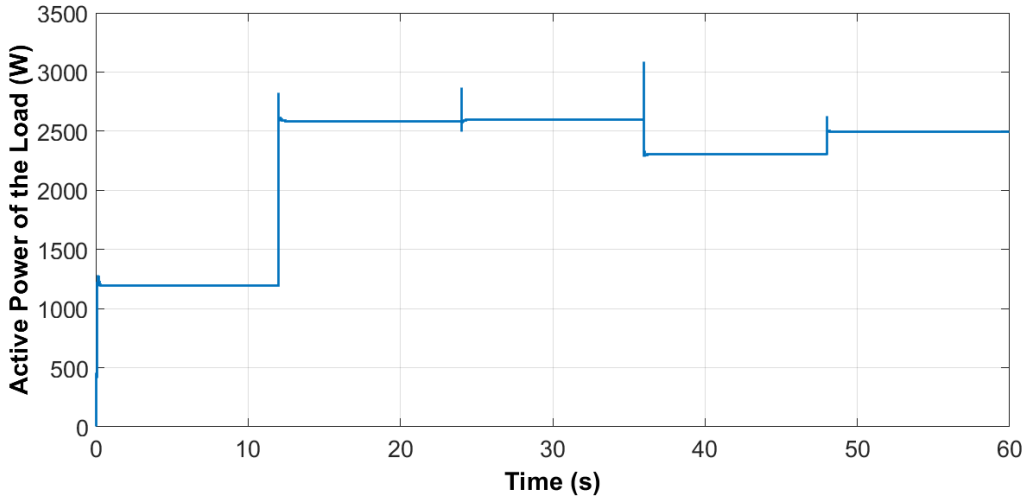

Figure 9a) Active Power of the load (Droop)

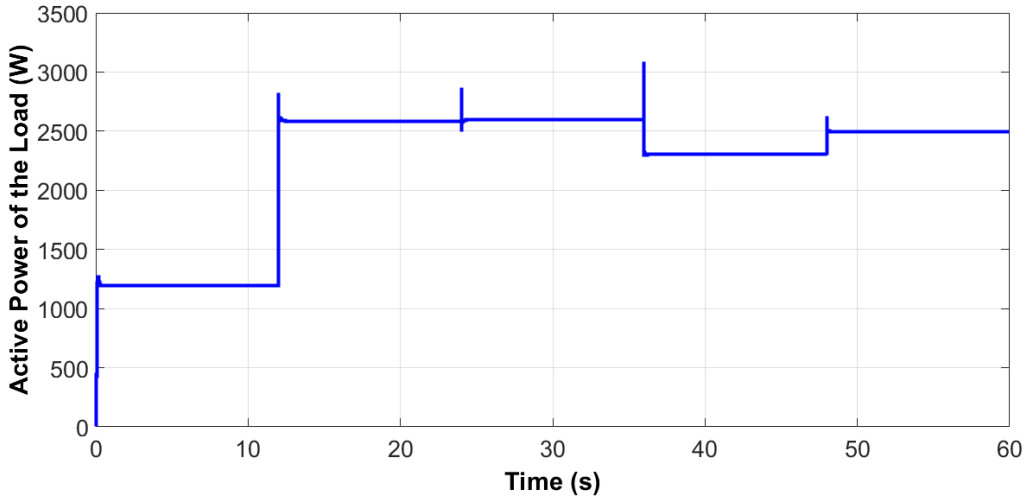

Figure 9b) Active Power of the load (Virtual Voltage)

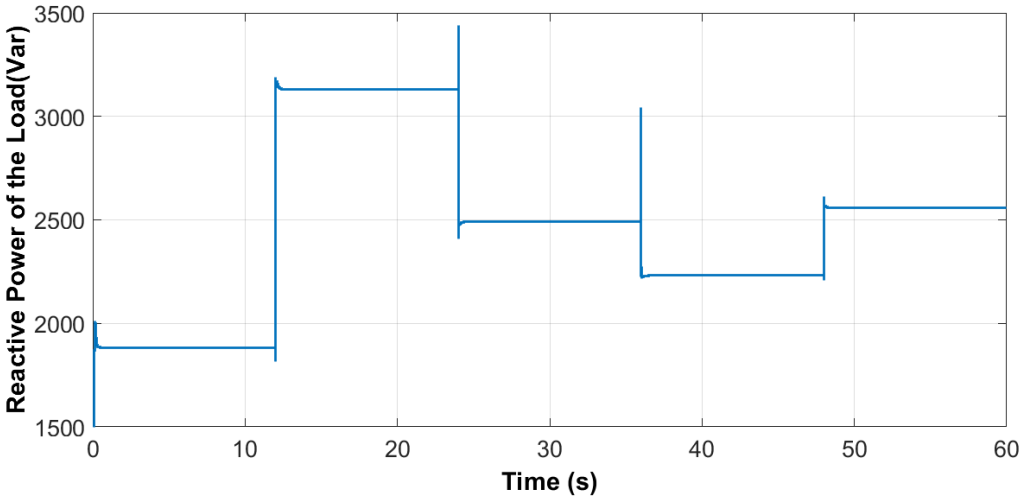

Figure 9c) Reactive Power of the Load (Droop)

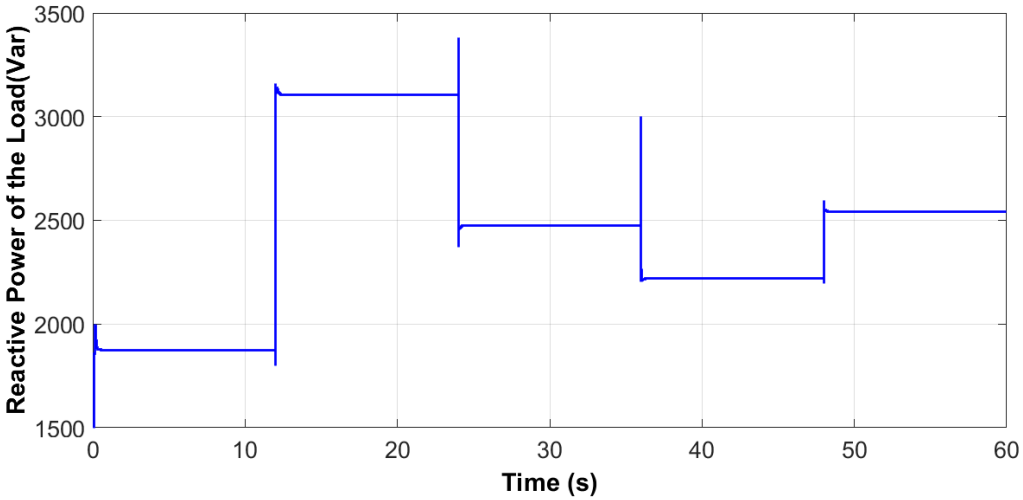

Figure 9d) Reactive Power of the Load (Virtual Voltage)

Figures 9(a)–9(d) show the active and reactive power in the MG node when multiple loads are connected and disconnected from the grid. The active and reactive powers increase depending on the amount of load connected to the node. The active power and reactive power consumed by the loads are the same regardless the control strategy used to regulate and keep the voltage stable in the node where the loads are connected and disconnected.

5.5 Conclusions

This document presented a new control strategy using a virtual voltage to share reactive power accurately between different generators distributed in an MG when electrical loads are connected and disconnected at different times. The results were obtained for a system with two distributed generators, with which it was possible to deliver reactive power accurately among the distributed generators of the MG in the presence of variable load changes. Variations of the load in the MG were presented at different times. After a few moments, the reactive power supplied by the distributed generators increases and in another period it decreases to regulate the voltage in the MG. Therefore, this control strategy based on an adaptive virtual voltage related to the output power of the inverters themselves works successfully. The proposed control strategy effectively regulates the frequency close to 50 Hz and also maintains the active and reactive powers to balance the network. The strategy is useful for the new MG to adapt and share active and reactive power accurately.

5.6 References

[1] J. M. Carrasco *et al.*, “Power-Electronic Systems for the Grid Integration of Renewable Energy Sources: A Survey,” *IEEE Trans. Ind. Electron.*, vol. 53, no. 4, pp. 1002–1016, Jun. 2006.

[2] K. Moslehi and R. Kumar, “A Reliability Perspective of the Smart Grid,” *IEEE Trans. Smart Grid*, vol. 1, no. 1, pp. 57–64, Jun. 2010.

[3] R.H.Lasseter, “MicroGrids,” pp. 305–308, 2002.

[4] R. H. Lasseter and P. Paigi, “Microgrid: a conceptual solution,” in *2004 IEEE*

35th Annual Power Electronics Specialists Conference (IEEE Cat. No.04CH37551), pp. 4285–4290.

[5] A. Molderink, V. Bakker, M. G. C. Bosman, J. L. Hurink, and G. J. M. Smit, “Management and Control of Domestic Smart Grid Technology,” *IEEE Trans. Smart Grid*, vol. 1, no. 2, pp. 109–119, Sep. 2010.

[6] J. M. Guerrero, L. GarciadeVicuna, J. Matas, M. Castilla, and J. Miret, “Output Impedance Design of Parallel-Connected UPS Inverters With Wireless Load-Sharing Control,” *IEEE Trans. Ind. Electron.*, vol. 52, no. 4, pp. 1126–1135, Aug. 2005.

[7] N. Pogaku, M. Prodanovic, and T. C. Green, “Modeling, Analysis and Testing of Autonomous Operation of an Inverter-Based Microgrid,” *IEEE Trans. Power Electron.*, vol. 22, no. 2, pp. 613–625, Mar. 2007.

[8] J. M. Guerrero, J. C. Vasquez, J. Matas, L. G. de Vicuna, and M. Castilla, “Hierarchical Control of Droop-Controlled AC and DC Microgrids—A General Approach Toward Standardization,” *IEEE Trans. Ind. Electron.*, vol. 58, no. 1, pp. 158–172, Jan. 2011.

[9] D. De and V. Ramanarayanan, “Decentralized Parallel Operation of Inverters Sharing Unbalanced and Nonlinear Loads,” *IEEE Trans. Power Electron.*, vol. 25, no. 12, pp. 3015–3025, Dec. 2010.

[10] J. He and Y. W. Li, “An accurate reactive power sharing control strategy for DG units in a microgrid,” in *8th International Conference on Power Electronics - ECCE Asia*, 2011, pp. 551–556.

[11] K. De Brabandere, B. Bolsens, J. Van den Keybus, A. Woyte, J. Driesen, and R. Belmans, “A Voltage and Frequency Droop Control Method for Parallel Inverters,” *IEEE Trans. Power Electron.*, vol. 22, no. 4, pp. 1107–1115, Jul. 2007.

[12] M. A. Zamani, T. S. Sidhu, and A. Yazdani, “Investigations Into the Control and Protection of an Existing Distribution Network to Operate as a Microgrid: A Case Study,” *IEEE Trans. Ind. Electron.*, vol. 61, no. 4, pp. 1904–1915, Apr. 2014.

[13] J. Rocabert, A. Luna, F. Blaabjerg, and P. Rodríguez, “Control of Power Converters in AC Microgrids,” *IEEE Trans. Power Electron.*, vol. 27, no. 11, pp. 4734–4749, Nov. 2012.

[14] I. U. Nutkani, P. C. Loh, and F. Blaabjerg, “Droop Scheme With Consideration of Operating Costs,” *IEEE Trans. Power Electron.*, vol. 29, no. 3, pp. 1047–1052, Mar. 2014.

[15] D. De and V. Ramanarayanan, “Decentralized Parallel Operation of Inverters Sharing Unbalanced and Nonlinear Loads,” *IEEE Trans. Power Electron.*, vol. 25, no. 12, pp. 3015–3025, Dec. 2010.

[16] C. K. Lee, B. Chaudhuri, and S. Y. Hui, “Hardware and Control Implementation of Electric Springs for Stabilizing Future Smart Grid With Intermittent Renewable Energy Sources,” *IEEE J. Emerg. Sel. Top. Power Electron.*, vol. 1, no. 1, pp. 18–27, Mar. 2013.

[17] K. De Brabandere, B. Bolsens, J. Van den Keybus, A. Woyte, J. Driesen, and R. Belmans, “A Voltage and Frequency Droop Control Method for Parallel Inverters,” *IEEE Trans. Power Electron.*, vol. 22, no. 4, pp. 1107–1115, Jul. 2007.

[18] C. N. Rowe, T. J. Summers, R. E. Betz, D. J. Cornforth, and T. G. Moore, “Arctan Power–Frequency Droop for Improved Microgrid Stability,” *IEEE Trans. Power Electron.*, vol. 28, no. 8, pp. 3747–3759, Aug. 2013.

[19] J. A. P. Lopes, C. L. Moreira, and A. G. Madureira, “Defining Control Strategies for MicroGrids Islanded Operation,” *IEEE Trans. Power Syst.*, vol. 21, no. 2, pp.

916–924, May 2006.

[20] M. Savaghebi, A. Jalilian, J. C. Vasquez, and J. M. Guerrero, “Autonomous Voltage Unbalance Compensation in an Islanded Droop-Controlled Microgrid,” *IEEE Trans. Ind. Electron.*, vol. 60, no. 4, pp. 1390–1402, Apr. 2013.

[21] J. Kim, J. M. Guerrero, P. Rodriguez, R. Teodorescu, and K. Nam, “Mode Adaptive Droop Control With Virtual Output Impedances for an Inverter-Based Flexible AC Microgrid,” *IEEE Trans. Power Electron.*, vol. 26, no. 3, pp. 689–701, Mar. 2011.

[22] W. Yao, M. Chen, J. Matas, J. M. Guerrero, and Z.-M. Qian, “Design and Analysis of the Droop Control Method for Parallel Inverters Considering the Impact of the Complex Impedance on the Power Sharing,” *IEEE Trans. Ind. Electron.*, vol. 58, no. 2, pp. 576–588, Feb. 2011.

[23] J. M. Guerrero, J. Matas, L. Garcia de Vicuna, M. Castilla, and J. Miret, “Decentralized Control for Parallel Operation of Distributed Generation Inverters Using Resistive Output Impedance,” *IEEE Trans. Ind. Electron.*, vol. 54, no. 2, pp. 994–1004, Apr. 2007.

[24] J. M. Guerrero, L. GarciadeVicuna, J. Matas, M. Castilla, and J. Miret, “Output Impedance Design of Parallel-Connected UPS Inverters With Wireless Load-Sharing Control,” *IEEE Trans. Ind. Electron.*, vol. 52, no. 4, pp. 1126–1135, Aug. 2005.

[25] P.-T. Cheng, C.-A. Chen, T.-L. Lee, and S.-Y. Kuo, “A Cooperative Imbalance Compensation Method for Distributed-Generation Interface Converters,” *IEEE Trans. Ind. Appl.*, vol. 45, no. 2, pp. 805–815, 2009.

[26] A. Mehrizi-Sani and R. Iravani, “Potential-Function Based Control of a Microgrid in Islanded and Grid-Connected Modes,” *IEEE Trans. Power Syst.*, vol. 25, no. 4, pp. 1883–1891, Nov. 2010.

[27] K. De Brabandere, B. Bolsens, J. Van den Keybus, A. Woyte, J. Driesen, and R. Belmans, “A Voltage and Frequency Droop Control Method for Parallel Inverters,” *IEEE Trans. Power Electron.*, vol. 22, no. 4, pp. 1107–1115, Jul. 2007.

[28] M. C. Chandorkar, D. M. Divan, and R. Adapa, “Control of parallel connected inverters in standalone AC supply systems,” *IEEE Trans. Ind. Appl.*, vol. 29, no. 1, pp. 136–143, 1993.

[29] A. Tuladhar, Hua Jin, T. Unger, and K. Mauch, “Control of parallel inverters in distributed AC power systems with consideration of line impedance effect,” *IEEE Trans. Ind. Appl.*, vol. 36, no. 1, pp. 131–138, 2000.

[30] R. Majumder, A. Ghosh, G. Ledwich, and F. Zare, “Angle droop versus frequency droop in a voltage source converter based autonomous microgrid,” in *2009 IEEE Power & Energy Society General Meeting*, 2009, pp. 1–8.

[31] J. M. Guerrero, J. Matas, L. G. de Vicuna, N. Berbel, and J. Sosa, “Wireless-control strategy for parallel operation of distributed generation inverters,” in *Proceedings of the IEEE International Symposium on Industrial Electronics, 2005. ISIE 2005.*, 2005, pp. 845–850 vol. 2.

[32] J. M. Guerrero, J. Matas, L. Garcia de Vicuna, M. Castilla, and J. Miret, “Decentralized Control for Parallel Operation of Distributed Generation Inverters Using Resistive Output Impedance,” *IEEE Trans. Ind. Electron.*, vol. 54, no. 2, pp. 994–1004, Apr. 2007.

[33] A. Tuladhar, Hua Jin, T. Unger, and K. Mauch, “Control of parallel inverters in distributed AC power systems with consideration of line impedance effect,” *IEEE Trans. Ind. Appl.*, vol. 36, no. 1, pp. 131–138, 2000.

[34] Yun Wei Li and Ching-Nan Kao, “An Accurate Power Control Strategy for Power-Electronics-Interfaced Distributed Generation Units Operating in a Low-

Voltage Multibus Microgrid," *IEEE Trans. Power Electron.*, vol. 24, no. 12, pp. 2977–2988, Dec. 2009.

[35] Q.-C. Zhong, "Robust Droop Controller for Accurate Proportional Load Sharing Among Inverters Operated in Parallel," *IEEE Trans. Ind. Electron.*, vol. 60, no. 4, pp. 1281–1290, Apr. 2013.

[36] C.-T. Lee, C.-C. Chu, and P.-T. Cheng, "A New Droop Control Method for the Autonomous Operation of Distributed Energy Resource Interface Converters," *IEEE Trans. Power Electron.*, vol. 28, no. 4, pp. 1980–1993, Apr. 2013.

6

6. Conclusions and Future Work

This chapter gathers the most relevant conclusions obtained in the development of the thesis and presents future works that can be investigated to continue the line initiated in this study.

One of the most interesting conclusions derived from the present work is the high complexity of the electrical system during load variation and the regulation of the voltage in the MG. This situation is solved by the enormous flexibility that power inverters can demonstrate in this type of situation. This flexibility of DGs is a fundamental aspect that must be highlighted and enhanced as it makes it possible to continue expanding and improving the introduction of DG systems in electric models.

In addition, the control strategies can provide safe operation even during severe load changes. This capability is an extremely powerful tool for new decentralized electrical models. The proposed control strategies, and others that will be developed in the future, allow MGs to autonomously provide better solutions and ensure power quality and reliability.

In Chapter 3, a new control strategy was proposed using a virtual RMS voltage to share the reactive power between different DGs in an MG when different electrical loads are connected over time in the MG. Results were obtained for a system with three DGs that shares reactive power between the DGs of the MG in view of load changes and according to variation of load in the MG. Therefore, at each moment, the active power and the reactive power supplied by the distributed generators both increase. Therefore, this control strategy, based on an adaptive virtual RMS voltage related to the RMS voltage of the load node, works successfully; that is, the strategy maintains the active and reactive power to balance the MG. This strategy is useful for new MGs to adapt and share active and reactive power.

In Chapter 4, this document presented a new control strategy to ensure that the power of the different DGs that conform the MG share the active and reactive power proportionally. It was achieved that the three DGs delivered the same output of active power, regardless where the electric vehicle is connected. In the case of reactive power sharing, it was possible to deliver a proportional power to the place where the load connection was made. In some moments the reactive power delivered to the MG by the DGs is greater and in other time periods it is less. Therefore, we conclude that this control strategy works properly to control the voltage of the different nodes in the MG. This control strategy manages to effectively control the frequency of the MG at a value close to 50 Hz. Furthermore, it effectively controls the active and reactive power delivered to each node when load changes in a certain time period. This strategy is useful for current distribution grids as they are not prepared to meet extra load, regardless the distance of connected and disconnected loads as in the case of electric vehicles shown in this thesis.

Chapter 5 presented a new control strategy using a virtual current to share reactive power accurately between different generators distributed in an MG when electrical loads are connected and disconnected at different time periods in the MG. Results were obtained for a system with two DGs, with which it was possible to deliver reactive power accurately among the DGs of the MG, according to the time period of the load variation in the MG. Therefore, this control strategy based on an adaptive virtual current related to the output power of the inverters themselves works successfully. The proposed control strategy effectively regulates the frequency close to 50 Hz and maintains the active and reactive power balance in the grid. This strategy is useful for new MGs to adapt and share active and reactive power accurately.

Chapter 6 presented a new control strategy using a virtual voltage to share reactive power accurately between different DGs in an MG when electrical loads are connected and disconnected at different time periods in a node. Results were obtained for a system with two DGs, with which it was possible to deliver reactive power accurately among the DGs of the MG when the different loads change. Therefore, in a few moments, the reactive power supplied by the DGs increases and, in another period, decreases to regulate the voltage in the MG. This strategy is useful for new MGs to adapt and share active and reactive power accurately.

6.1 Future work

Future works derived from this thesis include the following:

These strategies can be extended to multiple MGs connected in parallel and their behavior observed. It would be very interesting to observe the behaviors of a great number of inverters in the MG and their connection to different MGs when the load is connected and disconnected. However, a better communication must be implemented in order to send information among MGs.

Open communication infrastructure that includes Ethernet, Internet, and wireless fidelity (WiFi) is increasingly implemented for smart grid communications. However, delay or loss of data may occur during transmission. Therefore, the solution to reduce the cost and increase the margin of delay is one of the important research directions of MGs in the future.

This field is relatively underdeveloped at present, with few published works and with

simplified communication models. Everything indicates that these models will increase in complexity and that control strategies based on communications will be developed that give robustness and reliability to distributed generation plants during load changes and other disturbances.

Other ideas include working on several strategies, such as virtual voltage and current, at the same time. Even more, the control strategy for electric vehicles with bidirectional vehicles can be also studied to deliver active power and reactive power to the MG, whereas in this case we have only worked with unidirectional vehicles that consume energy.

7

ANEXES

Anexe 1

Understanding electricity saving behavior of rural indigenous communities in La Guajira Department, Colombia

Eder Molina[1], John E. Candelo-Becerra[1*], Edgar Ojeda-Camargo[2]

[1]Department of Electrical Energy and Automation, Universidad Nacional de Colombia, Sede Medellín, Carrera 80 No 65 – 223, Medellín Colombia. Email: eamolinav@unal.edu.co, *jecandelob@unal.edu.co

[2]Faculty of Engineering, Universidad de la Guajira, Km 5 Vía Maicao, Guajira, Colombia. E-mail: eojeda@uniguajira.edu.co

Abstract

This paper focuses on identifying how indigenous populations in the upper and middle zones of the La Guajira Department in Colombia save electricity or follow a plan based on an energy policy. To explore this, a survey among seven communities with electricity in the upper and middle zones of La Guajira and a quantitative and observational analysis were conducted. Results show that indigenous communities do not practice a culture of electricity-saving such as, for instance, often failing to turn off idle appliances. In addition, there are neither electricity-saving plans nor energy awareness measures to educate the area's indigenous communities. When comparing the energy consumption of Wayuu communities with that of the country's residential urban dwellers of similar socioeconomic level, few indigenous people using electricity

[1] Corresponding author

efficiently were found, particularly in terms of lighting and appliance use.

Keywords: consumption habits, electricity-saving, energy efficiency, indigenous people, rural communities, La Guajira, Colombia

7.1 Introduction

Energy efficiency leads to a reduction in the consumption of resources and changes any given community's consumption habits. Saving electricity is crucial both for the environment and the technical sustainability of power networks (Harmsen & Graus, 2013; Psomopoulos, Skoula, Karras, Chatzimpiros, & Chionidis, 2010). This importance is magnified for the country's economy (Ek & Söderholm, 2010; Lenzen et al., 2014), particularly for those located in non-interconnected rural areas (Consorcio Energético: CORPOEMA, 2010; Departamento Administrativo de Planeación de La Guajira, 2014; Gilbert, 2004; Mugi-Ngenga et al., 2016).

As seen in La Guajira Department of Colombia, a primary challenge for this type of situation is the annual reduction in the maximum value of electricity subsidized by the state. Determining the electricity saving of rural indigenous communities is, therefore, essential especially in gauging commitment to the country's energy policy plan. Understanding these elements will help the country set more specific and realistic goals, contribute to new and enhanced educational measures on electricity saving for these communities, develop new strategies for improving energy saving, review energy policy requirements, and provide new, optimally adjusted energy systems.

With respect to a rural community's energy supply, various authors have focused on

the economic development opportunities surrounding wind energy (Goodbody, Walsh, McDonnell, & Owende, 2013; Huesca-Pérez, Sheinbaum-Pardo, & Köppel, 2016; Munday, Bristow, & Cowell, 2011). Other authors have suggested that a state's provision of electric energy can be considered part of a plan to generate wealth and job opportunities while preserving the environment, as recently shown for the inhabitants of the Brazilian Amazon (Andrade, Rosa, & da Silva, 2011). Other authors have proposed the installation of energy sources in rural areas to solve the problem of energy access in remote areas (Byrnes, Brown, Wagner, & Foster, 2016; Gaona, Trujillo, & Guacaneme, 2015; Nie et al., 2012). Moreover, some have proposed a diffusion model based on classical diffusion theory, where the adoption rate becomes a function of awareness campaigns and social interaction (Radomes & Arango, 2015).

Many of these studies, however, explore energy development in indigenous communities in the United States (Necefer, Wong-Parodi, Jaramillo, & Small, 2015). In Colombia, two researchers conducted a survey of various actors involved in renewable energy systems (RES) projects to identify and analyze the social and political acceptance, market acceptance, and the community acceptance of RES (Rosso-Cerón & Kafarov, 2015). Finally, other researchers analyzed the viability of photovoltaics (PVs) in northern latitudes as part of the energy supply systems for nomadic camps far from indigenous communities dedicated to reindeer herding (Obydenkova & Pearce, 2016).

With respect to the use of electricity, one study recognized some household energy consumption patterns in rural areas in South Africa (Davis, 1998). Another study found that the perceptions of service and facility quality in rural small towns in the U.S. state of lowa were wholly dependent on a community's social organization (Wright Morton,

2003). Another study concluded that the electricity consumption of households depends on structural and motivational factors, with predictable patterns of interaction among members that influence their consumption, and that the total electricity saving effort depends on the strength of internalized norms, self-expectations, and factors related to self-efficacy (Thøgersen & Grønhøj, 2010). Another study revealed that providing households with a feedback system that gives information about electricity consumption empowers consumers to take energy-saving measures (Grønhøj & Thøgersen, 2011). A final study analyzed the perspectives of end users and their satisfaction with the quality of service in rural areas (Shyu, 2013).

In sum, there are few studies investigating electricity-saving behavior in rural communities, with even fewer focusing on rural indigenous communities. Those that did investigate indigenous communities focused on supplying electricity to them, typically by selecting the best renewable energy system (Huesca-Pérez et al., 2016). Furthermore, no study on this issue has been performed in Latin America. As a consequence, there is no evidence identifying the energy consumption patterns of rural indigenous communities in Latin America, how they might best use or save electricity, and the ways in which electricity service for these communities might be optimized. Consequently, before the installation of electricity services to indigenous communities, government entities must make an effort to create greater awareness to the customers about electricity-saving, as proposed in Grønhøj and Thøgersen (2011) and Thøgersen and Grønhøj (2010).

This research focuses on identifying how indigenous populations in the upper and middle zones of La Guajira Department in Colombia save electricity or follow a plan based on an energy policy. The methodology is based on descriptive observations,

applying surveys, and direct observation of electricity saving behavior within a randomly selected sample population. Data were analyzed and key aspects of user behavior in electrical energy consumption for the different communities described. Monthly electricity consumption of these groups was also studied, noting differences with the rest of the Colombian population, especially urban areas with similar weather conditions and socioeconomic level, where comparable appliances of customers were assumed. The results demonstrated that these communities have problems with electricity-saving measures, with stark consumption differences from those of urban populations.

This paper is organized as follows. Section 2 includes the methodology used in the investigation. Section 3 offers the study results and Section 4 discusses the results. Finally, Section 5 presents formal conclusions of the research along with important implications for future studies.

7.2 Methodology

This section presents the methodology applied in the research, where the population and samples are defined, and how electricity consumption is estimated. In this research, an exploratory descriptive methodology was applied that illustrates the current conditions of population, their access to electricity, and their perceptions of this service in their activities.

7.2.1 Population and Sample

La Guajira Department of Colombia was selected for this study. This department has an area of 20,848 km^2 and is divided into three zones: low, medium, and high Guajira

(Puerta Silva, 2004). The main municipalities in the middle and upper zones are Manaure, Uribia, Maicao, and Riohacha. All indigenous rural communities are politically associated with those urban jurisdictions.

According to the National Administrative Department of Statistics – DANE (DANE, 2006), there are about 5.1 people per household in La Guajira Department. The number of inhabitants in central and northern Guajira (219,646) was divided by 5.1, for a total of 43,068 households. Then, probability sampling for this population was applied because all households have the same probability of sample selection. A total of 283 households in seven rural indigenous communities with electricity were asked about the electricity service, consumption, and energy saving plan.

The survey was administered to people living in households of indigenous communities identified as the Wayuu ethnicity without including the survey consumption level of hospitals or rural schools as only residential users were comparable with other urban residential population with similar socioeconomic levels.

7.2.3 Estimated Electricity Savings

Total electricity consumption was estimated by identifying the use of electrical appliances, time of use, and other consumption habits for the target population. Then, the time of use of these appliances, the respective power usage for a 24-hour period, and the daily consumption of different families were obtained. This survey was conducted among the seven communities selected in the sample that had access to the electricity service.

For the population with electricity, a survey to identify behavior leading to the high electricity consumption of households in their daily activities was implemented including the use of appliances and the number and types of light bulbs. These data were compared with answers to the questions about the consumption behavior of these communities and to national consumption levels.

Table 1 shows the questions posed to communities with electricity to gauge their consumption patterns. We also tried to identify the practice of electricity savings, the kinds of appliances used, and the possibility that the respondents knew about the importance of saving electricity. All data were obtained from households.

Table 1. Questions for Indigenous Communities with Electricity

Number	Question	Range
1	What is your monthly consumption?	Low: (0.0–1.7) kWh/d Medium: 1.8–3.61 High: Greater than 3.61
2	Which months usually have the highest and lowest consumption rates?	First semester (January–June) Second semester (July–December)
3	Why do you think there is a high consumption rate in general?	The weather Family visit Acquisition of electrical appliance
4	How would you describe your usage of the electricity service?	Very good Good Regular Bad Very bad
5	What are some possible oversights that lead to high consumption rates?	Cultural aspects Needs to supply
6	How many lightbulbs do you use and what is their wattage?	Lightbulbs (1, 2, 3, …, 10) Steps of 100 Watts (1-100, 101-200, …, 901-1000)
7	Is there any information in your community about electricity-saving measures?	Yes No
8	Do you save electricity? (If yes, how? If no, why?)	Yes No
9	Do you have refrigeration equipment?	Yes No
10	What tasks do you need more electricity for?	Hobbies

		Needs

7.3 Results

7.3.1 Consumption Habits

Table 2 shows the consumption of electricity for those rural indigenous communities that have access to electricity. These communities are Nazareth—Uribía; Cristin López—Manaure; Paz—Maicao; Villa—Manaure; Pesuapa—Manaure; Santa Rosa—Maicao; and Aujero—Riohacha. The data were obtained as an average consumption of all users surveyed in each group.

Table 2. Electricity Consumption by Time of Day for Rural Indigenous Communities

	Communities with electricity						
	Nazaret	**Cristin Lopéz**	**La Paz**	**La Villa**	**Pesuapa**	**Santa Rosa**	**Aujero**
Hora	Carga (kW)	Carga (kW)	Carga (kW)	Carga (kW)	Carga (kW)	Carga (kW)	Carga (kW)
00:00 - 01:00	0.032	0.06	0.053	0.048	0.014	0.013	0.069
01:00 - 02:00	0.043	0.093	0.071	0.055	0.031	0.053	0.096
02:00 - 03:00	0.045	0.12	0.081	0.048	0.049	0.068	0.135
03:00 - 04:00	0.068	0.178	0.087	0.055	0.059	0.069	0.154
04:00 - 05:00	0.167	0.231	0.201	0.169	0.181	0.181	0.209
05:00 - 06:00	0.181	0.299	0.221	0.194	0.261	0.2	0.251
06:00 - 07:00	0.268	0.313	0.27	0.267	0.293	0.247	0.303
07:00 - 08:00	0.277	0.296	0.288	0.279	0.281	0.287	0.351
08:00 - 09:00	0.154	0.13	0.165	0.16	0.13	0.166	0.271
09:00 - 10:00	0.136	0.171	0.163	0.154	0.179	0.153	0.188
10:00 - 11:00	0.131	0.139	0.139	0.131	0.143	0.144	0.151
11:00 - 12:00	0.227	0.227	0.227	0.228	0.289	0.234	0.271
12:00 - 13:00	0.279	0.29	0.307	0.289	0.276	0.3	0.354
13:00 - 14:00	0.242	0.27	0.275	0.265	0.267	0.235	0.303
14:00 - 15:00	0.165	0.178	0.171	0.157	0.24	0.156	0.212
15:00 - 16:00	0.137	0.14	0.154	0.132	0.232	0.164	0.158
16:00 - 17:00	0.178	0.18	0.191	0.172	0.3	0.194	0.214
17:00 - 18:00	0.258	0.278	0.296	0.256	0.333	0.277	0.289
18:00 - 19:00	0.285	0.311	0.323	0.297	0.367	0.304	0.352
19:00 - 20:00	0.273	0.29	0.289	0.27	0.378	0.274	0.307
20:00 - 21:00	0.229	0.298	0.252	0.235	0.334	0.211	0.288
21:00 - 22:00	0.143	0.13	0.146	0.114	0.21	0.145	0.212

22:00 - 23:00	0.087	0.055	0.07	0.059	0.134	0.066	0.097
23:00 - 00:00	0.041	0.019	0.051	0.026	0.0012	0.035	0.061
Total	4.046	4.696	4.491	4.06	4.9822	4.176	5.296

The indigenous community of Aujero consumes electricity above the average rate of several other municipalities; this fact identifies important consumption habits among these indigenous communities along with variations from one community to another. Notably, the consumption peaks are always at the same time in the surveyed communities, even though electricity rates change from one community to another. The indigenous community of Aujero has the highest consumption peak until 1500 hours, when it is surpassed by Pesuapa. All these indigenous communities have consumption peaks in three periods instead of two—as in the urban population—i.e., consumption peaks between 0600 and 0800 hours, between 1200 and 1400 hours, and between 1800 and 2100 hours. Identifying communities with estimated electricity consumption near or above the subsistence limits allows us to identify the need for a new energy efficiency plan and to create awareness among these populations on the subject of electricity saving. Additionally, this comparison is useful for determining whether sustainable electricity production projects can be implemented to improve the social development of these communities (Akella, Saini, & Sharma, 2009; Coria & Calfucura, 2012; Valer, Mocelin, Zilles, Moura, & Nascimento, 2014).

7.3.2 Comparisons of Electricity Consumption

Table 3 shows the comparison of average power consumption of rural indigenous communities and the urban population. All information was obtained from population surveys conducted during this research, with information about urban areas obtained from Universidad Nacional de Colombia & Unidad de Planeación Minero Energética

(UPME, 2006). The differences in electricity consumption reveal the need for plans to use home appliances efficiently. Communities with a high consumption of electricity were also identified for the potential implementation of electricity-saving plans.

Table 3. Average Power Consumption of Rural Indigenous Communities and Urban Population

Rural indigenous communities		**Urban Population**	
	Electricity consumption per month (KWh - Month)		**Electricity consumption per month (KWh - Month)**
Manaure	145.1	**Pasto**	147.6
Maicao	127.2	**Medellín**	110.9
Uribía	121.3	**Barranquilla**	153.9
Riohacha	158.8	**Bogotá**	176.2

It is surprising how communities near the municipality of Riohacha have higher energy consumption than cities with the same climate, with the relevant comparator being the city of Barranquilla. Notably, as the second-most populous city in the country, Medellín has lower levels of consumption than all these communities. This is an important observation because these rural communities tend not to have high-consumption appliances, making it even more important for these populations to receive education on the culture of energy-saving, either by energy companies or the government itself. They need to learn these new consumption habits, which can become the basis for new projects that have the ultimate purpose of finding a renewable energy source.

Table 4 shows the comparison of the use of electrical appliances in indigenous communities and urban communities. The refrigerator is the main electrical appliance used by indigenous communities followed by the television and lighting. Therefore, urban communities experiencing the same weather conditions use fans in a very different way from indigenous communities and infer that these indigenous communities do not iron—possibly because they do not value the look of pressed clothes.

Table 4. Use of Electrical Appliances in Indigenous and Urban Communities

	Percentage of appliance use	
Household appliance	**Rural indigenous communities**	**Urban Population**
Lighting	24%	16%
TV	25%	8%
Refrigerator	25%	39%
Laundry machine	7%	2%
Fans	3%	28%
Cooking	4%	0%
Others	12%	7%

Figure 1 presents the number and types of light bulbs these communities used for lighting. The vast majority of indigenous populations do not use energy-saving light bulbs. The population uses an average of four to six light bulbs per household. When multiplied by the power consumed by each light bulb, this does not represent high consumption, yet a change is required in the type of light bulb to guarantee greater energy efficiency.

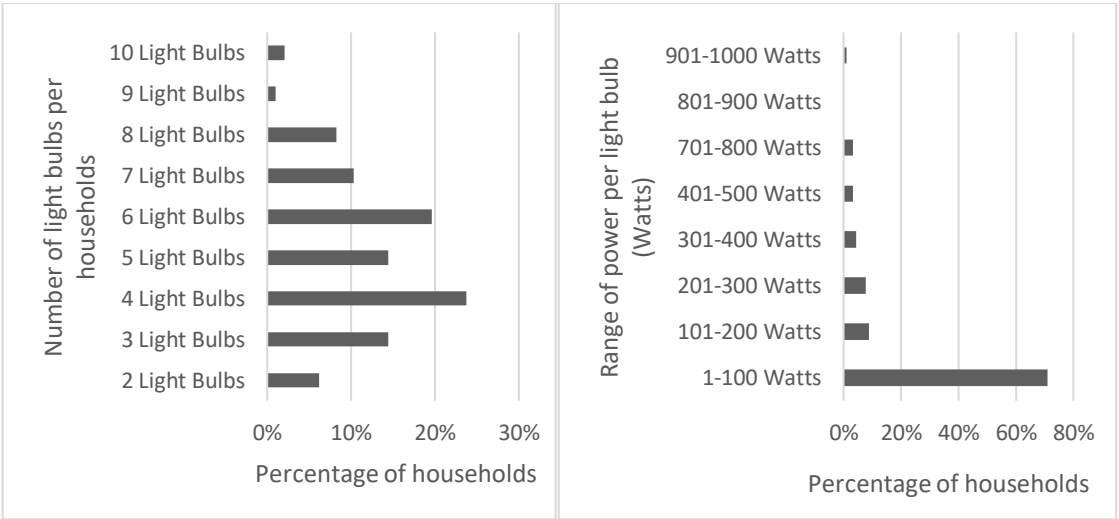

Figure 1. Power and number of light bulbs used per household.

7.3.3 Energy-saving plans

More than 90% of the population stated that they do not know anything about saving

electricity. This situation can be improved with pedagogic methods and publicity to create awareness on electricity-saving that has the potential to change the mindset of these indigenous communities (Hori, Shinozaki, Nogata, & Fujita, 2014). As illustrated in Figure 2, a significant number of people are not compromised with energy-saving plans.

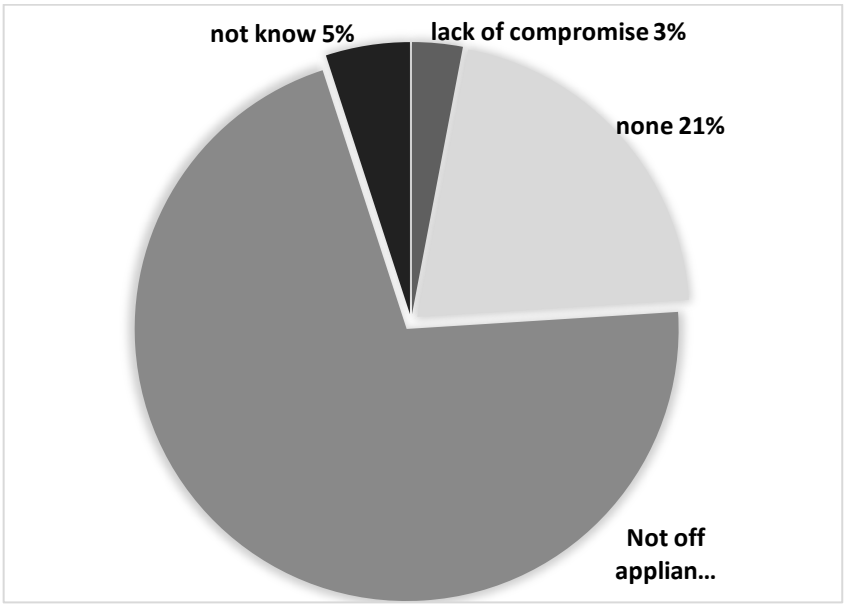

Figure 2. Percentage of people compromised with energy-saving plans.

People in indigenous communities were asked about the role that negligence might play in high energy consumption. Most answered that they did not turn off or unplug appliances because they were not aware that even after shutdown some appliances continue to consume energy. This demonstrates the necessity of campaigns on energy efficiency to create an electricity-saving culture in these communities. Through this research, it was possible to observe that rural indigenous communities living in the upper and middle zone of La Guajira were not aware of the importance of electricity-saving policies primarily because their energy supplier does not release information promoting or explaining such policies. Figure 3 shows that a large percentage of people in these communities simply do not know about energy-saving practices.

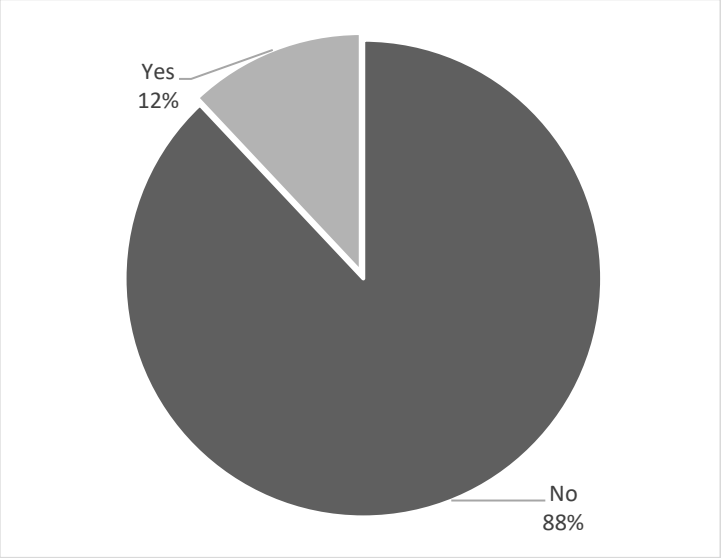

Figure 3. Percentage of people that know about energy-saving practices.

7.4 Discussion

Shortcomings in education about electricity-saving were found in the indigenous communities of middle and upper La Guajira, particularly through their misuse of certain appliances along with a lack of unawareness that their own habits generate more consumption (Grønhøj & Thøgersen, 2011; Kleinschafer & Morrison, 2014). This includes, for example, failing to unplug appliances when they are not in use. All of these awareness will allow the creation of new programs that enhance the energy consumption of indigenous communities (Ozaki, 2011; Sahakian & Steinberger, 2011).

The Aujero community showed a higher consumption of energy per month than the indigenous communities from Maicao or Manaure. In addition, consumption rates of this population are above those of populations living in cities with more industrial development and similar weather conditions (as in the case of Barranquilla). Some indigenous populations have higher power consumption than the lowest socio-economic strata of the city of Medellín. An apparent reason for this may be that

indigenous communities do not use electrical services efficiently, potentially because they lack electricity-saving habits.

The increase in energy consumption of indigenous communities in the upper and middle zones of La Guajira is directly related to its use for refrigeration (compared with cities with the same weather conditions), lighting, and the use of appliances, especially TV. Consumption rates are lower than in other places in general but when compared with lighting and TV use, their rates are much higher. Lighting is a particularly noteworthy topic because consumption rates are higher in these rural communities than in large cities. As such, indigenous communities require urgent reforms and new energy efficiency strategies and policies to reduce consumption in relation to the use of lighting and appliances as earlier proposed by Bernstein and Collins (2014) and Shwom and Lorenzen (2012).

As a result, it is imperative for electrical companies to implement pedagogical training interventions and design electricity-saving plans to promote an energy-saving culture among these communities. The results of the survey found that most indigenous people have never seen a television advertisement about saving electricity, a fact that has been previously confirmed for other cultures (Attari, DeKay, Davidson, & Bruine de Bruin, 2010). Most indigenous people do not know about electricity policies and this may be the main reason why they do not unplug their appliances and continue to use high-consumption lightbulbs above 100 W.

These results indicate that indigenous communities require continuous support that can be provided through public talks on saving electricity and on how new energy plans should be executed as has been done for other populations (Grønhøj & Thøgersen,

2011; Thøgersen & Grønhøj, 2010). Many community members are unaware of this support, which has the potential to improve their quality of life (Martins, 2005) even though such measures have never previously been implemented with any indigenous community. Furthermore, community acceptance plays a decisive role in the design of future energy projects, including the use of RES to optimize consumption (Ashok, 2007; Goodbody et al., 2013).

The indigenous communities surveyed tend not to make efficient use of their electrical service, which only underlines the need to implement pedagogic classes on electricity-saving topics. In the future, Colombian law may well require the design of energy-generation projects using alternative energy sources like solar energy, wind power plants, or the interconnection of different generation systems (Goodbody et al., 2013; Hoogwijk, de Vries, & Turkenburg, 2004; Prada Blanco, Vázquez Rodríguez, & Soliño Millán, 2007). Energy-saving plans would help optimize load consumption and, furthermore, as proposed by Gaona et al. (2015), it would help optimize generation systems and their installation in rural areas. Before providing electricity services in indigenous communities, it is necessary to design a special energy-saving plan in order to design optimal energy systems.

In analyzing the data from indigenous communities on their electricity use, we observed the high consumption for lighting. These indigenous communities use light bulbs that consume up to five times more power than more modern bulbs; thus, it is essential to change the lightbulbs these indigenous communities use and to promote an energy-saving mindset in this population (Thøgersen & Grønhøj, 2010). Government entities must provide guidance and advertisements to promote electricity-saving. This study can be applied to new electricity users among indigenous

populations, but much more work is required in the preparation of pedagogic material in the field of energy efficiency along with the generation of awareness of this matter throughout the entire community.

7.5 Conclusions

This paper focused on identifying how indigenous populations in the upper and middle zones of the La Guajira Department in Colombia save electricity or follow a plan based on an energy policy. From the results obtained in the research, it can be inferred that most of the indigenous population in the Colombian Guajira do not manage the culture of energy efficiency in terms of electricity consumption. Additionally, their consumption behavior does not follow a current regional or national-level energy policy plan. Some fail to turn off idle appliances when they do not need them and there are no energy awareness measures to educate indigenous communities. Comparison of electricity consumption of Wayuu communities and electricity consumption the country's residential urban dwellers with similar socioeconomic level revealed that few indigenous people use electricity efficiently as shown by the hours of use of lighting and some appliances.

Although electricity is used to perform basic activities, there is little justification for the high consumption rates of some communities, particularly those that exceed consumption rates of urban populations in low socio-economic strata. In the last few years, the electricity consumption threshold in Colombia's energy policy has been reduced, which is now a concern for indigenous households that are over the minimum value subsided. To counteract this trend, the inefficient use of electricity services in rural indigenous communities must be managed by government entities to avoid

affecting their economies in future. Our results are potentially useful for the design and future implementation of systems not already connected to the grid, such as generation systems based on solar or wind energy. These mechanisms may address the lack of access to electricity and improve the quality of life for these communities. Therefore, it is necessary to implement pedagogical measures to promote electricity saving. Future research should analyze the economic viability of possible cooperation between manufacturers and government to eliminate older lighting systems, many of which date to the last century. Our research also noted the lack of advertising around electricity-saving and this may be a primary cause of higher consumption rates.

7.6 References

Akella, A. K., Saini, R. P., & Sharma, M. P. (2009). Social, economical and environmental impacts of renewable energy systems. *Renewable Energy*, *34*(2), 390–396. http://doi.org/10.1016/j.renene.2008.05.002

Andrade, C. S., Rosa, L. P., & da Silva, N. F. (2011). Generation of electric energy in isolated rural communities in the Amazon Region a proposal for the autonomy and sustainability of the local populations. *Renewable and Sustainable Energy Reviews*, *15*(1), 493–503. http://doi.org/10.1016/j.rser.2010.09.052

Ashok, S. (2007). Optimised model for community-based hybrid energy system. *Renewable Energy*, *32*(7), 1155–1164. http://doi.org/10.1016/j.renene.2006.04.008

Attari, S. Z., DeKay, M. L., Davidson, C. I., & Bruine de Bruin, W. (2010). Public perceptions of energy consumption and savings. *Proceedings of the National Academy of Sciences*, *107*(37), 16054–16059. http://doi.org/10.1073/pnas.1001509107

Bernstein, M., & Collins, M. (2014). Saving energy through better information: a new energy paradigm? *Contemporary Economic Policy*, *32*(1), 219–229. http://doi.org/10.1111/j.1465-7287.2012.00330.x

Byrnes, L., Brown, C., Wagner, L., & Foster, J. (2016). Reviewing the viability of renewable energy in community electrification: The case of remote Western Australian communities. *Renewable and Sustainable Energy Reviews*, *59*, 470–481. http://doi.org/10.1016/j.rser.2015.12.273

Chaurey, A., Ranganathan, M., & Mohanty, P. (2004). Electricity access for geographically disadvantaged rural communities—technology and policy insights. *Energy Policy*, *32*(15), 1693–1705. http://doi.org/10.1016/S0301-4215(03)00160-5

Consorcio Energético: CORPOEMA. Plan de desarrollo para las fuentes no convencionales de energía en Colombia (2010).

Coria, J., & Calfucura, E. (2012). Ecotourism and the development of indigenous communities: The good, the bad, and the ugly. *Ecological Economics*, *73*, 47–55. http://doi.org/10.1016/j.ecolecon.2011.10.024

DANE. (2006). Boletin Censo General DANE 2005, 1–6.

Davis, M. (1998). Rural household energy consumption. *Energy Policy*, *26*(3), 207–217. http://doi.org/10.1016/S0301-4215(97)00100-6

Departamento Administrativo de Planeación de La Guajira. (2014). *Tercer Informe: La seguridad alimentaria de la media y alta Guajira*.

Departamento de Planeación Nacional, & Dirección de Desarrollo Territorial Sostenible. (2010). *Aspectos básicos grupo étnico indígenas*. Bogotá, Colombia.

Ek, K., & Söderholm, P. (2010). The devil is in the details: Household electricity saving behavior and the role of information. *Energy Policy*, *38*(3), 1578–1587. http://doi.org/10.1016/j.enpol.2009.11.041

Gaona, E. E., Trujillo, C. L., & Guacaneme, J. A. (2015). Rural microgrids and its potential application in Colombia. *Renewable and Sustainable Energy Reviews*, *51*, 125–137. http://doi.org/10.1016/j.rser.2015.04.176

Gilbert, A. (2004). Helping the poor through housing subsidies: lessons from Chile, Colombia and South Africa. *Habitat International*, *28*(1), 13–40. http://doi.org/10.1016/S0197-3975(02)00070-X

Giraldo Polanco, M. F., & Vega Gámez, M. I. (2015). Ethnography of the body and the motor function in the Wayuu culture. In *5º Coloquio Internacional de la Educación Corporal: modos de experiencia desde los cuerpos* (p. 6). Medellín - Colombia.

Goodbody, C., Walsh, E., McDonnell, K. P., & Owende, P. (2013). Regional integration of renewable energy systems in Ireland – The role of hybrid energy systems for small communities. *International Journal of Electrical Power & Energy Systems*, *44*(1), 713–720. http://doi.org/10.1016/j.ijepes.2012.08.012

Grønhøj, A., & Thøgersen, J. (2011). Feedback on household electricity consumption: learning and social influence processes. *International Journal of Consumer Studies*, *35*(2), 138–145. http://doi.org/10.1111/j.1470-6431.2010.00967.x

Harmsen, R., & Graus, W. (2013). How much CO2 emissions do we reduce by saving electricity? A focus on methods. *Energy Policy*, *60*, 803–812. http://doi.org/10.1016/j.enpol.2013.05.059

Hoogwijk, M., de Vries, B., & Turkenburg, W. (2004). Assessment of the global and regional geographical, technical and economic potential of onshore wind energy. *Energy Economics*, *26*, 889–919. http://doi.org/10.1016/j.eneco.2004.04.016

Hori, S., Shinozaki, M., Nogata, D., & Fujita, T. (2014). The role of CSR in promoting companies' energy-saving actions in two Asian cities. *Energy Policy*, *69*, 116–121. http://doi.org/10.1016/j.enpol.2014.01.030

Huesca-Pérez, M. E., Sheinbaum-Pardo, C., & Köppel, J. (2016). Social implications

of siting wind energy in a disadvantaged region – The case of the Isthmus of Tehuantepec, Mexico. *Renewable and Sustainable Energy Reviews*, *58*, 952–965. http://doi.org/10.1016/j.rser.2015.12.310

Kleinschafer, J., & Morrison, M. (2014). Household norms and their role in reducing household electricity consumption. *International Journal of Consumer Studies*, *38*(1), 75–81. http://doi.org/10.1111/ijcs.12066

Lenzen, M., Krishnapillai, M., Talagi, D., Quintal, J., Quintal, D., Grant, R., … Murray, J. (2014). Cultural and socio-economic determinants of energy consumption on small remote islands. *Natural Resources Forum*, *38*(1), 27–46. http://doi.org/10.1111/1477-8947.12030

Mancuso, A. (2005). Relaciones de género entre los Wayuu: estado de la investigación y nuevos campos de análisis. *Aguaita*, *13–14*, 39–61.

Martins, J. (2005). The Impact of the Use of Energy Sources on the Quality of Life of Poor Communities. *Social Indicators Research*, *72*(3), 373–402. http://doi.org/10.1007/s11205-004-5583-z

Mugi-Ngenga, E. W., Mucheru-Muna, M. W., Mugwe, J. N., Ngetich, F. K., Mairura, F. S., & Mugendi, D. N. (2016). Household's socio-economic factors influencing the level of adaptation to climate variability in the dry zones of Eastern Kenya. *Journal of Rural Studies*, *43*, 49–60. http://doi.org/10.1016/j.jrurstud.2015.11.004

Munday, M., Bristow, G., & Cowell, R. (2011). Wind farms in rural areas: How far do community benefits from wind farms represent a local economic development opportunity? *Journal of Rural Studies*, *27*(1), 1–12. http://doi.org/10.1016/j.jrurstud.2010.08.003

Necefer, L., Wong-Parodi, G., Jaramillo, P., & Small, M. J. (2015). Energy development and Native Americans: Values and beliefs about energy from the Navajo Nation. *Energy Research & Social Science*, *7*, 1–11.

http://doi.org/10.1016/j.erss.2015.02.007

Nie, S., Fu, X.-P., Li, P., Gao, F., Ding, C.-D., Yu, H., & Wang, C.-S. (2012). Analysis of the impact of DG on distribution network reconfiguration using OpenDSS. In *IEEE PES Innovative Smart Grid Technologies* (pp. 1–5). IEEE. http://doi.org/10.1109/ISGT-Asia.2012.6303390

Obydenkova, S. V., & Pearce, J. M. (2016). Technical viability of mobile solar photovoltaic systems for indigenous nomadic communities in northern latitudes. *Renewable Energy*, *89*, 253–267. http://doi.org/10.1016/j.renene.2015.12.036

Ozaki, R. (2011). Adopting sustainable innovation: what makes consumers sign up to green electricity? *Business Strategy and the Environment*, *20*(1), 1–17. http://doi.org/10.1002/bse.650

Prada Blanco, A., Vázquez Rodríguez, M. X., & Soliño Millán, M. (2007). Percepción social sobre generación de electricidad con fuentes de energía renovables en Galicia. *Revista Galega de Economía*, *16*(1), 1–20.

Psomopoulos, C. S., Skoula, I., Karras, C., Chatzimpiros, A., & Chionidis, M. (2010). Electricity savings and CO2 emissions reduction in buildings sector: How important the network losses are in the calculation? *Energy*, *35*(1), 485–490. http://doi.org/10.1016/j.energy.2009.10.016

Puerta Silva, C. (2004). Roles y estrategias de los gobiernos indígenas en el sistema de salud colombiano. *Revista Colombiana de Antropologia*, *40*(41), 85–125.

Radomes, A. A., & Arango, S. (2015). Renewable energy technology diffusion: an analysis of photovoltaic-system support schemes in Medellín, Colombia. *Journal of Cleaner Production*, *92*, 152–161. http://doi.org/10.1016/j.jclepro.2014.12.090

Rosso-Cerón, A. M., & Kafarov, V. (2015). Barriers to social acceptance of renewable energy systems in Colombia. *Current Opinion in Chemical Engineering*, *10*, 103–110. http://doi.org/10.1016/j.coche.2015.08.003

Sahakian, M. D., & Steinberger, J. K. (2011). Energy Reduction Through a Deeper Understanding of Household Consumption. *Journal of Industrial Ecology*, *15*(1), 31–48. http://doi.org/10.1111/j.1530-9290.2010.00305.x

Shwom, R., & Lorenzen, J. A. (2012). Changing household consumption to address climate change: social scientific insights and challenges. *Wiley Interdisciplinary Reviews: Climate Change*, *3*(5), 379–395. http://doi.org/10.1002/wcc.182

Shyu, C.-W. (2013). End-users' experiences with electricity supply from stand-alone mini-grid solar PV power stations in rural areas of western China. *Energy for Sustainable Development*, *17*(4), 391–400. http://doi.org/10.1016/j.esd.2013.02.006

Thøgersen, J., & Grønhøj, A. (2010). Electricity saving in households—A social cognitive approach. *Energy Policy*, *38*(12), 7732–7743. http://doi.org/10.1016/j.enpol.2010.08.025

Universidad Nacional de Colombia, & Unidad de Planeación Minero Energética UPME. (2006). *Determinación del consumo final de energía en los sectores residencial urbano y comercial y determinación para equipos domésticos de energía eléctrica y gas*. Bogotá, Colombia.

Valer, L. R., Mocelin, A., Zilles, R., Moura, E., & Nascimento, A. C. S. (2014). Assessment of socioeconomic impacts of access to electricity in Brazilian Amazon: case study in two communities in Mamirauá Reserve. *Energy for Sustainable Development*, *20*, 58–65. http://doi.org/10.1016/j.esd.2014.03.002

Wright Morton, L. (2003). Small Town Services and Facilities: The Influence of Social Networks and Civic Structure on Perceptions of Quality. *City and Community*, *2*(2), 102–120. http://doi.org/10.1111/1540-6040.00043

Anexe 2

Tracking AC Signals with Zero Average Dynamics and Fixed Point Induced Control

Fredy E. Hoyos[1], John E. Candelo-Becerra[2], Eder A. Molina[2]

Abstract – *This paper presents the theoretical and experimental results of a DC-AC buck converter configured as a DC-AC inverter when controlled by Zero Average Dynamics (ZAD) and Fixed Point Induced Control (FPIC) techniques. The system is modeled and implemented in an electric circuit to apply the control techniques and regulate voltage at the output to AC levels. The tests are based on comparing simulated and real results to identify the robustness of the circuit when subjected to disturbances. The results show that ZAD and FPIC controllers implemented digitally in a DSP meet the requirements of fixed frequency switching, robustness, and good performance in AC signal tracking tasks. For high frequencies, the value of the LC filter capacitor must be decreased when tracking AC signals; however, this increases ripple in the signal and tracking errors.*

Keywords*: DC-AC converter, zero average dynamics, fixed point induced control, nonlinear control, experimental test, rapid control prototyping, digital signal processing*

I. Introduction

Many applications require a regulated source that supplies accurate voltages [1]. However, equipment may suffer significant damage to internal components and loss of information, producing errors. Power converters help regulate voltages in the network and provide efficiency, security, fidelity, confidence, low cost, and smaller size. Regulated voltage is useful for networks with power quality issues and practical as in the case of critical loads such as electric welders, telecommunications equipment, and electromedical devices [2]. One of the most desired qualities in these devices is their performance efficiency, which is maximized through the use of properly implemented switching devices [3]. It is estimated that 90% of electrical energy is processed through power converters before its final use [4], [5].

In the literature, e.g., [6]–[9], the power converter is controlled by a pulse width modulation (PWM), using a sliding surface with two objectives: to calculate the duty cycle (d) and to enter the reference signal v_{ref}. The slip surface is defined as a first-order dynamic in the error, which is forced to have a zero average in each sampling period. This technique is known as ZAD (Zero Average Dynamics). This control technique guarantees robustness, low steady-state error, and fixed switching frequency [10].

The experimental prototype of a DC-AC converter controlled by the ZAD and FPIC strategy has been previously studied in [10] and [11]. Additionally, it has been used in theoretical models, analysis, and simulation of power converters to obtain results including: knowledge of the satisfactory operation range for parameter values through bifurcations [10], [11]; characterization, selection, and execution of different types of control applied to the system; regulation of the output voltage at a desired value [12]; and simplification in the design and implementation of prototypes among other [10].

Therefore, it is necessary to now implement real prototypes that corroborate the numerical results calculated in the simulations; moreover, experimental results have not been published using voltages close to residential 110 AC voltage values. By performing this experimental tests, new operating conditions are expected to be found, such as: sensors warming, short circuit risk, damage risk of digital devices, signal saturation, electromagnetic noise, large values in chaos and dynamic behaviors, and others [13]; which contribute to future research.

Because the system with ZAD presents dynamic behavior when the parameters are

varied, it is necessary to determine the working conditions that allow adequate operation. In order to stabilize unstable equilibria, the FPIC control technique is implemented, which at the theoretical and simulation levels has returned excellent results as shown in [10], [11].

Therefore, the experimental test of a controlled power converter with ZAD and FPIC techniques is proposed. This device can deliver a signal that is a regulated by the user and lower than the supply voltage to regulate AC and DC signals at the output. For this, the voltage in the capacitor (υ_c), the current in the inductor (i_L), and the value of the connected load (R) are sensed, which for this study will be linear and variant in time.

The electronic prototype consists of hardware and software. The first comprises the inverter, the LC filter, and signal conditioning. The second is the digital part, programmed in the DS1104 board, which is where the ZAD and FPIC control techniques are implemented.

The controllers are implemented in the MATLAB-Simulink platform and are downloaded to the DSP to work in real time. The voltage signals in the capacitor (υ_c), current in the inductor (i_L), and current in the load (i_R) are sampled at a frequency of 25 kHz. The reference is configured using Simulink blocks, with some constant parameters entered in the controllers. The control techniques are executed and, finally, the signals PWMC (modulator by centered pulse width) and PWMCinv (inverted centered pulse width modulator) are configured at a frequency of 5 kHz to close the control loop. For this purpose, Section 2 presents the Research Method, Section 3 shows the control strategies, and Section 4 presents the results and analysis where the comparison of the three models with the theoretical, simulation, and experimental tests are performed. Finally, Section 5 reports the conclusions.

II. Research Method

The power converter under study is configured as shown in Figure 1. The converter has a switch that makes the commutation, an LC filter, and the load to be fed is a pure resistance (R). With this configuration, the system starts from a non-regulated DC voltage (E) at the input and by centered pulse width modulation with constant frequencies (FC) up to 5 kHz. It is possible to have a regulated DC or AC output, variable in frequency and amplitude, according to the application requirement of the user and with the characteristic that the output is smaller in magnitude to the power supply because it is a buck power converter.

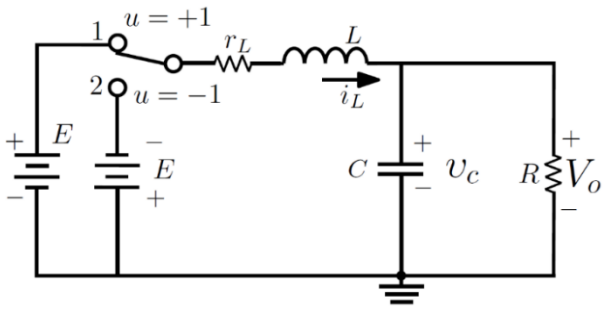

Fig. 1. DC-AC power converter

The switch is placed in position 1 or 2 depending on the control signal $u = +1$ or $u = -1$ as shown in Figures 1 and 2, where the final outputs are the signals *d*, PWMC, and PWMCinv. These control signals are responsible for controlling the time in which each source will be connected to the LC filter. The signals taken for the control techniques are the current in the inductor (i_L), the voltage in the capacitor (v_c), and the current in the load (i_R). These signals together with the reference signal (v_{ref}) are processed digitally using the ZAD control technique and FPIC to calculate the duty cycle (d). The duty cycle generates the control signals (Figure 2) that affect the switching of the power transistors to activate $+E$ or $-E$ at the LC filter input to close the control loop.

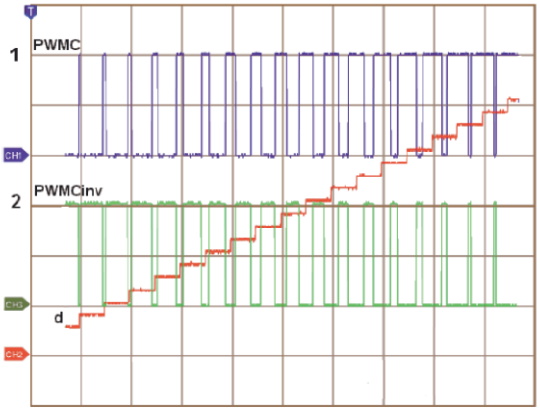

Fig. 2. PWM and PWMinv signals controlled by d

If the reference is a sinusoidal signal, then the converter will behave like a DC-AC converter. However, if the reference is a continuous signal, then the converter will behave like a DC-DC converter. Figure 2 shows the control signals that indicate how long the supply $+E$ or $-E$ will be connected to the LC filter. The fraction of the period T in which the source $+E$ is connected is called the “duty cycle” (d).

The presence of the PWM generates a control signal that allows modeling the system as one of variable structure as described in Equation (1), where the state variables are the voltage in the capacitor (v_c) and the current through the inductance (i_L). This system switches from one topology to another; each time, the control signal changes (u), which changes in PWM form. This fact allows the introduction of a controller based

on a sliding surface described as $s(x) = (v_c - v_{ref}) + K_s(\dot{v}_c - \dot{v}_{ref})$, where taking into account the reference signal, the voltage sensed at the output, the variation of the load, and doing some approximations, the duty cycle (d) is calculated:

$$\begin{bmatrix} \dot{v}_c \\ \dot{i}_L \end{bmatrix} = \begin{bmatrix} -\frac{1}{RC} & \frac{1}{C} \\ -\frac{1}{L} & -\frac{r_L}{L} \end{bmatrix} \begin{bmatrix} v_c \\ i_L \end{bmatrix} + \begin{bmatrix} 0 \\ \frac{E}{L} \end{bmatrix} u. \quad (1)$$

The system is fed back through high-frequency control pulses that activate $+E$ or $-E$ at the input to feed the converter, thereby reducing the difference between the real voltage v_c and the reference voltage v_{ref}. Then, a sliding surface $s(x)$ is defined, with first-order dynamics in the error that force it to have a zero average in each sampling period to guarantee a regulated voltage at the output, robustness, fixed switching frequency, and low steady-state error.

II.1. Control strategies

In this work, ZAD and FPIC control techniques are applied to control the power converter. This is important to perform real-time calculation of the duty cycle (d), which is required to determine the time for the switching period (T), the time the switch will be ON (d), and the time the switch will be OFF ($T - d$). Therefore, it is necessary to have an expression for the calculation of (d) in which the variables of the real circuit are considered, such as voltage value in the capacitor (v_c), current in the inductance (i_L), and value of the load (R). Starting from the ZAD technique and then applying the FPIC technique, the system in (1) will be controlled by means of PWM.

II.2. Control with ZAD

Control with ZAD ensures that the average of the function $s(x)$ is zero in each switching period. Making assumptions of linearity to sections on the sliding surface $s(x)$ [10], the duty cycle is calculated with Equation (4), considering Equations (2) and (3).

$$\int_{KT}^{(K+1)T} s(x(t))dt = 0 \quad (2)$$

$$\int_0^T s(x(t))dt = \int_0^{d/2} s(x(t))dt + \int_{d/2}^{T-d/2} s(x(t))dt + \int_{T-d/2}^{T} s(x(t))dt = 0 \quad (3)$$

$$d\_zad(kT) = \frac{2s(x(kT)) + T\dot{s}_-(x(kT))}{\dot{s}_-(x(kT)) - \dot{s}_+(x(kT))} \quad (4)$$

where:

$$s\big(x(KT)\big) = (1 + aK_s)x_1(KT) + K_s h x_2(KT) - x_{1ref} - K_s \dot{x}_{1ref} \quad (5)$$

$$\dot{s}_{+}\big(x(KT)\big) = (a + a^2K_s + hK_sm)x_1(kT) + (h + ahK_s + hK_sp)x_2(KT) + hK_s\frac{E}{L} - \dot{x}_{1ref} - K_s\ddot{x}_{1ref}\,, \quad (6)$$

$$\dot{s}_{-}\big(x(KT)\big) = (a + a^2K_s + hK_sm)x_1(kT) + (h + ahK_s + hK_sp)x_2(KT) - hK_s\frac{E}{L} - \dot{x}_{1ref} - K_s\ddot{x}_{1ref}\,. \quad (7)$$

Herein, $(x_1 = v_c)$, $(x_2 = i_L)$, K_s is the parameter of the ZAD control, $x_{1ref} = v_{ref}$ is the reference signal and $\dot{x}_{1ref}$, $\ddot{x}_{1ref}$ are their derivatives [10], and the other parameters are given in (8).

$$a = -\frac{1}{RC}, \quad h = \frac{1}{C}, \quad m = -\frac{1}{L}, \quad p = -\frac{r_L}{L} \quad (8)$$

II.3. Control with FPIC

The control technique FPIC designed by [6] and [10] is useful for autonomous and non-autonomous systems, and is especially used to control discrete systems. This is based on the theorem of continuity of the eigenvalues and useful to stabilize orbits of one or more periods in unstable and/or chaotic systems, and does not require the measurement of state variables. This forces the system to evolve to a fixed point; therefore, it is necessary to know previously the equilibrium point of the control signal.

Assuming that $x_1 = x_{1ref}$, $\dot{x}_1 = \dot{x}_{1ref}$ (in the steady state), and $\dot{x}_1 = ax_1 + hx_2$, Equation (4) is transformed into Equation (9):

$$dss = \frac{T\left[x_{1ref}(hm - ap) + \dot{x}_{1ref}(a + p) - \ddot{x}_{1ref} - \right.}{-2h\frac{E}{L}} \quad (9)$$

II.4. *Control with ZAD and FPIC*

The expression that defines the duty cycle (d) to be applied in each iteration according to ZAD and FPIC control techniques is given by Equation (10). With this equation, the converter is controlled in real time using ZAD and FPIC control techniques at the same time:

$$d(kT) = \frac{d_{zad(kT)} + N * dss}{N + 1}. \quad (10)$$

Then, with Equation (10), the control variable (d) is calculated at a frequency of $(1/T)$ kHz to close the control loop. If the converter regulates the voltage at the output when considering variable loads, then it is necessary to sense and input the value of the load resistance. Thus, the alternative is to sense the current in the load (i_R) and the voltage in the same to calculate the resistance value.

III. Results and Analysis

The results presented below are taken from the schematic diagram shown in Figure 3 and of the respective experimental prototype shown in Figure 4. The parameters of the converter and the controllers are listed in Table 1.

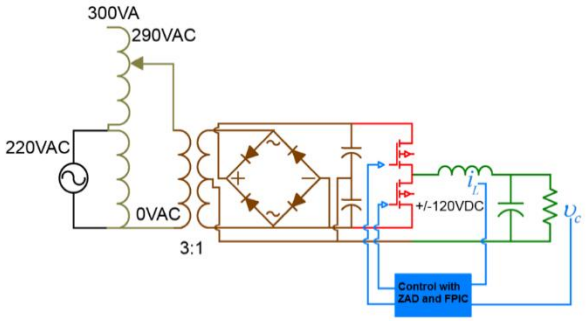

Fig. 3. Schematic diagram of the experiment

TABLE I

PARAMETERS USED FOR THE CIRCUIT

Parameter	Description	Value
R	Resistance of load	$151.3\ \Omega$
C	Capacitance	$57.68\ \mu f$
L	Inductance	$3.945\ mH$
r_L	Internal resistance	$4\ \Omega$
E	Input voltage	$\pm$130 V DC
FC	Switching frequency	5 kHz
Fs	Sampling frequency	25 kHz
N	Control parameter of FPIC	1
K_s	Control parameter of ZAD	5

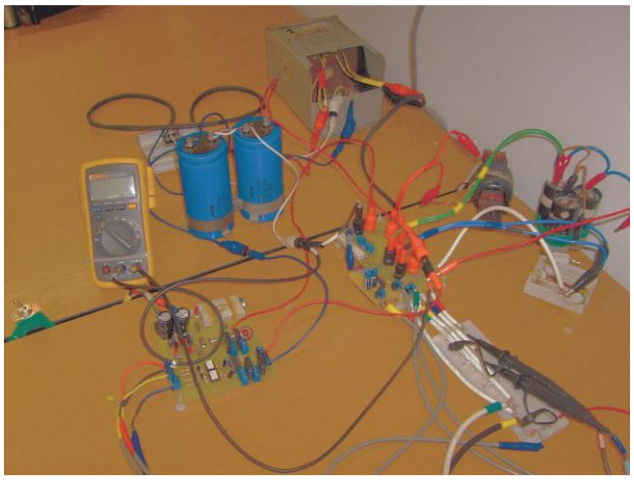

Fig. 4. Experimental prototype

In Figure 5, the performance of the control techniques is shown when the signal is a sinusoidal form of $110 * sen(2\pi * 60t)$ V. In the upper part (CH1), in yellow color, the power output that feeds the LC filter, this signal is PWM type pulse centered of ±130 V. Note that this channel has a gain of 50 V/div and this signal is switching to a constant frequency of 5 kHz. In blue (CH2) the output voltage in the load v_c (controlled signal)

is also shown with a gain of 50 V/div.

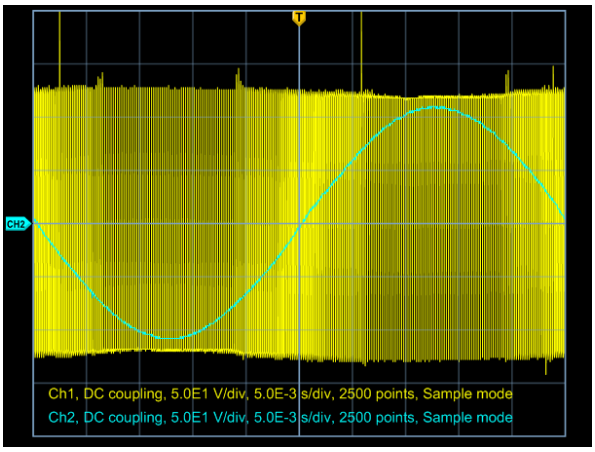

Fig. 5. PWMC and v_c when $v_{ref} = 110sen(2\pi * 60t)$

Figure 6 shows the experimental results when the reference signal $v_{ref} = 100sen(2\pi * 60t)$ V. The figure shows the signals measured with the oscilloscope in the following way: in yellow (CH1), the voltage of the PWM at ±130 V; in blue (CH2), the regulated voltage signal of the output v_c; in pink (CH3), the current in the inductor (i_L); and in green (CH4), the current in the load (i_R).

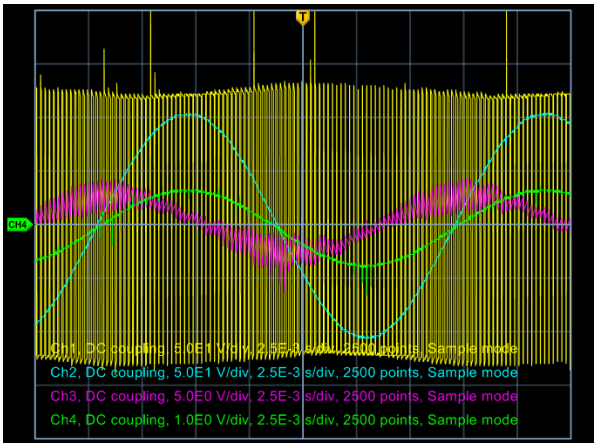

Fig. 6: PWMC and v_c when $v_{ref} = 100sen(2\pi * 60t)$

Figure 7 shows the voltage in the capacitor (v_c), the current in the inductor (i_L), and the current in the load (i_R). Furthermore, Figure 8 shows the voltage in the capacitor (v_c), the duty cycle (d), and the error of the voltage output ($Error$) in percentage. The signals shown in the two figures are acquired in the ControlDesk program for the same reference signal $20 * sen(2\pi * 20t)$. These two figures show that the duty cycle is not saturated, the form is the same as the voltage wave measured in the output, the error is in the range of ±5%, and the current through the inductor (i_L) is lagged with respect to the voltage signal (v_c). The current in the inductor has a large ripple due to the switching of the transistors at 5 kHz; for this case, however, only the signal sampled at 5 kHz is shown. In Figure 9, the same signals for the reference signal $v_{ref} = 20 * sen(2\pi * 20t)$, taken in this case by the oscilloscope, are also shown. Figure 10 displays the numerical results for the same reference signal. In the simulation, the transient wave has been included to show the speed with which the controller responds; however, as can be seen in Figure 10, the signals in steady-state have the same behavior as those obtained experimentally.

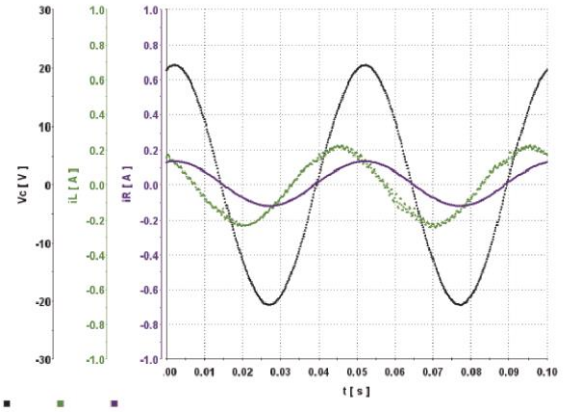

Fig. 7. v_c, i_L, and i_R views in ControlDesk

when $v_{ref} = 20sen(2\pi * 20t)$

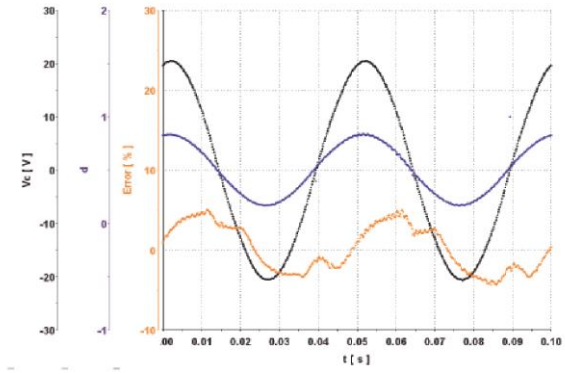

Fig. 8. v_c, d, and $Error$ views in ControlDesk

when $v_{ref} = 20sen(2\pi * 20t)$

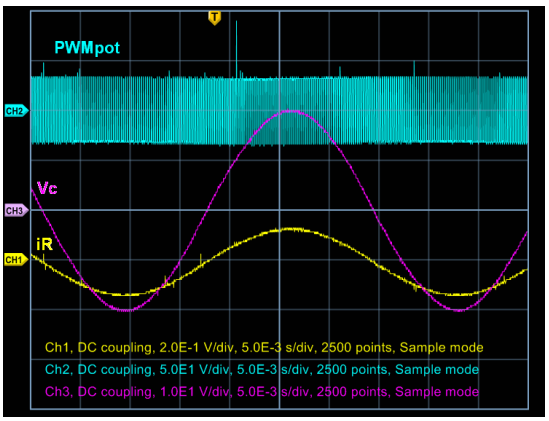

Fig. 9. PWMC, v_c, and i_R when $v_{ref} = 20sen(2\pi * 20t)$

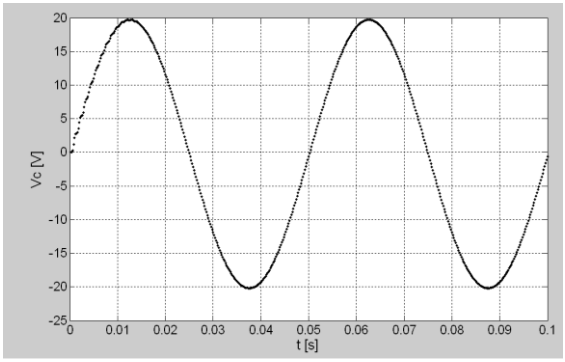

(a)

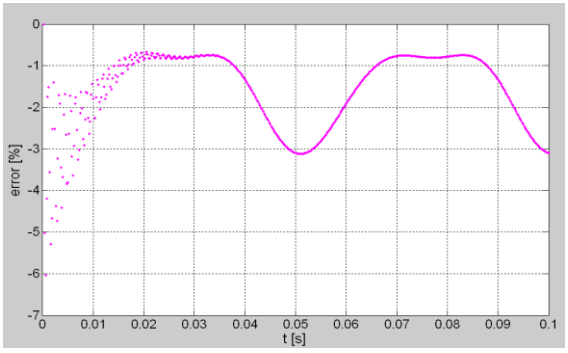

(b)

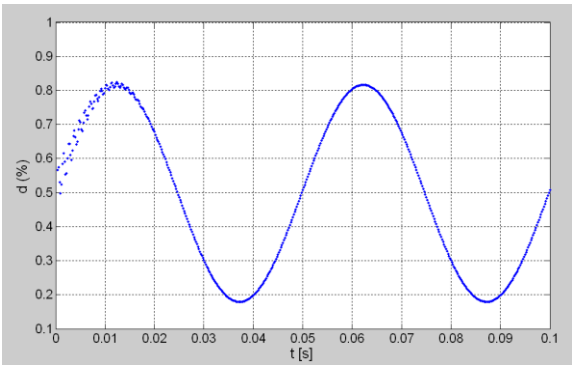

(c)

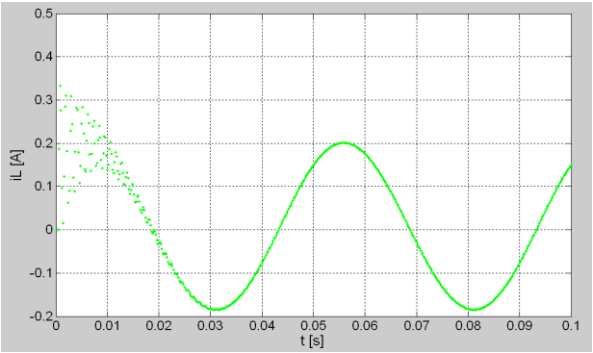

(d)

Fig. 10. Simulation results for the reference signal $v_{ref} = 20sen(2\pi * 20t)$. (a) v_c, (b) $Error$, (c) d, and (d) i_L

IV. Conclusion

In the implementation of this and another class of controllers at the experimental level, it is very important to keep in mind the sampling frequency with which the real signals are going to be acquired as this was one of the biggest drawbacks due to noise and flickering. Thus, it was found necessary to apply a sampling signal of at least 10 times the maximum frequency of the reference signal. The ZAD and FPIC controllers implemented digitally in a DS1104 meet the requirements of fixed frequency switching, robustness, and good performance in AC signal tracking tasks. Because the maximum switching frequency of the PWM output is 5 kHz, a higher regulation error occurs when the frequency of the reference signal is increased. Therefore, we have this limitation on the frequency of the signal we wish to control. For tracking high-frequency AC signals, the value of the LC filter capacitor must be decreased to avoid control effort. However, this causes the ripple of the signal to increase at the output and this generates an increase in the tracking error.

Acknowledgements

This work was supported by the Universidad Nacional de Colombia - Sede Medellín, under the projects HERMES-41917 and HERMES-36911. The authors thank to the School of Physics, the Department of Electrical Energy and Automation of the Universidad Nacional de Colombia.

References

[1] M. H. Rashid, *Power electronics handbook : devices, circuits, and applications* (Butterworth-Heinemann, 2011).

[2] D. W. Hart, *Electrónica de potencia* (Prentice Hall, 2001).

[3] F. Angulo, J. E. Burgos, and G. Olivar, Chaos stabilization with TDAS and FPIC in a buck converter controlled by lateral PWM and ZAD, *Mediterranean Conference on Control & Automation, Athens, Greece, January 2008.*

[4] S. Banerjee, G. C. Verghese, *Nonlinear Phenomena in Power Electronics:*

Bifurcations, Chaos, Control, and Applications (Wiley-IEEE Press, 2001).

[5] J. A. Taborda, F. Angulo, G. Olivar, Estimation of parameters in Buck converter with Digital-PWM control based on ZAD strategy, *IEEE Second Latin American Symposium on Circuits and Systems (LASCAS), Bogotá, Colombia, February 2011.*

[6] E. Fossas, R. Griñó, D. Biel, Quasi-Sliding control based on pulse width modulation, zero averaged dynamics and the L2 norm, in Advances in Variable Structure Systems, *6th IEEE International Workshop on Variable Structure Systems, October 2000.*

[7] D. Biel, E. Fossas, R. Ramos, A. Sudria, Programmable logic device applied to the quasi-sliding control implementation based on zero averaged dynamics, *Proceedings of the 40th IEEE Conference on Decision and Control, Orlando, FL, USA, December 2001.*

[8] R. R. Ramos, D. Biel, E. Fossas, F. Guinjoan, A fixed-frequency quasi-sliding control algorithm: application to power inverters design by means of FPGA implementation, *IEEE Trans. Power Electron., Vol. 18(Issue 1): 344–355, January 2003.*

[9] D. Biel, R. Cardoner, E. Fossas, Tracking Signal in a Centered Pulse ZAD Power Inverter, *International Workshop on Variable Structure Systems, Alghero, Sardinia, Italy, June 2006.*

[10] F. E. Hoyos, D. Burbano, F. Angulo, G. Olivar, N. Toro, J. A. Taborda, Effects of Quantization, Delay and Internal Resistances in Digitally ZAD-Controlled Buck Converter, *International Journal of Bifurcation and Chaos, Vol. 22(Issue 10): 1250245, October 2012.*

[11] F. E. Hoyos Velasco, N. T. García, Y. A. Garcés Gómez, Adaptive Control for Buck Power Converter Using Fixed Point Inducting Control and Zero Average Dynamics Strategies, International Journal of Bifurcation and Chaos, Vol. 25(Issue 04): 1550049, April 2015.

[12] F. E. Hoyos, J. E. Candelo, J. I. Silva-Ortega, Performance evaluation of a DC-AC inverter controlled with ZAD-FPIC, *INGE CUC, Vol. 14(Issue 1): 9–18, January 2018.*

[13] S. Ashita, G. Uma, P. Deivasundari, Chaotic dynamics of a zero average dynamics controlled DC–DC Ćuk converter, *IET Power Electron., Vol. 7(Issue 2): 289–298, February 2014.*